



International Committee for Future Accelerators

Sponsored by the Particles and Fields Division of IUPAP

Beam Dynamics Newsletter

No. 78

**Issue Editor:
J. Byrd, Argonne National Laboratory**

**Editor in Chief:
Ingo Hofmann, GSI/TUD**

December 2019

Contents

1	FOREWORD	5
1.1	FROM THE CHAIR.....	5
1.2	FROM THE EDITOR.....	6
2	SUPERCONDUCTING UNDULATORS	8
2.1	DEVELOPMENT OF SUPERCONDUCTING UNDULATORS AT THE ADVANCED PHOTON SOURCE.....	8
2.1.1	Introduction	8
2.1.2	Superconducting Undulators for the APS.....	8
2.1.2.1	Planar Undulators SCU0 and SCU18-1/2	8
2.1.2.1.1	Magnet.....	9
2.1.2.1.2	Cryostat	12
2.1.2.1.3	Performance	13
2.1.2.2	Helical Superconducting Undulator - HSCU	14
2.1.3	Superconducting Undulators for the APS Upgrade.....	17
2.1.3.1	Planar Undulators.....	17
2.1.3.2	SCAPE	18
2.1.4	Developments of Nb ₃ Sn SCU	21
2.1.5	Development of Undulators for FELs	22
2.1.5.1	FEL SCU Prototype	22
2.1.5.2	FEL SCU Module Prototype	23
2.1.6	Summary	24
2.1.7	References	25
2.2	SUPERCONDUCTING UNDULATOR ACTIVITIES AT KIT.....	27
2.2.1	Introduction	27
2.2.2	Development of Planar SCUs towards a Commercial Product [2]	27
2.2.2.1	Layout	28
2.2.2.2	Magnetic Measurements	29
2.2.2.3	Installation and Operation of SCU15 and SCU20 in the KIT Synchrotron	31
2.2.3	In House Developments.....	33
2.2.3.1	Measurement Systems.....	33
2.2.3.1.1	CASPER II.....	33
2.2.3.1.2	COLDDIAG.....	35
2.2.3.2	Period Length Doubling.....	36
2.2.3.3	Jointless High Temperature Superconducting Tape Stacked Undulator.....	37
2.2.4	Possible Future Applications of SCUs to Xray-FELs	38
2.2.5	Summary	39
2.2.6	References	39

2.3	CRYOSTATS AND CRYOGENIC SYSTEMS FOR SCUS	42
2.3.1	Introduction	42
2.3.2	Cryostat Design - APS First Generation	42
2.3.3	Second-Generation APS Cryostat	44
2.3.4	SCU Cryostats for FELs	47
2.3.5	Cooling Systems	49
2.3.6	Alignment Systems	50
2.3.7	Beam Vacuum Chambers	50
2.3.8	References	50
2.4	SCU ACTIVITIES IN THE UK	52
2.4.1	Introduction	52
2.4.2	Planar SCU Activities	52
2.4.2.1	Parameters and Design Choices	52
2.4.2.2	Prototype Construction and Testing	53
2.4.2.3	Prototype Test with CLARA	55
2.4.2.4	Next Steps	57
2.4.3	Helical SCU Activities	58
2.4.3.1	Motivation for Helical	58
2.4.3.2	Magnet Modelling	58
2.4.3.3	Open Questions	59
2.4.4	Conclusion	59
2.4.5	References	59
2.5	PRACTICAL SUPERCONDUCTING MATERIALS FOR HIGH-FIELD UNDULATORS.....	61
2.5.1	Introduction	61
2.5.2	Practical Superconducting Materials for SCUs	62
2.5.2.1	Niobium Titanium (NbTi)	64
2.5.2.2	Niobium-Tin (Nb ₃ Sn).....	65
2.5.2.3	Second-Generation High-Temperature Superconductors (2G-HTS).....	68
2.5.3	Conclusion and Outlook.....	71
2.5.4	References	71
2.6	SUPERCONDUCTING UNDULATOR DEVELOPMENTS AT LAWRENCE BERKELEY NATIONAL LABORATORY	74
2.6.1	Introduction	74
2.6.2	SCU Design	75
2.6.3	SCU Fabrication.....	76
2.6.4	Magnet Training.....	79
2.6.5	Magnetic Measurements.....	80
2.6.6	Local Field Error Correction System	81
2.6.7	Conclusions	84
2.6.8	References	85
3	WORKSHOP AND CONFERENCE REPORTS	86
3.1	ICFA MINI-WORKSHOP ON “MITIGATION OF COHERENT BEAM INSTABILITIES IN PARTICLE ACCELERATORS” (MCBI 2019).....	86

3.2	THE 63 RD ICFA ADVANCED BEAM DYNAMICS WORKSHOP ON ENERGY RECOVERY LINACS, ERL2019	88
4	RECENT DOCTORAL THESES	95
5	FORTHCOMING BEAM DYNAMICS EVENTS	100
5.1	ICFA BEAM DYNAMICS PANEL MEMBERS	101

1 Foreword

1.1 From the Chair

This Newsletter is edited by John Byrd, Director of the Accelerator Systems Division at the Advanced Photon Source and Director of the Argonne Accelerator Institute.

The thematic part of it is on *Superconducting Undulators*. We are grateful to John Byrd for having taken the responsibility for this compilation of highly interesting works, which includes six contributions from international researchers in this field. They describe the status and developments of this exciting topic at participating laboratories as well as the many technical challenges that had to be met before this technology could be realized successfully in a steadily increasing number of accelerators worldwide.

ICFA, the “International Committee for Future Accelerators”, will hold its 85th meeting at the SLAC National Laboratory, February 20-22, 2020. A central topic will be again – as already during the March and August ICFA meetings in 2019 - the future of the International Linear Collider (ILC) project. A decision of the Japanese government on the role of Japan as host country – with strong international participation - is still pending.

Section 3 is reporting about relevant ICFA BD meetings in the second half of 2019. Section 4 includes 7 PHD thesis reports.

In Section 5, we are glad to announce more details on the so far approved Advanced Beam Dynamics Workshops for 2020:

- The [64th ICFA Advanced Beam Dynamics Workshop on High Luminosity Circular e+e- Colliders](#), 14 - 16 September 2020 on Elba (INFN-LNF), Italy.
- The [65th ICFA Advanced Beam Dynamics Workshop on High-Intensity and High-Brightness Hadron Beams](#), 5–9 October 2020, FNAL, USA (note: dates changed from earlier announced 28 September – 2 October, 2020)

Ingo Hofmann, Panel Chair

1.2 From the Editor

John Byrd, Argonne National Laboratory

I have chosen the topic of superconducting undulators (SCUs) for this edition of the ICFA Beam Dynamics Newsletter. It is a subject I am not very familiar with and therefore very eager to learn from the experts in our community. I am extremely grateful to all of my colleagues for their contributions to this edition to help inform the rest of the community of the tremendous progress in this area.

In my opinion, we are currently in a golden age of development of synchrotron light sources. Third generation storage ring light sources, developed, designed, constructed, and operated over the past four decades, were optimized to provide low emittance beams with lattices that maximized the available straight sections for insertion devices, typically undulators, that increased the number of high brightness beamlines. There are currently over 50 light sources operating around in over a dozen countries around the world. The second facet of this golden age is the development of free electron lasers (FELs) as operating light source facilities. There are several operating facilities and several more planned, based on normal and superconducting linacs with low emittance injectors that provide high brightness, high peak current electron beams for lasing. Each of these FELs require dozens of exquisitely aligned undulators for the lasing action to occur.

Undulators are very attractive sources of synchrotron radiation. They provide bright narrowband beams at the fundamental and multiple odd harmonics. One of the essential features of an undulator is its tuneability, achieved by varying the peak magnetic field on axis. The large majority of undulators in use are hybrid permanent magnet undulators that combine high field permanent magnets and steel in an array with a period of a few centimeters housed in a rugged mechanical structure. The peak magnetic field is varied by changing the gap between the two arrays, typically arranged above and below the beam, using the mechanical structure to compensate for the magnetic forces between the two arrays. The maximum peak field is achieved by using the strongest permanent magnet material and minimizing the separation of the magnet arrays, limited by either the vacuum chamber or the beam stay-clear for the case of in-vacuum devices. Higher fields have been achieved by cryogenically cooling the permanent magnets. During the original development of undulators, permanent magnets were the only means for achieving Tesla-level fields with such short periods.

Superconductivity has always been considered a means of generating even higher peak fields on axis in short period undulators, especially given the tremendous success of superconducting magnets in accelerators. However, a number of engineering challenges needed to be met before it could be incorporated in undulators. These include cryogenic and mechanical design that allows for cooling with cryocoolers, minimization of heating mechanisms such as resistive beam heating, mechanical design that provides satisfactory magnetic field performance when cooled, long term performance in a radiation environment, and rugged design to allow a decade or more of operation in an accelerator. Over the past few decades, many researchers around the world have addressed and answered these challenges and we now have several SCUs in operation in existing accelerators with many more either in fabrication or in development. This issue describes many of these challenges and the solutions that have been adopted.

Third generation sources are now giving way to a new generation of ultralow emittance rings using multibend achromat (MBA) lattices that will provide two to three

orders of magnitude increase in photon beam brightness, primarily by a corresponding decrease in the horizontal beam emittance. These concepts have led to many new projects to upgrade or build new machines around the world. Two new machines have already been built: the MAXIV ring in Lund, Sweden and Sirius in Campinas, Brazil. The Sirius ring is currently under commissioning. The ESRF-EBS, a major upgrade to the ESRF storage ring, is also currently undergoing commissioning. There are many of these new sources expected in the next five years that will revitalize x-ray science and provide many opportunities for innovation.

Another very interesting feature of the MBA machines is that they are pushing towards on-axis injection schemes due to small dynamic aperture of the ultralow emittance designs. One of the consequences of this approach is that the vacuum chamber cross sections in the straight sections have aspect ratios much closer to unity than in third generation machines that have wide flat chambers. This will allow a much range of magnetic field configurations compared with the typical planar magnet array that are above and below the flat vacuum chambers. One of the biggest challenges for SCUs will be to build magnetic structures in the plane of the synchrotron radiation and manage the heat load from the radiation of upstream dipoles.

One of the most exciting potential applications is for x-ray FELs. Firstly, the higher potential peak magnetic field allows a broader tuning range. Secondly, SCUs are ideal for helical magnetic field configurations. This allows a shorter total FEL length and higher potential peak FEL power. There are significant challenges to achieve this. One of these will be to achieve the exquisite electron-photon beam alignment between undulators needed to maintain the lasing over several undulator lengths when cooled to cryogenic temperatures. I believe that SCUs will be a major component in the next generation of FEL designs if these challenges can be addressed.

My thanks to Cathy Eyberger for help in putting together this edition of the newsletter and again to the contributors of this edition. Please enjoy.

John Byrd, Argonne National Laboratory

2 Theme Section

2.1 Development of Superconducting Undulators at the Advanced Photon Source

Efim Gluskin and Yury Ivanyushenkov

Mail to: gluskin@anl.gov and yury@anl.gov

Advanced Photon Source, Argonne National Laboratory, Lemont, IL 60439, USA

2.1.1 Introduction

In the last three decades, driven by immense growth in the number of synchrotron radiation facilities around the world, advancements in permanent magnet undulator technology were quite significant. These advancements, including in-vacuum undulators, resulted from large and steady investments in undulator technology made by major synchrotron radiation facilities. But currently permanent magnet undulators—in-vacuum cryogenically cooled—are very close to the limit of their performance in terms of undulator peak field for a given period length and magnetic gap. Superconducting undulators (SCUs) offer a possibility to reach the magnetic fields not achievable by other undulator technologies. Magnetic simulations and recent experimental results confirm [1, 2] that SCUs outperform most advanced permanent magnet undulator technologies.

It is safe to state that the next generation of undulators will rely more and more on superconducting technology. About a decade ago, in anticipation of such a shift, the APS started an intense program of developing superconducting undulators. This program included the development of undulator magnet arrays, a stand-alone cryogenic system, and a magnet measurement system. To support all these developments, a special dedicated facility, which included a magnet winding machine, an epoxy impregnation setup, cryocoolers, liquid helium testing cryostats, control systems, and auxiliary mechanical systems, was built. A dedicated team of scientists, engineers, and technicians was formed, and this team, supported by the APS and DOE accelerator R&D projects, succeeded in designing and building a set of SCUs that now successfully operate at the APS. Capitalizing on this success, the APS upgrade project has included several SCUs in its baseline design.

The APS SCU team continues to develop different types of undulators to meet the current and future needs of storage ring- and FEL-based light sources.

2.1.2 Superconducting Undulators for the APS

2.1.2.1 *Planar Undulators SCU0 and SCU18-1/2*

Development of superconducting undulators at the APS started in the first decade of this century with an intensive R&D phase aimed at design and fabrication of an SCU magnetic structure. This paved the way to the first superconducting undulator, SCU0, which was completed and installed on sector 6 of the APS in the winter of 2012-13 [3]. Two years later a 1.1-m-long undulator, SCU1 (SCU18-1), was installed in sector 1, and

in 2016 a similar undulator, SCU18-2, replaced SCU0. There are currently two planar undulators—SCU18-1 (Figure 1) and SCU18-2—in operation at the APS.



Figure 1: Superconducting undulator SCU18-1 installed in the APS storage ring.

The parameters of these devices, as well as of SCU0, are given in Table 1.

Table 1: Parameters of APS planar undulators.

<i>Parameter</i>	<i>Unit</i>	<i>SCU0</i>	<i>SCU18-1/2</i>
Electron beam energy	GeV	7	7
Photon energy at the fundamental	keV	20-25	11.7-25
Period length	mm	16	18
Number of periods	...	20.5	59.5
Vacuum gap	mm	7.2	7.2
Design magnetic field	T	0.64	0.97
Achieved magnetic field	T	0.8	0.97
Achieved undulator parameter K	...	0.96	1.63
Magnetic length	m	0.33	1.075
Cryostat length	m	2.063	2.063

2.1.2.1.1 Magnet

As in planar permanent magnets or hybrid undulators, the magnetic field in the superconducting undulator is created by a pair of identical magnets, separated by a vertical gap that accommodates a beam vacuum chamber, see Figure 2.

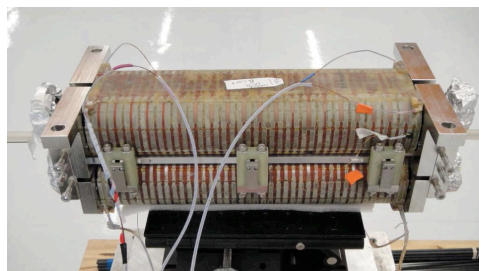


Figure 2: Photograph of an SCU0 magnet assembly.

A set of multiple racetrack coils are formed when a NbTi superconducting wire is wound into the former (or core) grooves. The current is flowing in opposite directions in the adjacent coil packs, therefore generating an alternating field profile along the beam axis. The SCU0 magnets are wound with a round NbTi 0.7-mm wire while a 0.6-mm wire was used for winding the SCU18-1/2 magnets; both superconducting wires are from Supercon Inc. [4]. For the SCU0, an assembled design of the magnetic core was chosen where individual, precisely ground and lapped poles are inserted in slots machined in the polished sub-core, as shown in Figure 3. In this design, the groove surface has a $0.4\text{-}\mu\text{m}$ finish to help avoid electrically shorting the wire to the core during the winding process. The SCU0 core is designed to wind the undulator coil first in one direction into alternate grooves for the full coil length. After making a 180° turn, the wire is then similarly wound into the remaining grooves in the opposite direction to form an undulator magnet coil without any splicing.

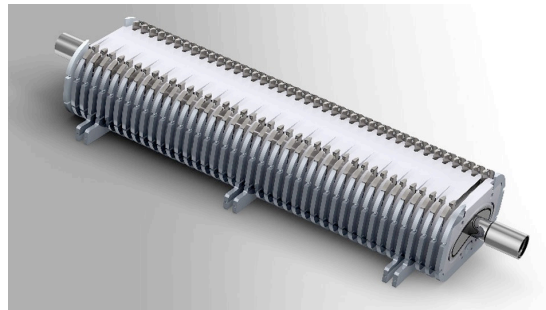


Figure 3: SCU0 undulator magnet core.

In the SCU18-1/2 magnet, the superconducting wire makes a 180° turn on the back side of the core around a pin (Figure 4) after being wound into a groove. The number of wire turns in a winding pack depends on the undulator period length and the groove dimensions. For example, a 16-mm-period SCU0 magnet contains 39 turns of 0.6-mm round wire in a groove, while there 53 turns in a winding pack of the SCU18-1/2 cores. The core and the superconducting wire are cooled to 4.2 K with liquid helium (LHe) passing through a channel in the core, also seen in Figures 3 and 4.

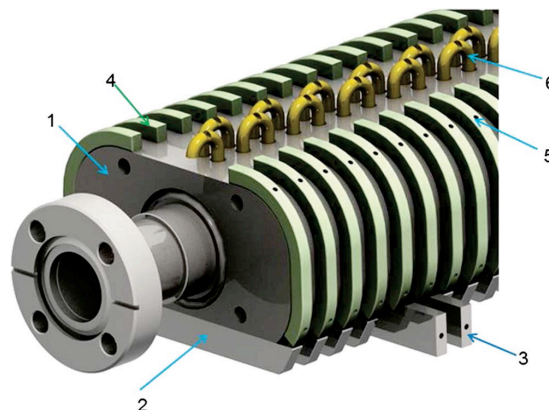


Figure 4: SCU18-1/2 undulator upper magnet core.

Several correction coils are available during operation of the planar SCU. All the correction coils are inside the cryostat. As a result of winding the undulator magnet with

an odd number of main coil packs, there is a vertical field along the length of the undulator that is zero at the center of the magnet and increases linearly toward its ends. This field causes the electron trajectory to take an “S” shape. On each core there are correction coils wound in the two end grooves where there are a reduced number of turns of the main coil, see Figure 5. These end corrector coils are wound with the same conductor as the main coil and are used to straighten the electron trajectory as well as adjust the magnetic strength of the end poles.

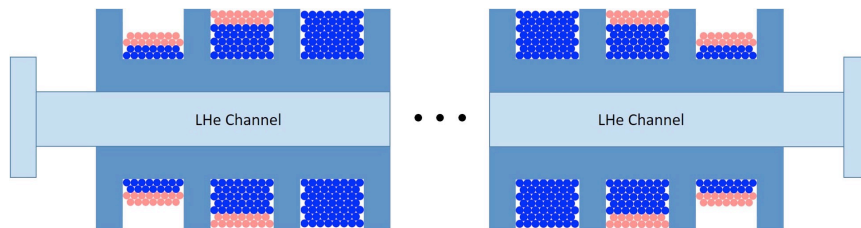


Figure 5: Winding scheme of the SCU1 magnet. There are 53 conductors in a full main coil pack (blue), 38 main coil conductors in the second to last grooves, and 15 main coil conductors in the end grooves. There are 15 conductors (red) wound over the top of the main coil to form the corrector coil in the last two grooves at either end.

In order to correct the first field integral due to the undesirable dipole field, first noticed in SCU18-1, there is a Helmholtz-like coil that is wound from ten turns of 0.7-mm-diameter NbTi superconducting wire. These coils are placed above and below the assembled SCU magnet, as shown in Figure 6.

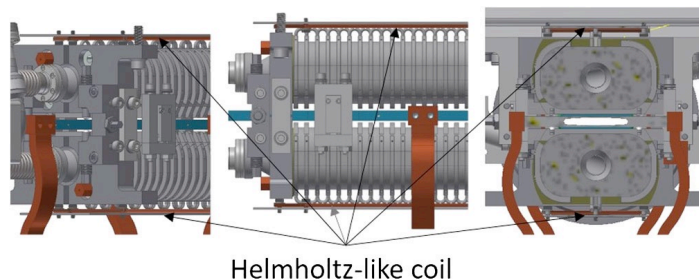


Figure 6: Helmholtz-style coil to correct the dipole vertical field along the length of the device.

The last type of correction coils available are used to adjust the second field integral. These are the dipole coils that are installed inside the cryostat upstream and downstream of the magnetic structure, as seen in Figure 7. The coils are wound using 22 American wire gauge copper magnet wire.

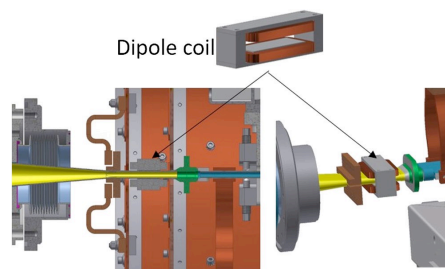


Figure 7: Dipole coils installed upstream and downstream of the undulator magnet inside the cryostat that can be used to compensate the second field integral.

Magnetic performance of the APS superconducting undulators was measured using a dedicated horizontal magnetic measurement system [5]. It is based on the concept of a warm-bore guide tube developed at the Budker Institute of Nuclear Physics (INP), Novosibirsk, Russia [6]. The APS measurement system utilizes a room-temperature Ti tubing that is tensioned inside but thermally isolated from the cold Al beam chamber. The Ti tubing is a guide tube for a carbon fiber Hall probe assembly driven by a 3.5-m-long linear stage. The measurement system also utilizes wire coils for integrated field measurements and is configured without interfering with the cryogenic or vacuum systems of the SCU cryomodule.

2.1.2.1.2 Cryostat

Undulators SCU0 and SCU18-1/2 use similar 2-m-long SCU0-type cryostats. The design of the SCU0 cryostat is based on the concept developed at the INP and implemented in the superconducting wigglers that have been built by the INP team for several light sources worldwide [7]. The SCU0-type cryostat is a stainless-steel vacuum vessel that contains two copper radiation shields and a cold mass, as shown in Figure 8. The cold mass consists of the superconducting magnet assembly, including a beam vacuum chamber, and a 100-liter LHe tank with piping making a closed-loop 4 K circuit. The central part of the beam vacuum chamber is made of aluminum alloy 6063-T5 with a stainless-steel transition on each end. A stainless-steel frame supports both the magnet assembly and the LHe tank and is supported inside the vacuum vessel by a set of Kevlar strings. The cryostat also incorporates two turrets not visible in Figure 8 and a helium fill turret. One of the most important conceptual points in the cryostat design is that the superconducting cores are thermally isolated from the vacuum chamber. This substantially reduces the heat load from the beam on the superconducting magnet. The vacuum chamber can then be cooled independently and does not need to be at the temperature—typically 4 K—of the superconducting coils. The SCU0-type cryostat cooling system consists of four 2-stage cryocoolers delivering cooling power at three temperature levels with design values of 4 K (magnet cores), 20 K (beam chamber and internal radiation shield), and 60 K (outer radiation shield and current leads).

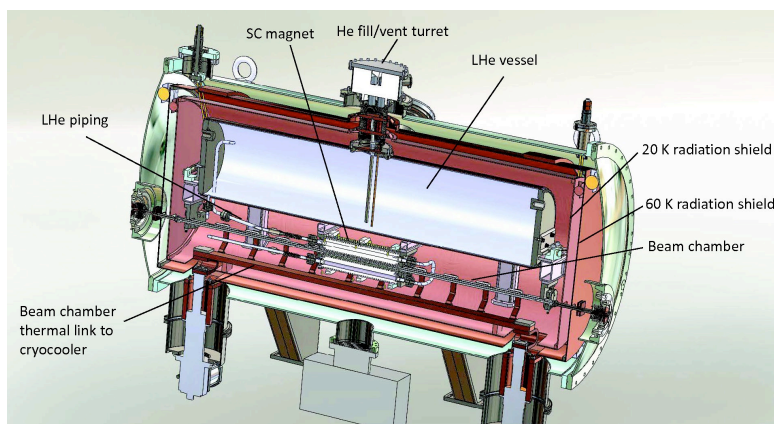


Figure 8: Solid model cutaway view of the inside of the SCU0 cryostat.

The SCU18-1/2 undulators use cryostats that are improved versions of the SCU0 cryostat [8]. Modifications include the addition of optical windows in the cryostat vacuum vessel that allow direct observation and measurement of the cold mass vertical position

inside the cryostat. Also, several thermal links were added to improve cooling of the cold mass support frame. The Kevlar strings that support the cold mass in the cryostat have been improved as well.

2.1.2.1.3 Performance

The performance of superconducting undulators was measured after installation of these devices on the APS storage ring. The SCU0 was characterized by measuring the photon flux passing through a bent-Laue monochromator and comparing the SCU0 photon flux with that from an in-line 3.3-cm-period length permanent magnet hybrid undulator, U33. At 85 keV, the 0.33-m-long SCU0 produced $\sim 45\%$ higher photon flux through an aperture than the 2.3-m-long U33. Figure 9 shows the simulated photon flux calculated from the measured magnetic fields compared to the measured photon flux at 85 keV for SCU0, and the measured photon flux for U33 (inset). In these measurements, the U33 gap was scanned from 11.0 mm to 12.0 mm to maximize the photon flux. Smaller than expected flux from SCU0 is likely due to an alignment error of the aperture (0.5 mm \times 0.5 mm), located 40 m from the undulator, with respect to the photon beam. Nevertheless, this measurement demonstrates the enhanced capability of SCU0 for generating higher photon fluxes at higher energies.

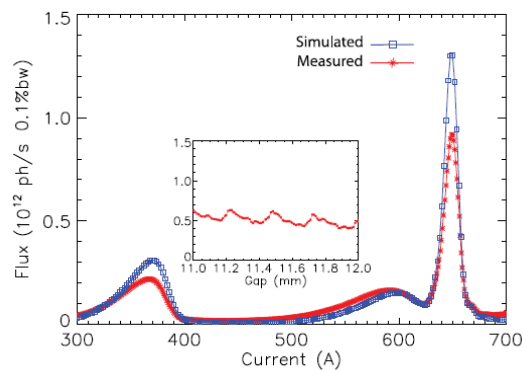


Figure 9: Photon flux comparisons at 85 keV. Main: simulated and measured SCU0 photon flux as the main coil current is scanned. Inset: measured photon flux of in-line U33 as the gap is scanned. Inset vertical axis units are the same as the main plot.

Figure 10 shows the flux comparison among hybrid undulators U33 and U23, and SCU18-1 (SCU1) sources, measured with monochromatized radiation over 40–140 keV at the APS1-ID, under the same beamline conditions [9]. The advantage of the superconducting undulator is apparent.

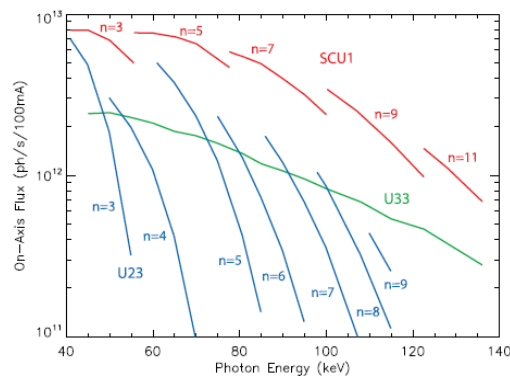


Figure 10: Measured odd-harmonic SCU1-1 (SCU1) tuning curves of monochromatic flux through a $0.5 \times 0.5 \text{ mm}^2$ aperture at 27.5 m compared with those of 11-mm minimum gap permanent magnet devices U33 (continuous tuning curve envelope) and U23 (even and odd harmonics).

2.1.2.2 *Helical Superconducting Undulator - HSCU*

The successful development and operation of planar APS SCUs have laid the groundwork for the expansion of SCU technology toward helical magnet geometry. There is a set of motivations to pursue the helical SCU technology. One of them is to demonstrate that a helical SCU could deliver higher field strength compared with widely used APPLE-type undulators, and at the same time it is quite competitive in providing well-controlled radiation properties, such as polarization. The first step in such a demonstration is the development of a robust HSCU design and fabrication of a HSCU magnet that meets the design specifications of 3rd- and 4th-generation light sources. A second step is the demonstration of HSCU radiation performance along with operational reliability at the storage ring.

In 2015 the APS, supported by DOE BES accelerator R&D funding, started the design and construction of the HSCU in order to continue advancement of SCU technology and provide APS users with a unique radiation source for novel x-ray experiments.

The x-ray energy range utilized for coherence-based x-ray scattering experiments at APS sector 7, chosen to house the HSCU, is within 6.5 to 10 keV. This range and allowable—by APS storage ring operational requirements—aperture of the vacuum chamber in the HSCU primarily affect the choice of undulator period. In addition, the energy bandwidth should be as low as possible in order to use x-rays without a monochromator. The design optimization of the HSCU period and magnetic aperture resulted in the parameters shown in Table 2.

Table 2: Design parameters of the HSCU.

<i>Parameter</i>	<i>Value</i>
Electron beam energy (GeV)	7
Photon energy at the fundamental (keV)	6-12
Period length (mm)	31.5
Number of periods	38.5
Electron beam aperture (mm)	26×8
Coil inner diameter (mm)	31
Coil outer diameter (mm)	39.09
Conductors per helix	138
Conductor diameter (mm)	0.7
On-axis magnetic field $B_x=B_y$ (T)	0.41
Undulator parameter $K_x=K_y$	1.2

The magnet concept utilized a well-known bifilar helical coil arrangement [10-12]. Magnetic modeling and several practical constrains guided the choice of coil pack dimensions, the geometry of the winding mandrel, as well as the impregnation mold material and its shape. There were also several important factors that influenced the design and the process of magnet fabrication. One of these factors was continuous, non-interrupted coil winding; another was gradual reduction of the field at each end of the

magnet. A third very important factor was use of the impregnation mold as the magnet strongback to provide the required rigidity and secure the magnet's straightness.

Several short prototypes of the HSCU with a period of 20 mm and bore diameter of 15 mm were manufactured to test different winding schemes followed by a 0.3-m-long prototype of the final design. Some of these prototypes and the preliminary configuration of the turn-around structure are shown in Figure 11.



Figure 11: Top: Al and 1020 steel, 20-mm-period prototype HSCU mandrels with the turn-around structures not installed. Bottom: One end of the prototypes with the turn-around structures installed.

The 0.3-m-long, 31.5-mm-period prototype shown in Figure 12 was impregnated with epoxy and went through the process of quench training and magnet measurements in the vertical, LHe-filled cryostat.



Figure 12: The 0.3-m-long, 31.5-mm-period prototype HSCU after winding.

Following the successful conclusion of the prototype program, the 1.2-m full-length HSCU magnet was built. That included winding the full-length magnet, consisting of 38.5 full periods with two periods at each end devoted to the conductor turn-around geometry and consequent epoxy impregnation of the coil. Then the magnet, incapsulated in the impregnation mold, was quench-trained and measured in the vertical LHe bath cryostat. The HSCU magnet and the mold are shown in Figure 13.

Magnet measurements in the vertical cryostat confirmed that the HSCU achieved designed peak field on the axis at the designed current level with more than 20% quench-safe margin. Prior to the installation of the HSCU magnet in the horizontal cryostat, described in J. Fuerst's paper of this Newsletter, the set of corrector magnets had been attached to both ends of the mold. These SC magnets provide compensation for 1st and

2nd field integrals in order to contain the values of both integrals within APS ID specifications. Cryogenic tests and magnet measurements of the HSCU in the horizontal cryostat have been completed [13]. They resulted in the lookup tables for the corrector magnets and confirmed the readiness of the device for installation on the APS storage ring.

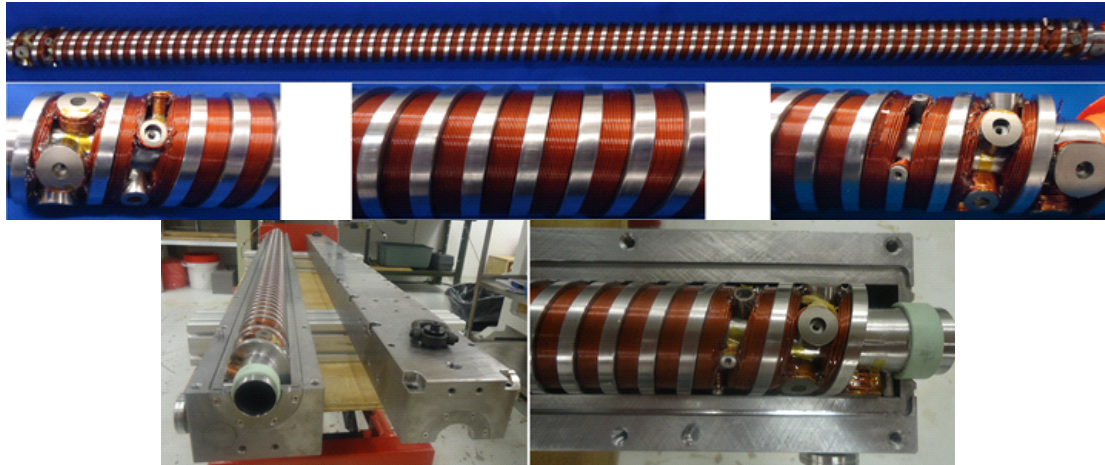


Figure 13: Top: HSCU magnet after winding. Bottom: HSCU magnet test fit into the mold before epoxy impregnation.

The HSCU was installed on the straight section of sector 7 of the APS storage ring during the December 2017-January 2018 scheduled shutdown. Figure 14 shows the HSCU installed on the APS ring. After rapid and successful commissioning, the HSCU was transferred to user operations. Although the commissioning process was mostly routine, one specific feature of the HSCU vacuum chamber—relatively limited horizontal aperture—forced introduction of a horizontal trajectory angle bump adjacent to the straight section bending magnet. Such a bump eliminated the access of hard x-ray radiation to the inbound wall of the vacuum chamber and significantly reduced the heat-leak-produced Compton-scattered hard x-rays. After the commissioning with e-beam, the radiation properties of the HSCU were also measured, and the predicted spectral performance was confirmed.

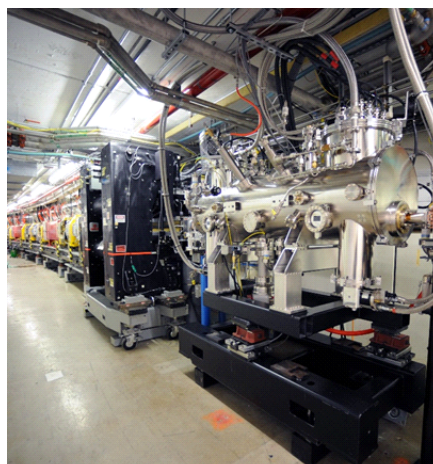


Figure 14: Helical superconducting undulator in sector 7 of the APS storage ring.

The HSCU has been operating with 100% reliability for almost two years. Using the unique radiation properties of the HSCU, scientists at sector 7 have been able to significantly advance x-ray phase contrast imaging techniques for studies of fast processes in the soft matter. The APS HSCU is also an extremely useful test bed for future FEL undulator lines.

2.1.3 Superconducting Undulators for the APS Upgrade

The upgrade of the APS (APS-U) is now in progress with a goal of replacing the existing storage ring with a new multi-bend achromat lattice and developing or updating x-ray beamlines. Several new SCUs will be built for the upgrade: eight planar undulators assembled in pairs in four long cryostats, and a Superconducting Arbitrarily Polarizing Emitter – SCAPE.

2.1.3.1 Planar Undulators

The APS-U undulators contain two undulator magnets configured either in-line or canted in 4.8-m-long cryostats as listed in Table 3.

Table 3: Scope of the APS-U planar undulators.

<i>Period length (mm)</i>	<i>Magnet length (m)</i>	<i>Configuration</i>	<i>Quantity of cryostats</i>
16.5	1.9	Two in-line	2
16.5	1.5	Two canted	1
18.5	1.2	Two canted	1

Unlike the APS, where superconducting undulators occupy only half of a straight section, in the APS-U the SCUs will occupy the complete length of the straight section, as shown in Figure 15.

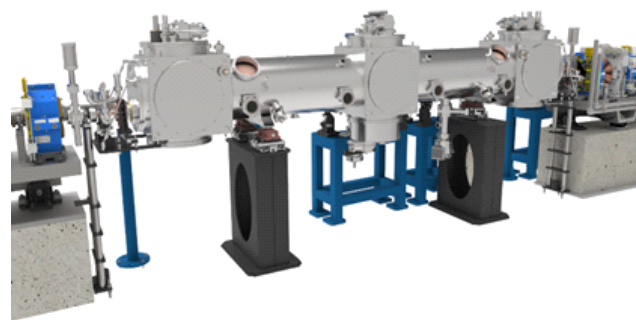


Figure 15: Layout of APS-U straight section with an SCU.

The design of APS-U SCUs is based on the experience of building and operating SCUs for the APS. The cryostat overall layout is similar to the HSCU cryostat—a cold mass is assembled inside a 20”-diameter vacuum vessel that also contains a single thermal shield; cooling is provided by cryocoolers, as seen in Figure 16 [14].

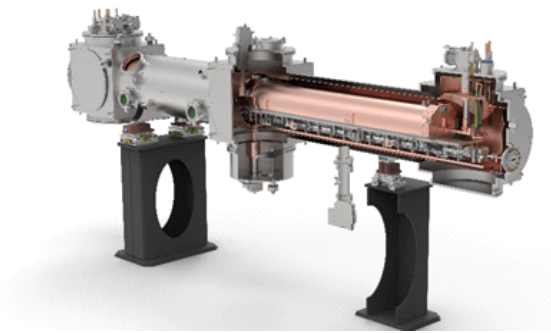


Figure 16: A layout of the APS-U SCU cryostat.

Five cryocoolers (Sumitomo RDK-418D4) maintain the magnet cooling circuit at 4.2 K, and up to two cryocoolers (Sumitomo RDK-408S) can be used to provide cooling to the electron beam vacuum chamber in order to maintain the chamber below 20 K. The first stages of all the cryocoolers are connected to the thermal radiation shield and the warm end of the high temperature superconducting leads. A preliminary thermal analysis has been completed and excess capacity at 4.2 K is expected, which will allow the SCU cryostat to operate without losing LHe inventory [15].

It is desirable to have the ability to measure the magnetic field and monitor the alignment of the magnets within the production cryostat when the system is under normal operating conditions, i.e., under vacuum and at cryogenic temperatures. To achieve this, a new magnetic measurement system is being developed [16], and eight optical windows have been incorporated into the cryostat to perform survey and alignment measurements at any time during operation. Horizontal and vertical displacements of the magnets can be measured through the optical windows using a precision 2D laser scanning tool developed at the APS [17].

2.1.3.2 *SCAPE*

SCAPE is a novel concept of a universal superconducting undulator capable of generating both planar and circular polarized radiation [18]. The SCAPE magnetic structure consists of two pairs of planar-like cores—one vertical and one horizontal— assembled around a beam vacuum chamber, as seen in Figure 17.

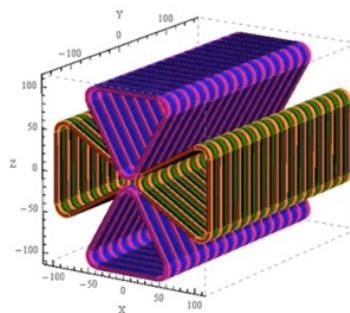


Figure 17: Concept of SCAPE. Superconducting coils model in RADIA.

The horizontal pair is shifted against the vertical pair by a quarter of the period length. Such a magnet generates a planar magnetic field when one of the core pairs is energized—either the vertical or the horizontal one—or it generates a helical field when all the core pairs are energized. Since the cores are wound with a superconducting wire, the magnetic

field on axis exceeds the values reachable with a permanent magnet technology. Figure 18 shows a mechanical 3D design model of a SCAPE magnet and a beam chamber.

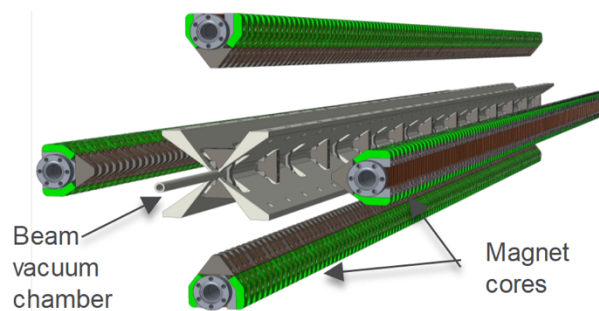


Figure 18: SCAPE 3D design model.

The beam chamber can be made of an Al extrusion, which contains a central tube with integrated longitudinal fins that are used for extraction of the electron-beam-generated heat. The magnet cores, which are also made of Al extrusion, contain magnetic pole tips. The cores and superconducting windings are cooled by liquid helium, which passes through the core channels.

A 0.5-m-long SCAPE prototype with a period length of 30 mm and a magnetic gap (pole-to-pole) of 10 mm was built and successfully tested. The mechanical structure of the prototype is shown in Figure 19, and a core winding is shown in Figure 20. The magnet was tested in a LHe-bath cryostat and achieved a field of 0.73 T in the planar and helical modes.



Figure 19: SCAPE prototype mechanical structure.



Figure 20: SCAPE core winding.

The SCAPE undulator will use the same or a similar cryostat as the APS-U planar superconducting undulators. Two SCAPE devices up to 1.7 m long will be in the cryostat in order to obtain switchable polarization, which is a requirement for the SCAPE by the beamline. A baseline option for polarization switching is based on the electron beam trajectory manipulation with two pairs of kicker magnets outside the SCAPE and a canting magnet between two undulator magnets inside the cryostat. In this scheme, the electron beam is collinear with the magnetic axis of one undulator but is angled in the other; therefore only one photon beam reaches the beamline target while the other goes into a beam stop, see Figure 21 [19]. Preliminary calculations suggest that about a 30- μ -rad bump is sufficient to achieve the desired rejection.

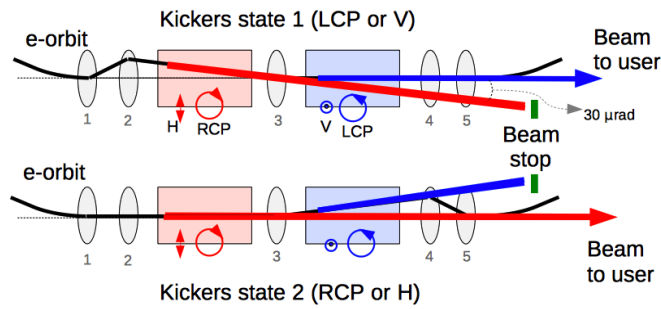


Figure 21: Polarization switching with electron beam bumps.

The other possibility for polarization switching is to use ‘current bumps’ in the SCAPE magnets. As in the previous scheme, the SCAPE magnets are preset to particular polarization modes; for instance, the upstream magnet is set to a linear-horizontal mode while the downstream one is set to a linear-vertical mode. Then by increasing or decreasing the current in the second magnet, one is shifting its radiation spectrum out of the bandwidth of the monochromator located downstream of the SCAPE undulator. In this situation, the monochromator filters out the radiation from the detuned undulator and accepts the radiation from the tuned one, see Figure 22 [19]. It is expected that detuning of undulators with this scheme can be achieved by rapid increasing/decreasing currents in the SCAPE magnets at a level of about 10 A.

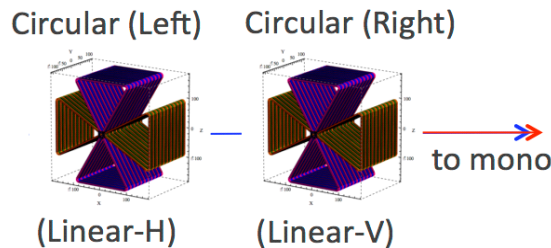


Figure 22: Polarization switching by using a monochromator to reject radiation from a detuned undulator.

The latter scheme requires operation of SCAPE superconducting magnets in AC-modulated DC mode. It is known that a superconductor exhibits heating when energized with such a current. This challenging request has triggered R&D to study heating of SCAPE coils by AC currents. For this study, a short model was built, and the heating was measured at various DC levels and AC amplitudes and frequencies. Preliminary studies suggest that the heating power is independent of the DC value and rises quadratically with the AC amplitude but only linear with the AC frequency. To decrease the AC heating, one suggestion is to use a double-layer winding with the main coil wound with a ‘standard’ superconductor, which is energized by a DC current, while an AC-optimized conductor (usually a multi-filament conductor with extremely small diameter filaments and a special matrix) is used for winding an extra layer that is powered by an AC power supply. According to preliminary studies, this allows reduction of the overall conductor heating by about 40% [20]. A more detailed study is underway. Once the level of heating is well understood, a scheme for polarization switching—either a static SCAPE with the electron beam bumps or an AC-modulated SCAPE—will be chosen.

2.1.4 Developments of Nb₃Sn SCU

Previous sections of this paper illustrated the successful developments of NbTi-based SCU technology. Several SCUs were built, and they became reliable sources of a wide spectrum of x-rays and sources of choice for experiments with hard x-rays. However, a further drive toward smaller-period SCUs is limited by the maximum achievable field attainable with NbTi technology. Hence, like many other SC technology applications, there are attempts to use different SC materials that could outperform NbTi for SCU applications. Such attempts have been made in the last ten years by different development groups. So far they have not resulted in operational devices similar to NbTi-based SCUs. In 2018, the APS in collaboration with Fermilab and LBNL started a project to develop a Nb₃Sn SCU with a final goal of installing it on the APS storage ring and utilizing it for user operations [21]. The project is supported by the DOE BES accelerator R&D program, and it should be completed in 2021, several months prior to the APS upgrade shutdown.

The first phase of the project included the design, fabrication, and testing of short, only several-period Nb₃Sn SCU magnets. There were several goals for that phase of the project. They included establishing a robust design for the ends of the magnet, fine-defining and verifying the well-controlled and repeatable processes of high-temperature treatment of the Nb₃Sn magnet coils, and detailed quench analysis. In the second phase of the project, capitalizing on the experience gained with the short prototypes, a 0.5-m-long Nb₃Sn SCU will be built and tested. If at the end of the second phase the expected technical performance of a 0.5-m-long Nb₃Sn SCU is achieved, the project will move to its third and final phase of fabricating and testing a 1.2-m-long Nb₃Sn SCU and installing it on the APS storage ring. Currently, the project is close to the end of the second phase.

A total of six short prototypes of the Nb₃Sn SCU have been built, and four of them have been tested in the LHe cryostat at phase one of the project. One of these prototypes is shown in Figure 23. The prototypes incorporated step-by-step improvements in the mechanical design, included testing of different wires and fine-tuning of the heat treatment cycle that was conducted in a special, high-temperature oven at Fermilab. The results of quench training for four prototypes are shown in Figure 24.



Figure 23: A picture of a short model magnet #6 (SMM6) after winding and reaction before the epoxy impregnation.

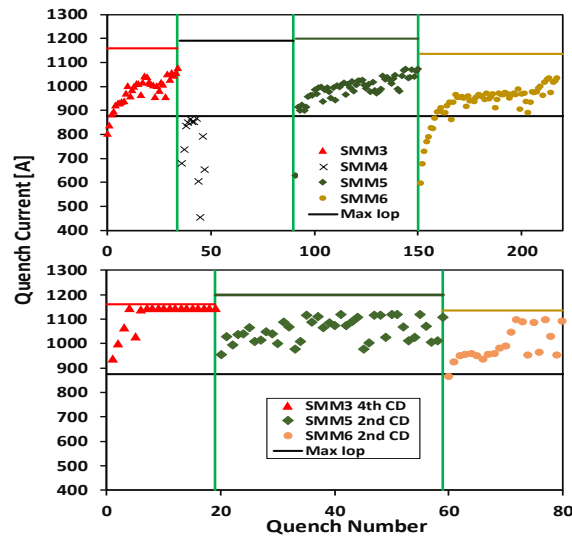


Figure 24: Training curves for SMM3-6 in the first cool down (CD) (top panel) and after repeated cool down(s) (bottom panel) except for SMM4, which was damaged in the first CD. Magnets reached the maximum operating current and required a few quenches. The second CD showed that the magnet has very good memory and requires almost no training to reach the maximum operating current.

Detailed analysis of quench training results provided benchmarking parameters for the final design of the quench protection system developed at LBNL.

Recently one 0.5-m-long Nb₃Sn SCU magnet was fabricated and quench-trained. The magnet met technical requirements. More details about these latest results are in the paper by I. Kesgin et al., in this Newsletter.

2.1.5 Development of Undulators for FELs

2.1.5.1 FEL SCU Prototype

The advantages of SCU technology for achieving higher magnetic field compared with PM undulators make the SCU an obvious candidate for FEL undulator lines. It has been shown that SCUs have the potential to extend the spectral range of existing FEL sources, and they can be fit in shorter tunnels without degrading FEL performance. In order to demonstrate the viability of SCU technology for FELs, in 2013-2016 a collaborative R&D effort between ANL, LBNL and SLAC was executed with the purpose of developing and comparing two planar SCU magnet technologies: NbTi and Nb₃Sn. ANL and LBNL built and tested two SCU magnets of the same 1.5-m length but used different superconducting wire: ANL - NbTi, and LBNL - Nb₃Sn. Although the Nb₃Sn magnet did not reach its full excitation current (< 75%), the NbTi magnet demonstrated all technical specifications, including an rms phase-shake of < 5 degrees, x and y first field-integrals of < 40 μT-m, and x and y second field-integrals of < 150 μT-m², etc. [22]. The parameters of the NbTi device are listed in Table 4. The most challenging requirement— achieving a phase error below 5° rms over a 1.5-m-long magnet— triggered a dedicated study of the field error sources in a planar SCU. The precise measurements of the core geometry after each fabrication step revealed deformation of a core during a vacuum resin impregnation. In order to compensate the magnetic gap

enlargement due to this core bowing, design changes were implemented and a method of measuring the magnetic gap of the magnet assembly was developed [23]. As a result, the external mechanical clamps are installed onto the magnet assembly at gap spacer locations distributed along the length of the device. In this arrangement, the magnetic gap is defined by the precision of the gap spacers that are machined to 10 μm rms. The technique was first tested in the LCLS SCU magnet where five clamps were installed over 1.5 m. This magnet has achieved a phase error of 3.8° rms, thus meeting the specification requirement of 5° rms.

Table 4: Parameters of LCLS SCU prototype.

<i>Parameter</i>	<i>Unit</i>	<i>Specification</i>	<i>Measured</i>
Magnetic length	m	1.5	1.5
Period length	mm	21	21
Vacuum gap	mm	5.7	5.7
Magnetic gap	mm	8.0	8.0
Magnetic field	T	1.67	1.67
Undulator parameter K	...	3.26	3.26
Phase error rms	deg	5	3.8±0.3
1st field integral (x and y)	$\mu\text{T}\cdot\text{m}$	±40	31±3
2 nd field integral (x and y)	$\mu\text{T}\cdot\text{m}^2$	±150	-80±3
Cryostat length	m	2.063	2.063

The developed gap compensation scheme was fully implemented in the SCU18-2 magnet, which achieved a phase error as low as 2° rms. For comparison, the phase errors in the SCU18-1 magnet, which does not have gap compensation clamps, are greater than 5° rms.

2.1.5.2 *FEL SCU Module Prototype*

Successful development and operation of high quality, high performance SCUs at the storage ring, as well as demonstration of the performance of a NbTi SCU within FEL specified requirements, set the stage for the next step in the process of adopting SCU technology for FEL light sources. This step would be the design and construction of an SCU-based FEL undulator module prototype that should include not only undulator magnets, but also a phase shifter, focusing magnets, and a precise electron beam position monitor. All these components plus the alignment system should be integrated in a cryostat and tested as a unit to validate the FEL-required performance, including predicted gain, required accuracy beam diagnostics, and ability to perform beam-based alignment. The schematic of a FEL SCU cryomodule prototype is shown in Figure 25.

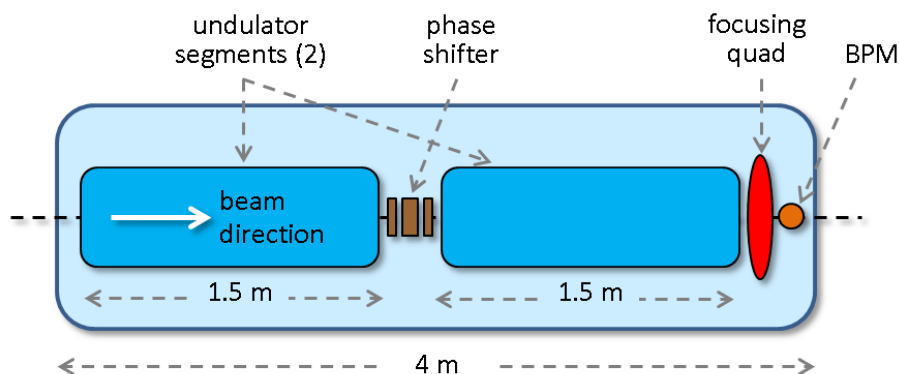


Figure 25: Schematic of a FEL SCU cryomodule prototype with two 1.5-m-long magnets, a cold quad, phase shifter, and BPM.

The design and construction of the FEL SCU module would greatly benefit from the APS-U SCU developments and construction efforts. In particular, most of the APS-U SCU cryoengineering could be directly applied to the FEL SCU module prototype. Although for the long FEL SCU line the approach of a local, self-contained cryogenic system very likely is not the most optimal, and a relatively small cryoplant would be more cost effective and technically efficient than a multitude of cryocoolers. Use of the cryoplant would drive the different design of the cryostat vessel and LHe distribution system but would not affect most of the module's internal components.

R&D effort on the FEL SCU module prototype in addition to the SCU magnets would include: design a cold mass that can accommodate either a planar or helical SCU magnet with an option to position a planar undulator magnet at orthogonal axial positions; design, fabricate, and test a “cold,” tunable phase shifter with well-compensated 1st and 2nd integrals in x and y directions; implement measurement and control techniques to maintain required rms phase “shake”; design, build, and test an alignment system that permits component-to-component, component-to-fiducial alignment with warm and cold components; design, build, test, and demonstrate high, <1 micron, resolution of a cold e-BPM; design, build, and test cold quadrupoles.

The main motivation of advancing SCU technology toward FEL sources is illustrated in Figure 26. It shows significant improvement in the spectral performance of LCLS-II in the case of replacement of current permanent magnet undulators with SCUs. Also, use of helical SCUs with smaller periods increases the spectral range further and allows for better use of existing undulator tunnels.

2.1.6 Summary

In the last decade APS has invested significant resources and efforts in the development of SCU technology. It resulted in building of the dedicated facility for development, construction and characterization of SCUs, and the team of physicists, engineers and support technical staff capable to design and construct state-of-the-art SCUs. Several SCUs, built and successfully operated by this team at the APS, became radiation sources of choice for hard x-ray and coherent scattering programs. These programs will be further enhanced by use of advanced SCUs installed on the upgraded APS storage ring.

APS SCU team continues to explore existing and new superconducting materials for the development of novel SCUs, as well as new magnet geometries to generate and control polarization properties of x-ray radiation.

SCU superior performance and high operational reliability make these devices quite attractive for all types of light sources: storage rings or FELs.

2.1.7 References

1. J. Bahrtdt and E. Gluskin, "Cryogenic permanent magnet and superconducting undulators," *Nucl. Instr. and Methods in Physics, Research A* 907 (2018) 149-168.
2. E. Moog, R. Dejus, S. Sasaki, "Comparison of achievable magnetic fields with superconducting and cryogenic permanent magnet undulators - a comprehensive study of computed and measured values," APS Light Source Note, ANL/APS/LS-348, 2017.
3. Y. Ivanyushenkov *et al.*, "Development and operating experience of a short-period superconducting undulator at the Advanced Photon Source," *Physical Review Accelerators and Beams* 14(4), (April 2015) 040703.
4. Supercon Inc., 830 Boston Turnpike, Shrewsbury, MA 01545, USA.
5. C. L. Doose and M. Kasa, "Magnetic Measurements of the First Superconducting Undulator at the Advanced Photon Source," in *Proc. North American Particle Accelerator Conf. (NAPAC'13)*, Pasadena, CA, USA, Sep.-Oct. 2013, paper THPBA06, pp. 1238-1240.
6. N. Mezentsev, private communication, 2009.
7. N. A. Mezentsev, "Superconducting magnets for SR generation in Budker INP," in *Proc. Russian Particle Accelerator Conference 2006 (RUPAC)*, JINR, Dubna (2006).
8. J. Fuerst, C. Doose, Q. Hasse, Y. Ivanyushenkov, M. Kasa, E. Moog, J. Pfothenauer, D. Potratz, D. Skiadopoulos, V. Syrovatin, and E. Trakhtenberg, "Cryostat design and development for a superconducting undulator for the APS," *AIP Conf. Proc.* 1434 (2012) 901.
9. Y. Ivanyushenkov *et al.*, "Development and operating experience of a 1.1-m-long superconducting undulator at the Advanced Photon Source," *Physical Review Accelerators and Beams* 20(10), (October 2017) 100701.
10. D. F. Alferov, Yu. A. Bashmakov, and E. G. Bessonov, "Generation of circularly polarized electromagnetic radiation," *Soviet physics. Technical physics*, 21(11) (1976) 1408-1411.
11. L. R. Elias and J. M. Madey, "Superconducting helically wound magnet for the free-electron laser," *Review of Scientific Instruments* 50(11), (Nov. 1979) 1335.
12. G. Kezerashvili and P. Voroboyov, "Colliding beams polarization measurements using superconducting helical undulator at the VEPP-2M storage ring," BINP Preprint 91-84, 1991.
13. M. Kasa *et al.*, "Design, construction, and magnetic field measurements of a helical superconducting undulator for the Advanced Photon Source," in *Proc. of IPAC2018*, pp. 1263-1265, Vancouver, Canada (2018).
14. E. Anliker, J. Fuerst, Q. Hasse, Y. Ivanyushenkov, M. Kasa and Y. Shiroyanagi, "A new superconducting undulator cryostat for the APS upgrade," in *Proceedings of CEC-ICMC 2019*, Hartford, Connecticut, USA (2019)

- <https://indico.cern.ch/event/760666/contributions/3390968/>
15. Y. Shiroyanagi, E. Anliker, Q. Hasse, Y. Ivanyushenkov, M. Kasa and J. Fuerst, “Thermal analysis of a superconducting undulator cryostat for the APS upgrade,” in *Proceedings of CEC-ICMC 2019*, Hartford, Connecticut, USA (2019) <https://indico.cern.ch/event/760666/contributions/3390935/>
 16. M. Kasa, E. R. Anliker, Y. Ivanyushenkov, and Y. Shiroyanagi, “New Superconducting Undulator Magnetic Measurement System for the Advanced Photon Source Upgrade,” in *Proc. 10th Int. Particle Accelerator Conf. (IPAC’19)*, Melbourne, Australia, May 2019, pp. 1881-1883.
 17. W. Jansma, J. Fuerst, K. Goetze, and J. Rix, “Precision 2D Laser Scanning: Overview and Applications,” *The Journal of the CMSC* 12(2), (2017) 6-13.
 18. Y. Ivanyushenkov, J. Fuerst, Q. Hasse, M. Kasa, Y. Shiroyanagi, and E. Gluskin, “Conceptual Design of a Novel SCAPE Undulator,” in *Proc. 8th Int. Particle Accelerator Conf. (IPAC’17)*, Copenhagen, Denmark, May 2017, pp. 1596-1598.
 19. D. Haskel, private communication, 2018.
 20. I. Kesgin, private communication, 2019.
 21. I. Kesgin *et al.*, “Development of a Nb₃Sn superconducting undulator for the Advanced Photon Source,” in *Proc. of the International Conference on Magnet Technology (MT26)*, Vancouver, Canada, 2019.
 22. P. Emma *et al.*, “A Plan for the Development of Superconducting Undulator Prototypes for LCLS-II and Future FELs,” in *Proc. 36th Int. Free Electron Laser Conf. (FEL’14)*, Basel, Switzerland, Aug. 2014, paper THA03, pp. 649-653.
 23. M. Kasa, C. L. Doose, J. D. Fuerst, E. Gluskin, and Y. Ivanyushenkov, “Progress on the Magnetic Performance of Planar Superconducting Undulators,” in *Proc. North American Particle Accelerator Conf. (NAPAC’16)*, Chicago, IL, USA, Oct. 2016, pp. 477-479.

2.2 Superconducting Undulator Activities at KIT

Sara Casalbuoni*, Nicole Glamann, Andreas Wolfgang Grau,
Tomas Holubek, David Saez de Jauregui

Mail to: sara.casalbuoni@kit.edu

KIT, Karlsruhe, Germany

Cristian Boffo**, Thomas Gerhard, Melanie Turenne, Wolfgang Walter
Bilfinger Noell GmbH, Würzburg, Germany

2.2.1 Introduction

Superconducting undulators (SCUs) can produce higher photon flux and can cover a wider photon energy range compared to permanent magnet undulators (PMUs) with the same vacuum gap and period length. This potential has been demonstrated with real devices operating with electron beam only in the past few years both at the Advanced Photon Source (APS) at Argonne National Laboratories (ANL) and at the Karlsruhe Institute of Technology (KIT) synchrotron at KIT. A recent comparison between SCUs and cryogenic PMUs (CPMUs), which are the PMUs with highest peak field on axis for the same geometry, showing the superior magnetic performance of SCUs can be found in Ref. [1]. Another advantage of SCUs with respect to PMUs is radiation hardness, widely demonstrated for NbTi magnets, which is and will become an increasingly important issue with the small gaps in the newest machines as round beam diffraction limited storage rings and X-ray FELs.

The progress made in the last years by the collaboration between the Karlsruhe Institute of Technology (KIT) and Bilfinger Noell GmbH (Noell) to develop SCUs for present and future light sources will be presented. The first important milestone of the collaboration was reached in 2015, with the successful test of a full-scale planar SCU with 15 mm period length (SCU15). The lessons learned have now been implemented in a new full-scale SCU with 20 mm period length (SCU20), which has reached series-production readiness.

The design of both SCUs, their installation and operation in the KIT synchrotron light source will be described. Afterwards, the progress achieved by the KIT in house development will be outlined focusing on: i) the instrumentation to characterize the magnetic field properties and to measure the beam heat load to a cold bore needed for the cryogenic design of SCUs, ii) SCUs with period length doubling, iii) and a jointless compact high temperature superconducting (HTS) tape stacked undulator with a novel winding scheme for table top free electron lasers (FELs). At the end possible applications of SCUs in X-ray FELs will be described, and a summary will be presented.

2.2.2 Development of Planar SCUs towards a Commercial Product [2]

The Karlsruhe Institute of Technology (KIT) and the company Bilfinger Noell GmbH (Noell) are developing superconducting undulators (SCUs) for the KIT synchrotron, for low emittance storage rings and FELs. The involvement of the industrial partner from the very beginning permits now the commercialization of SCUs.

As mentioned above, the first SCU developed by the collaboration is SCU15. This was the first full scale SCU reaching a higher peak field on axis with respect to the competing cryogenic permanent magnet technology with the same vacuum gap and

* on leave at European XFEL, Schenefeld, Germany

**now with FNAL, IL, USA

period length, in operation with electron beam [3]. The lessons learned from SCU15 have been implemented in the new SCU20, which is more robust, compact and easier to use [2].

The SCUs developed by the collaboration are based on NbTi wire technology. A big advantage for the users is that the KIT/Noell SCUs are conduction cooled, which means that there is no need of liquid helium or nitrogen to operate or cool them to the operating temperature of about 3-4 K. Both SCU15 and SCU20 have a movable beam vacuum chamber, and can be powered with a fixed vacuum gap of 7 mm. However, when the magnets are not powered, the gap can be opened up to 15 mm, which is required at the electron storage ring KARA (Karlsruhe Research Accelerator) of the KIT synchrotron during electron beam injection. All other existing and planned superconducting insertion devices have beam vacuum chambers with fixed gap, easier to be designed and manufactured. In case of small gap (4-7 mm) insertion devices, accelerator physicists and operators are used to the possibility to open the vacuum chamber, which is typical for in vacuum permanent magnet undulators. This feature is not a ‘MUST’ for low emittance light sources, however it is of great advantage during commissioning and “nice to have” during operation [2].

2.2.2.1 *Layout*

A sketch comparing SCU15 and SCU20 is shown in Fig. 1. The main parameters of SCU15 and SCU20 are listed in Table I. The design has been simplified. The manufacturing process of the different components is more structured and reliable while keeping and even improving the performance. SCU20 is robust, compact and straightforward to use. The main improvements are described below.

The structure and material of the yoke have been modified. Each yoke of the superconducting coils in SCU20 is made by 11 blocks approximately 0.15 m long, instead of 206 plates used in SCU15. The material of the yoke is changed from cobalt-iron, difficult to be procured and machined, to low carbon steel. The NbTi wire used in SCU20 is thicker (0.76 mm insulated diameter) than in SCU15 (0.54 mm x 0.34 mm insulated), so more robust, and it is round offering better electrical insulation [2-4].

While the compensation of the field integrals of SCU15 was performed using storage ring correctors, in SCU20 the vertical field integrals are corrected with Helmholtz coils and auxiliary coils wound with a thin NbTi wire (0.254 mm diameter insulated) on the last grooves of the iron yoke. The horizontal field integrals of SCU20 are compensated with two copper correctors at room temperature located at the entrance and at the exit of the cryostat [2-5].

The beam vacuum chamber, which for both devices needs to vertically open from 7 mm to 15 mm, and it is a critical component of the SCUs has been made more compact and easier to fabricate.

Magnetic length as well as the length of the cryostat is the same for both SCUs. In both undulators a passive quench protection system based on cold diodes is applied to the magnet. Quench detection is included in the main power supply and triggered by a voltage difference of 100 mV within 100 ms across the two coils.

The layout of both SCUs is designed to sustain a beam heat load up to 4 W. Experiments performed with electron beam showed that SCU20 can safely work also with 8 W [5].

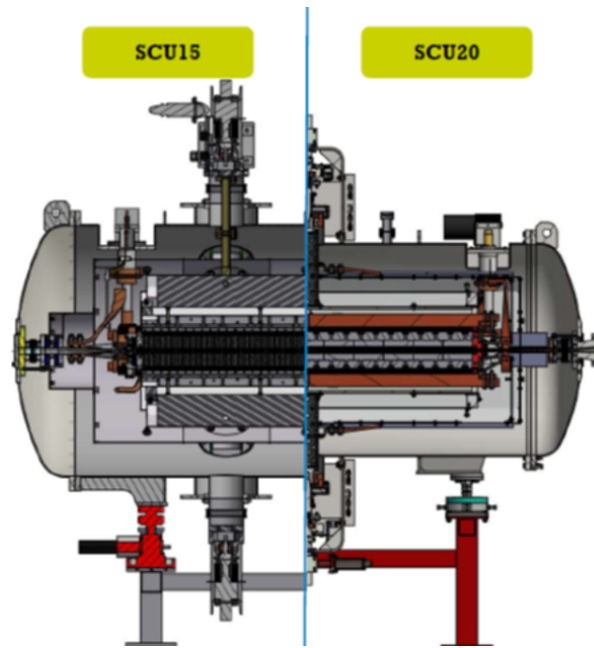


Figure 1: A sketch comparing SCU15 (left) and SCU20 (right).

Table 1: Main parameters of SCU15 and SCU20 [2].

<i>Parameter</i>	<i>Unit</i>	<i>SCU15</i>	<i>SCU20</i>
period length	mm	15	20
maximum peak field on axis	T	0.73	1.18
number of fully wound periods	...	100.5	74.5
magnetic length	m	1.555	1.554
magnetic gap	mm	8	8
vacuum gap closed (open)	mm	7 (15)	7 (15)

2.2.2.2 *Magnetic Measurements*

The KIT IBPT horizontal conduction cooled test facility CASPER II (Characterisation Setup for Field Error Reduction), which had to be developed in house (see section 1.1.3.1.1) was still under development and not ready to measure the coils of SCU15, which have been characterized in a LHe bath in vertical configuration at CERN [6].

Training of the SCU20 coils together with measurements of the magnetic field quality have been performed in CASPER II. As mentioned above, the vertical field integrals have been minimized by adjusting the current in the auxiliary and Helmholtz coils. The measurements of the first field integral at different transverse coordinate x (on the magnetic plane and perpendicular to the magnetic axis) positions have been used to measure the corresponding multipoles, which resulted to be low enough not to change the dynamic aperture of the KIT synchrotron operating at 2.5 GeV. The roll-off was also measured to be sufficiently small not to induce a dynamic kick [4, 5, 7].

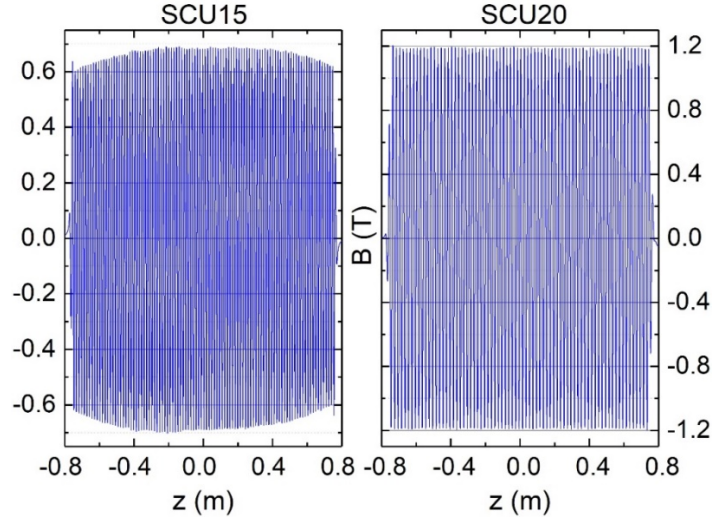


Figure 2: Left. Magnetic field profile along the undulator length of the SCU15 coils measured at a current of 135 A (max. current 150 A) with a Hall probe. The SCU15 coils were measured in a liquid helium bath vertical cryostat at CERN. Afterwards the SCU15 coils were mechanically shimmed to remove the observed bending and improve the field quality [3, 6]. Right. Magnetic field profile of SCU20 coils powered with 395 A (max. current 400 A). SCU20 coils were measured in the KIT IBPT test facility CASPER II in the horizontal orientation [2, 7].

Long range deviations turned out to be a concern for SCU15 coils. After the first cooldown a bending was observed in the magnetic field profile, reflecting a bend at the ends of each coil of about $250\ \mu\text{m}$ away from the gap [3, 6]. The coils were successfully pre-bent (mechanically shimmed) during final assembly. The measured magnetic field profile for SCU15 before pre-bending (mechanical shimming) is shown on the left side of Fig. 2. The SCU20 coils are mounted on a newly developed support structure avoiding long range deviations, thus improving the magnetic field quality. This is demonstrated on the right side of Fig. 2.

The flux produced by the undulator through a slit of $50\ \mu\text{m} \times 50\ \mu\text{m}$ at 10 m from the source is calculated using the measured magnetic field and the KARA storage ring parameters shown in Table 2. Such small pinhole has been used to give a reference in terms of brilliance. In Fig. 3 the flux calculated from the measured SCU20 magnetic field shown on the right plot of Fig. 2 is compared to the one from an ideal SCU20, i.e. without mechanical errors and with perfect end fields. A slight reduction in flux for the odd harmonics (less than 28% up to 30 keV) is observed between the spectra from the ideal and measured SCU20 magnetic fields. This is due to mechanical accuracies and a non-ideal end field configuration in the real undulator. A comparison with an ideal CPMU as the one built at SOLEIL for the same vacuum gap allowed in the KARA storage ring of 7 mm is also made. The SOLEIL CPMU has 18 mm period length (CPMU18), 2 m magnetic length and a peak magnetic field of 0.82 T for 7 mm vacuum gap [8]. Figure 3 shows the better spectral performance of SCU20 with respect to the ideal CPMU18. Figure 3a demonstrates that SCU20 produces up to five times larger flux at high photon energies, while Figure 3b the larger photon energy range reached with SCU20.

Table 2: Parameters at the KARA storage ring [2].

<i>Parameter</i>	<i>Unit</i>	<i>Value</i>
electron beam energy	GeV	2.478
electron beam current	mA	100
energy spread	...	0.001
horizontal emittance	nm rad	41
vertical emittance	nm rad	0.3
β_x	m	19
β_y	m	1.7

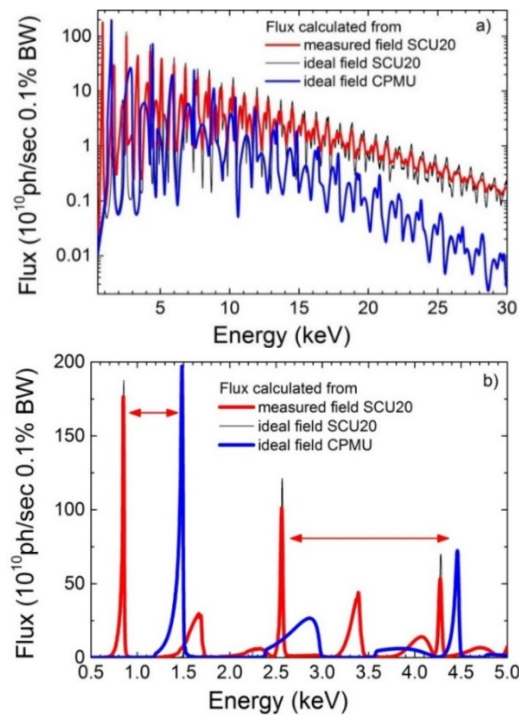


Figure 3: a) Flux through a slit of $50 \mu\text{m} \times 50 \mu\text{m}$ placed at 10 m from the source calculated with B2E for the measured magnetic field of the SCU20 at 395 A (red line), as well as for a SCU20 (black line) and a CPMU18 (blue line) with ideal field profile (without mechanical errors and perfect end fields), with 1.5 m and 2 m magnetic length, respectively. b) Zoom of (a) in the low energy range and with a linear scale: the red arrows indicate the extended energy region available with the SCU20 with respect to the CPMU18 [4]. Reproduced under the terms of the [Creative Commons Attribution 3.0 license](https://creativecommons.org/licenses/by/3.0/).

2.2.2.3 Installation and Operation of SCU15 and SCU20 in the KIT Synchrotron

The assembly procedure of the SCUs foresees alignment, which can be and is performed at room temperature since the devices are designed to keep the magnetic plane in place after cooldown. A laser tracker is used to measure the position of the magnetic axis with respect to four fiducials placed out of the cryostat with a precision of ± 0.1 mm vertically and ± 0.2 mm horizontally, as well to align the cryostat in the storage ring with a precision of ± 0.15 mm vertically and horizontally [3].

The installation required the venting of a 5 m long straight section (on a ring of 110.4 m circumference). The beam lifetime was recovered in about five weeks of beam operation of the storage ring at 2.5 GeV for SCU15, and in only about three for SCU20 [5].

The cooldown and warmup times are kept below one week. This allows installation in practicable times compatible with shutdowns of the order of three-four weeks. Since SCU20 is more compact and it has a smaller mass, its cooldown time is improved from the seven days needed for SCU15 to five days. Warmups have been performed in about four days for both SCUs [2, 3]. However, if needed, it would be possible to shorten this time for SCU20 by about one day.

After cooldown the coils are ramped to reach the maximum operating current. In general, since they have a memory effect, few quenches are needed to reach the maximum operating current and no complete new training is needed. While SCU15 had a couple of quenches, SCU20 reached 400 A (maximum operating current) after the first ramp, so no training was needed [5]. A quench was observed few minutes after that the coils reached the 400 A for the first time. For both SCUs the coils recover the operating temperature after about 15 minutes from the quench, which allows to power them again.

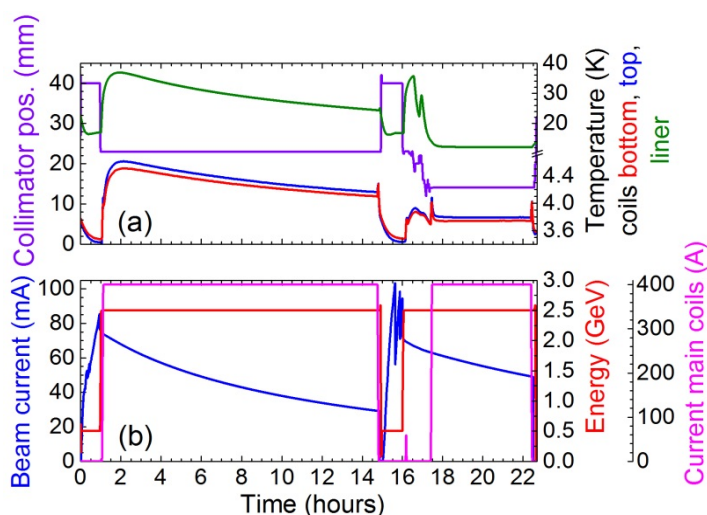


Figure 4: (a) Position of the horizontal collimator (violet line) and the temperature of the top (blue line) and bottom (red line) coils as well as of the liner (green line) as a function of time. (b) Beam current (blue line), beam energy (red line), and current in the main coils (magenta line) of the SCU20 as a function of time [5]. Reproduced under the terms of the [Creative Commons Attribution 3.0 license](https://creativecommons.org/licenses/by/3.0/).

SCU15 was successfully tested for one year with electron beam. No quench occurred while operating with electron beam at 2.5 GeV (normal operation mode). Two quenches took place with electron beam energy of 1.3 GeV while trying to reach the so-called low-alpha operation mode, due to poor orbit control [3]. SCU20 was installed during the winter shutdown in December 2018. It is operating with beam in the KIT synchrotron since January 2018 without quenches [2, 5].

The reliability of both SCUs is due to the robust design, manufacturing and assembly based on the excellent thermal decoupling between the liner and the coils, separated by only 0.2 mm along a length of 1.5 m. This result has been reached despite the aggressive approach of minimizing the difference between the magnetic gap and vacuum gap by 1 mm and has allowed SCU15 to be the first full scale length SCU reaching a higher peak

field on axis than a CPMU for the same geometry [3]. Figure 4 demonstrates that SCU20 could be operated with a beam heat load of 8 W, which is twice the nominal one. A horizontal collimator installed upstream with respect to SCU20 with the function to screen the synchrotron radiation from the upstream bending magnet was moved to allow 8 W of beam heat load. While the temperature of the liner increases from about 11 K to 35 K, the one of the coils grows from 3.8 K to about 4.6 K, and the coils stably operate at maximum current.

Installation of SCUs is straightforward, as it is their commissioning. The first X-rays produced by SCU20 have been observed at the NANO beamline just after three days of machine operation.

SCU15 could be operated using vertical correctors out of the cryostat. SCU20 is transparent to the electron beam with values of correctors very close to the ones measured in CASPER II. This gives confidence in the CASPER II measuring system and in the assembly procedure followed. Adjustment of the currents in the vertical and horizontal correctors was performed in few hours. Experiments involving all beamlines have been performed showing that the tuning of SCU20 is compatible with the operation of all the beamlines of the KIT synchrotron while performing their most sensitive experiments [5].

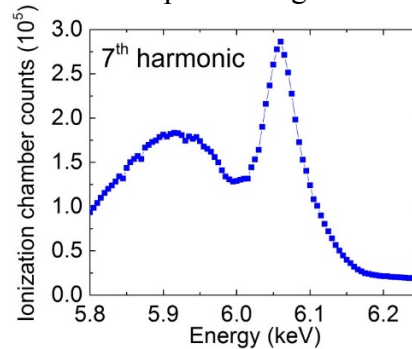


Figure 5: Seventh harmonic of SCU20 measured at the NANO beamline through $0.1 \mu\text{rad} \times 3 \mu\text{rad}$ with an ionization chamber (gain 9) at 2.5 GeV electron beam energy. The values are normalized to 100 mA electron beam current [5].

The spectral performance of SCU15 was thoroughly characterized at the IMAGE beamline and it is described in detail in Ref. [3]. An accurate spectral characterization of SCU20 is ongoing at the NANO beamline. Preliminary measurements of the photon spectrum, reported in Fig. 5, show from the position of the 7th harmonic that the peak field on axis of 1.18 T is in very good agreement with the one measured in the KIT test facility CASPER II described in the next section [5].

2.2.3 In House Developments

2.2.3.1 Measurement Systems

2.2.3.1.1 CASPER II

A good field quality of the undulators is necessary to maximize their spectral response. To this end, mechanical accuracies of about $50 \mu\text{m}$ for the pole and winding heights and of about $10 \mu\text{m}$ for the period length of the SCU coils are needed to be reached at room temperature and to be kept down to 4 K for lengths of the order of 2 m.

A precise measuring system is needed to qualify the magnetic field. A unique instrument has been developed at KIT IBPT named CASPER II (Characterisation setup for Field Error Reduction). CASPER II, shown in Fig. 6, is described in several publications [9-11]. CASPER II is a horizontal test stand to characterize conduction cooled undulator coils up to about 2 m long. The cryostat has a shell structure, used to facilitate the exchange of the coils to be measured.

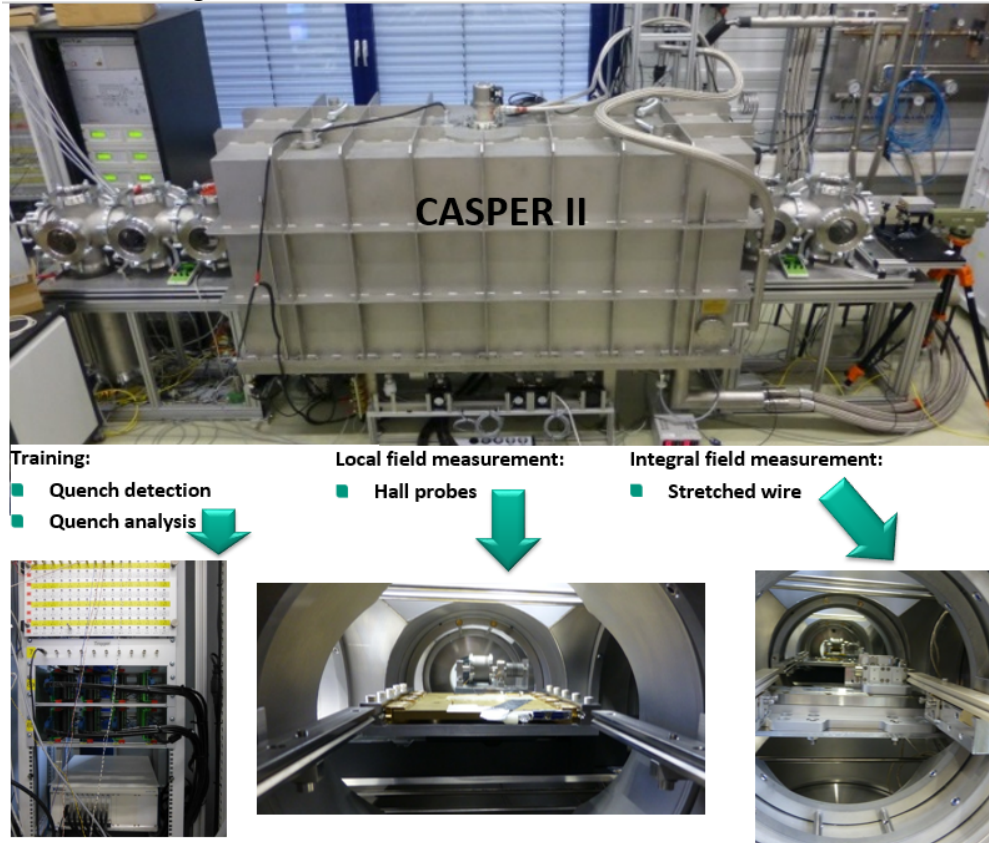


Figure 6: CASPER II test facility to characterize conduction cooled superconducting undulator coil in horizontal configuration.

The coils are in a configuration very similar to the one in which they are in the final cryostat. They are trained using an in house designed quench detection system (built by the Institute for Data Processing and Electronics at the KIT) and a fast data acquisition system from National Instruments [11]. The local field measurements are performed using calibrated Hall probes located on a sledge moving along the undulator axis on precisely machined guiding rails. The sledge temperature ranges from 15 K–45 K [7]. The Hall probes have been calibrated at the Institute of Technical Physics at KIT between 4 K–77 K and -2 T and 2 T. The accuracy of the calibration is in the operating conditions ± 90 μ T [7, 12]. The longitudinal position of the Hall probe is measured with sub- μ m resolution by means of a laser interferometer (from SIOS). The roll-off is obtained by horizontally shifting one Hall probe and measuring the longitudinal magnetic field profile at different horizontal positions. The field integrals and multipoles are measured using the stretched wire system. The spatial resolution is ± 0.5 mm. The repeatability of the first and second field integrals is measured to be within $\pm 3.5 \times 10^{-6}$ T m and $\pm 1.0 \times 10^{-5}$ T m² [11]. Local and integral field measurements can be performed during the same cool down.

With the aim of characterizing the SCU coils in the final cryostat the lessons learned with CASPER II will be implemented in a new system shown in Fig. 7.

Within the same cooldown, three different measuring techniques are planned to be applied: local field mapping with a Hall sensor, the moving stretched wire and pulsed wire technique [13].

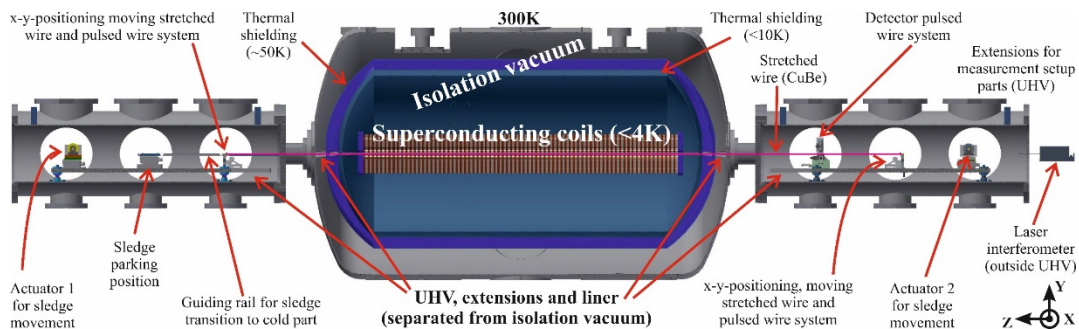


Figure 7: Sketch of the planned measurement system for SCU coils in the final cryostat [13].

2.2.3.1.2 COLDDIAG

The beam heat load is needed as input parameter for the cryogenic design of superconducting insertion devices. Since the heating of the superconducting coils due to beam was a limiting performance issue for earlier developments, a cold vacuum chamber for diagnostics (COLDDIAG) has been developed to measure the beam heat load to a cold vacuum chamber in different light sources and has been manufactured by Noell.

The results of the measurements performed with COLDDIAG at the Diamond Light Source (DLS), together with impedance bench measurements performed at KIT open onto solutions applied to the design of the new devices; in particular, the tapering of the vacuum chamber have been moved from the cold regions to the ones between the thermal shield and room temperature [14, 15]. Moreover, the measurements performed with electron beam demonstrate that the electron beam heat load can be handled [15].

COLDDIAG consists of two warm and one cold section (see Fig. 8). All sections are equipped with the same diagnostics: temperature sensors and heaters to measure the beam heat load, pressure gauges to measure the pressure, mass spectrometers to determine the gas content, and retarding field analyzers to measure charged particles hitting the wall.

With such retarding field analyzer, it was possible for the first time to precisely measure [14] the energy spectrum of photo-desorbed electrons hitting the cold chamber. A similar device as COLDEX [16], built to validate the Large Hadron Collider (LHC) vacuum system, has electrodes, sensitive to the amount of charged particles impinging on the wall but unable to measure their energy.

Together with the determination of the beam heat load such diagnostics allows to investigate the contribution of different beam heating mechanism as synchrotron radiation, impedance, and bombardment of low energy charged particles onto the vacuum chamber surface.

The possibility to use COLDDIAG for studies of interaction of electron and positron beams with a cold surface at DAFNE [17], of interest for a future circular collider, is under consideration.



Figure 8: COLDDIAG installed in the Diamond Light Source.

2.2.3.2 *Period Length Doubling*

Non in-vacuum permanent magnet undulators with switchable period length called revolvers, in which different magnetic structures are rotated [18] are applied in different synchrotron light sources with the goal of putting at disposal of the users a broader energy spectrum of the emitted photons.

Superconducting undulator technology allows a cheaper and more compact solution using the same magnetic structure to switch the period length. This is obtained by changing the current direction in one of the separately powered subset of winding packages of the superconducting coils (see Fig. 9) [19].

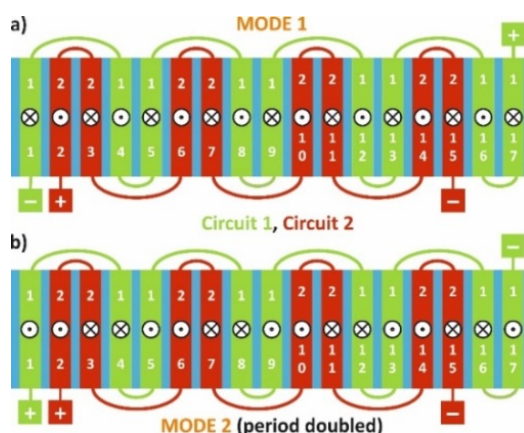


Figure 9: Scheme of period length doubling for a superconducting undulator coil by changing the current direction in one subset of windings. a) The circuits are powered to have the smallest period. b) The current direction of circuit 1 is changed to obtain period doubling [19]. Reproduced under the terms of the [Creative Commons Attribution 3.0 license](https://creativecommons.org/licenses/by/3.0/).

Undulator coils with switchable doubling of the period length from 17 mm (SCU17) to 34 mm (SCU34) to operate at a magnetic gap of 6 mm (vacuum gap 5 mm) and 0.41 m long, shown in Fig. 10 have been designed, manufactured and successfully tested in liquid helium [20].

A superconducting undulator with such coils allows to reach full tunability with SCU17 and high brilliance in the soft X-ray regime with the 1st harmonic of SCU34 to measure some or all M-absorption edges of metals like V, Cr, Mn and Fe, going as low as few tens of eV in a low emittance light source with 3 GeV electron beam energy.

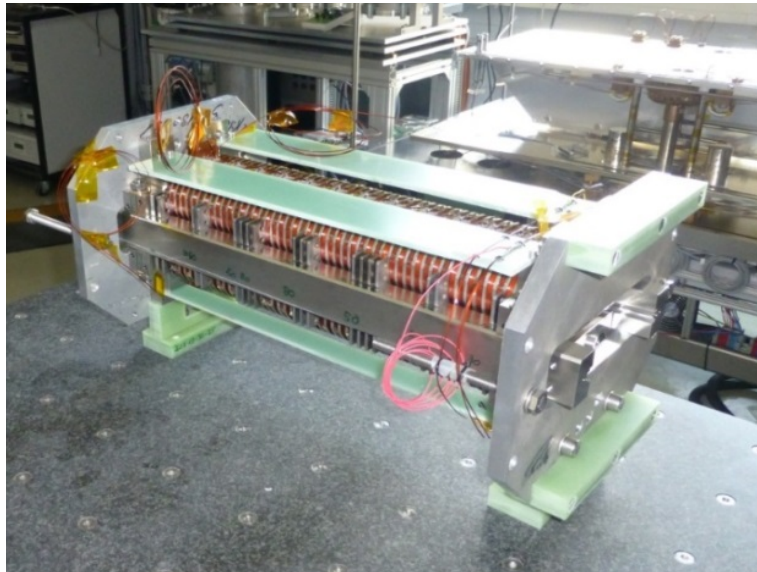


Figure 10. Superconducting undulator coils with switchable period length (between 17 and 34 mm) and a magnetic length of 0.41 m [20]. Reproduced under the terms of the [Creative Commons Attribution 3.0 license](https://creativecommons.org/licenses/by/3.0/).

2.2.3.3 *Jointless High Temperature Superconducting Tape Stacked Undulator*

Promising for future applications to SCU technology are HTS tapes. Their engineering current density is rapidly increasing and they can sustain higher heat loads than NbTi. Another advantage of HTS tapes with respect to other materials with higher critical current than NbTi as Nb₃Sn, is that they do not need any heat treatment, which endangers the goal of reaching high mechanical accuracies, necessary for undulator applications. It is possible to just substitute the HTS to NbTi in the usual planar undulator configuration similar to the one of SCU15 and SCU20. The other possibility is the one proposed by the group in LBNL to stack structured HTS tapes [21]. The proposal was to structure the tapes with lithography. At KIT the HTS tape is structured with a picosecond YAG laser and a novel winding scheme to avoid joints between the tapes has been proposed and implemented in a prototype [22], shown in Fig. 11. This configuration is particularly suitable for short period lengths < 10 mm and narrow magnetic gaps < 4 mm, favoring it among other competitive technologies to be used for FELs. The first magnetic field measurements on 30 stacked HTS structured tapes, measured in a LHe bath are shown in Fig. 12.

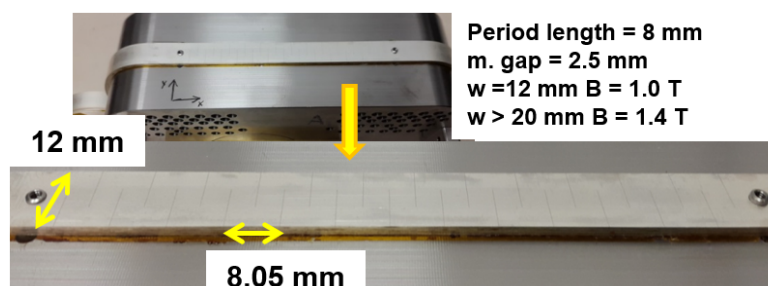


Figure 11: Prototype of a jointless high temperature superconducting tape stacked undulator coil with 30 HTS tapes with a width $w = 12$ mm. Top right: the achievable values of the peak field on axis with a magnetic gap of 2.5 mm, a period of 8 mm and widths of the tape of 12 and >20 mm.

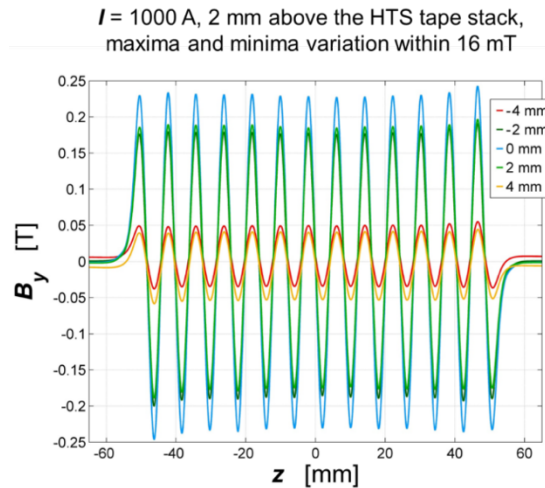


Figure 12. First magnetic field measurements of the prototype shown in Fig. 9 at 2 mm from the HTS tape stack with a current of 1000 A measured in a LHe bath.

Several issues need to be solved mainly from the HTS tape producer before this concept can be scaled up to build full scale undulators reliably operating with beam [22, 23]. However for table top FELs the technical solution might not be too far in the future.

2.2.4 Possible Future Applications of SCUs to Xray-FELs

SCU technology could be used to increase the energy range now available for the XFEL users. The possibility of a future very hard X-ray SASE line [24] as well as for the THz-SCU [25] for the European XFEL have been studied.

A SASE line, at the European XFEL operating with an electron beam energy of 17.5 GeV, filled with short period SCUs (15 mm -20 mm) can increase the photon spectrum up to about 100 keV. The high X-ray photon energies in combination with XFEL properties such as ultra-short pulse duration and, intense pulses arriving at MHz rates will open up new possibilities into research of dense matter. For example, this would allow MHz rate X-ray microscopy able to reveal bulk dynamics in materials such as crack propagation or shockwave propagation previously possible to be observed only ex-situ. A possible upgrade of the linac of the European XFEL to CW (continuous wave) with a corresponding reduction of electron beam energy down to 7.8 GeV is under consideration. In this case such SCU SASE line covers up to 25 keV, as now done with existing SASE1/2 lines with permanent magnet undulators with 40 mm period length. Moreover, including period length doubling in the SCU SASE line, for example with 18 mm and 36 mm, permits to further increase the available photon energies to range from about 2 to 90 keV [24].

Superconducting technology has also been proposed to generate superradiant undulator radiation after a SASE line to provide THz pulses in a frequency range between 3 and 30 THz with exceptional THz pulse energies. The ultrahigh brightness and the

ultrashort duration of the pulses generated at the European XFEL can be exploited in a "pump-probe" configuration, to probe non-equilibrium states of a matter sample that can be excited by previous interaction with THz radiation. This would be possible at European XFEL with a NbTi based SCU with a period length of about 1 m [25].

2.2.5 Summary

The collaboration between KIT and its industrial partner Noell developed in the last years cryogen free NbTi based planar undulators, which are now commercially available and the developed technology can be applied to next generation light sources, too.

A substantial effort sustaining this activity has been done at KIT developing CASPER II, a unique and precise magnetic measurement system to characterize the magnetic field of conduction cooled superconducting undulator coils, as well as COLDDIAG to study the beam heat load to a cold vacuum chamber.

KIT has conducted in house research to further apply superconducting undulator technology to the next generation light sources, focusing on period length switching of interest in particular for European XFEL, and on a jointless HTS structured tape undulator competitive for compact light sources with respect to existing technologies.

2.2.6 References

1. J. Bahrtdt and E. Gluskin, "Cryogenic permanent magnet and superconducting undulators," *Nucl. Instrum. Methods Phys. Res. A*, **907** 149-168 (2018).
2. S. Casalbuoni, N. Glamann, A. Grau, T. Holubek, D. Saez de Jauregui, S. Bauer, C. Boffo, T. Gerhard, M. Turenne, and W. Walter, "Superconducting Undulators: From Development towards a Commercial Product," *Synchrotron Radiat. News*, **31**(3) 24-28 (2018)
<https://www.tandfonline.com/doi/full/10.1080/08940886.2018.1460171>
3. S. Casalbuoni, A. Cecilia, S. Gerstl, N. Glamann, A. Grau, T. Holubek, C. Meuter, D. Saez de Jauregui, R. Voutta, C. Boffo, Th. Gerhard, M. Turenne, and W. Walter, "Characterization and long term operation of a novel superconducting undulator with 15 mm period length in a synchrotron light source," *Phys. Rev. ST Accel. Beams*, **19** 110702 (2016)
<https://doi.org/10.1103/PhysRevAccelBeams.19.110702>
4. S. Casalbuoni, N. Glamann, A. Grau, T. Holubek, D. Saez de Jauregui, C. Boffo, Th. Gerhard, M. Turenne, and W. Walter, "Field quality of 1.5 m long conduction cooled superconducting undulator," *IOP Conf. Series: Journal of Physics: Conf. Series*. **874** 012015 (2017) <https://doi.org/10.1088/1742-6596/874/1/012015>
5. S. Casalbuoni, E. Blomley, N. Glamann, A. Grau, T. Holubek, E. Huttel, D. Saez de Jauregui, S. Bauer, C. Boffo, Th. Gerhard, M. Turenne, and W. Walter, "Commissioning of a full scale superconducting undulator with 20 mm period length at the storage ring KARA," *AIP Conf. Proc.* **2054** 030025 (2019)
<https://doi.org/10.1063/1.5084588>
6. S. Casalbuoni, T. Baumbach, S. Gerstl, A. Grau, M. Hagelstein, D. Saez de Jauregui, C. Boffo, J. Steinmann and W. Walter, "Training and Magnetic Field Measurements of the ANKA Superconducting Undulator," *IEEE Trans. Appl. Supercond.* **21**(3) 1760-1763 (2011) DOI: 10.1109/TASC.2010.2085070
7. S. Casalbuoni, N. Glamann, A. Grau, T. Holubek, D. Saez de Jauregui, C. Boffo,

- Th. Gerhard, M. Turenne and W. Walter, "Magnetic Field Measurements of Full-Scale Conduction-Cooled Superconducting-Undulator-Coils," *IEEE Trans. Appl. Supercond.* **26**(3) 4100704 (2018) DOI: 10.1109/TASC.2018.2791953
8. C. Benabderrahmane, M. Valléau, A. Ghaith, P. Berteaud, L. Chapuis, F. Marteau, F. Briquez, O. Marcouillé, J.-L. Marlats, K. Tavakoli, A. Mary, D. Zerbib, A. Lestrade, M. Louvet, P. Brunelle, K. Medjoubi, C. Herbeaux, N. Béchu, P. Rommeluere, A. Somogyi, O. Chubar, C. Kitegi, and M.-E. Couprie, "Development and operation of a Pr₂Fe₁₄B based cryogenic permanent magnet undulator for a high spatial resolution x-ray beam line," *Phys. Rev. Accel. Beams* **20** 033201 (2017).
 9. A. Grau, T. Baumbach, S. Casalbuoni, S. Gerstl, M. Hagelstein, T. Holubek and D. Saez de Jauregui, "Cryogen-free setup for local and integral field magnetic field measurements of superconducting undulator coils," *IEEE Trans. Appl. Supercond.* **22** 9001504 (2012).
 10. S. Gerstl, S. Casalbuoni, A. Grau, N. Glamann, T. Holubek, D. Saez de Jauregui, R. Voutta, C. Boffo, Th. Gerhard, M. Turenne and W. Walter, "First characterization of a superconducting undulator mock-up with the CASPER II magnetic measurement system," in *Proc. 6th International Particle Accelerator Conf.*, Richmond, VA, USA (2015) 2815-7 (2015).
 11. A. Grau, S. Casalbuoni, S. Gerstl, N. Glamann, T. Holubek, D. Saez de Jauregui, R. Voutta, C. Boffo, Th. Gerhard, M. Turenne and W. Walter, "Characterization of 30-cm-long superconducting undulator coils with the magnetic measurement system CASPER II," *IEEE Trans. Appl. Supercond.* **26** 4100804 (2016).
 12. S. Casalbuoni, "A review of magnetic field measurements of full scale conduction cooled superconducting undulator coils," *Supercond. Sci. Technol.* **32** 023001 (2019).
 13. A. W. Grau, S. Casalbuoni, N. Glamann, and D. Saez de Jauregui, "Cryogenic, in-Vacuum Magnetic Measurement Setup for Superconducting Undulators," in *Proc. 10th Int. Particle Accelerator Conf. (IPAC'19)*, Melbourne, Australia, 1709-1712 (2019).
 14. S. Gerstl, R. Voutta, S. Casalbuoni, A. W. Grau, T. Holubek, D. Saez de Jauregui, R. Bartolini, M. P. Cox, E. C. Longhi, G. Rehm, J. C. Schouten, R. P. Walker, G. Sikler, M. Migliorati, and B. Spataro, "Cold vacuum chamber for diagnostics: Instrumentation and first results," *Phys. Rev. ST Accel. Beams* **17** 103201 (2014). DOI:10.1103/PhysRevSTAB.17.103201
 15. R. Voutta, S. Gerstl, S. Casalbuoni, A. W. Grau, T. Holubek, D. Saez de Jauregui, R. Bartolini, M. P. Cox, E. C. Longhi, G. Rehm, J. C. Schouten, R. P. Walker, M. Migliorati, and B. Spataro, "Cold vacuum chamber for diagnostics: Analysis of the measurements at the Diamond Light Source and impedance bench measurements," *Phys. Rev. ST Accel. Beams* **19** 053201 (2016). DOI: <https://doi.org/10.1103/PhysRevAccelBeams.19.053201>
 16. V. Baglin, I. R. Collins, and B. Jenninger, "Performance of a cryogenic vacuum system (COLDEX) with an LHC type beam," *Vacuum* **73** 201 (2004).
 17. S. Casalbuoni, "Using DAFNE to study the physics of e⁺/e⁻ beam interaction with vacuum devices," *DAFNE-TF Workshop*, Frascati, 17 December 2018. https://agenda.infn.it/event/16334/attachments/23692/26956/Casalbuoni_DAFNE-TF_2018.pdf

18. T. Hara, T. Tanaka, T. Seike, T. Bizen, X. Maréchal, A. Nisawa, S. Fukushima, Yoshikawa, H. Kitamura, “Revolver undulator for BL15XU at SPring8,” *Nucl. Instr. Meth. A* **161** 467-468 (2001).
19. T. Holubek, S. Casalbuoni, N. Glamann, S. Gerstl, C. A. Meuter, D. Saez de Jauregui, “Design and Tests of Switchable Period Length Superconducting Undulator Coils,” in *Proc. 9th Int. Particle Accelerator Conf. (IPAC'18)*, Vancouver, BC, Canada, 4226-4228 (2018). doi:10.18429/JACoW-IPAC2018-THPMF067
20. S. Casalbuoni, N. Glamann, A. W. Grau, T. Holubek, D. Saez de Jauregui, “Superconducting Undulator Coils with Period Length Doubling,” *J. Phys.: Conf. Ser.* **1350** 012024 (2019).
21. S. Prestemon, D. Dietderich, A. Madur, S. Marks, R.D. Schlueter, “High performance short-period undulators using high temperature superconductor tapes,” in *Proc. PAC'09*, Vancouver, BC, Canada, WE5RFP075 (2009).
22. T. Holubek, S. Casalbuoni, S. Gerstl, N. Glamann, A. Grau, C. Meuter, D. Saez de Jauregui, R. Nast and W. Goldacker, “A novel concept of high temperature superconducting undulator,” *Supercond. Sci. Technol.* **30** 115002 (2017). DOI: <https://doi.org/10.1088/1361-6668/aa87f1>
23. S. Casalbuoni, “High temperature superconducting tapes for undulator technology,” *Supercond. Sci. Technol.* **30** 070501 (2017). DOI: <https://doi.org/10.1088/1361-6668/aa6f63>
24. S. Serkez, G. Geloni, S. Karabekyan, Y. Li, T. Tanikawa, S. Tomin, F. Wolff-Fabris, S. Casalbuoni, C. Boffo, M. Dohlus, E. Schneidmiller, M. Yurkov, I. Zagorodnov, A. Trebushinin, “Super-X: Simulations for Extremely Hard X-ray Generation with Short Period Superconducting Undulators for the European XFEL,” in *Proc. FEL2019*, Hamburg, Germany, TUP061 (2019).
25. T. Tanikawa, S. Karabekyan, S. Kovalev, S. Casalbuoni, V. Asgekar, S. Serkez, G. Geloni and M. Gensch, “A superradiant THz undulator source for XFELs,” *J. Inst.* **14** P05024 (2019). DOI: <https://doi.org/10.1088/1748-0221/14/05/P05024>

2.3 Cryostats and Cryogenic Systems for SCUs

Joel Fuerst
SLAC National Accelerator Laboratory
Mail to: fuerst@slac.stanford.edu

2.3.1 Introduction

The superconducting magnets of an SCU must operate at a temperature below the conductor's critical temperature given the surrounding magnetic field. Other SCU subsystems like current leads, thermal radiation shields, and particle beam vacuum chambers also operate at different temperature levels and require active cooling. The SCU therefore requires a cryogenic system comprised of two main elements: a multi-level cooling system to reach and maintain operating temperature and a containment system (the cryostat) to reduce heat transfer from the ambient.

The design of both the cooling system and cryostat depend on the magnitude and characteristics of the heat load. "Dynamic" loads arise from SCU operation (for magnets and current leads) as well as from particle beam operation (for the beam vacuum chamber). "Static" loads are caused by heat transport from the ambient and are present whenever the device is at operating temperature. Cryostat design represents an optimization exercise where the combined static and dynamic heat loads together with their relative contributions affect the complexity and cost of the cryostat.

Cooling system design depends not only on the cryostat itself but also the number of SCUs in the system and their proximity to each other. For a few SCUs spread among the insertion device locations of a storage-ring light source, independent cryocooler-based cooling systems are an appropriate choice. On the other hand, a contiguous array of SCUs in a free electron laser (FEL) source may implement a centralized cryoplant supporting the SCUs via a cryogenic distribution system.

2.3.2 Cryostat Design - APS First Generation

Cryogenic devices such as SCUs are housed in a cryostat capable of maintaining the necessary operating environment. The cryostat supports the device mechanically and provides the interface between the device and the cooling system, support and alignment system, electrical systems, and other subsystems. The first SCU at the APS resulted from a collaboration with the Budker Institute of Nuclear Physics (BINP) following their successful designs [1]. It consists of an outer vacuum vessel (eliminating convection heat transfer) containing two levels of copper thermal radiation shielding (minimizing radiation heat transfer) which surround the cold mass (magnet and supporting liquid helium (LHe) reservoir). Conduction heat transfer is minimized by careful design of the mechanical supports between the vacuum vessel, shields, and cold mass. Support design typically includes low-conductivity material, optimized lengths vs. cross-sections, and intermediate heat stationing – the use of intermediate thermal shields to intercept the heat conducting from room temperature to the cold mass. Figure 1 shows a representation of the design while Figure 2 shows the device installed in the APS storage ring.

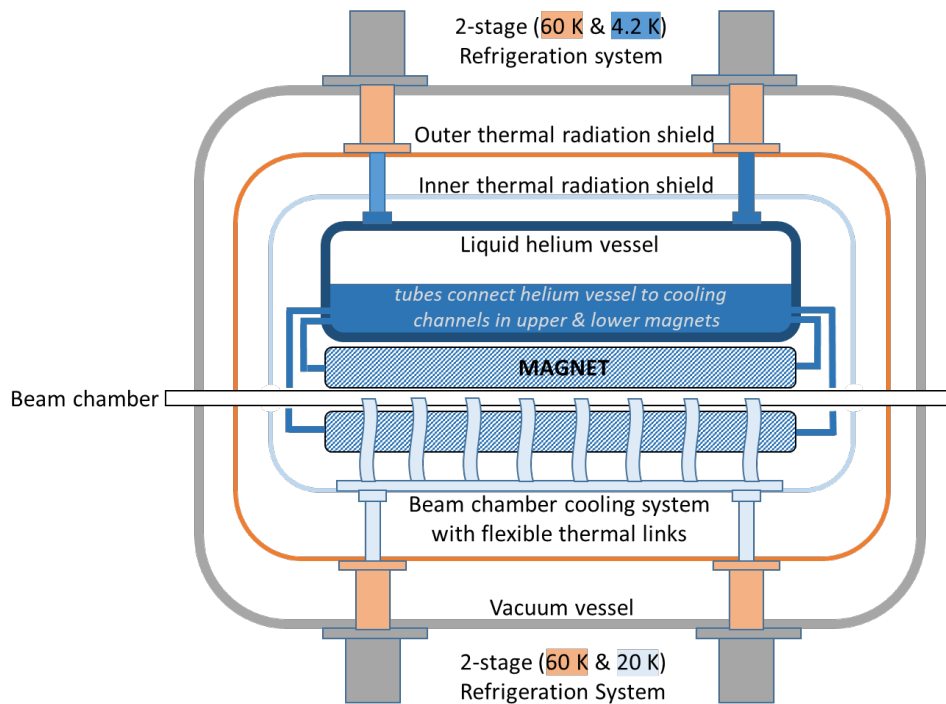


Figure 1: Graphical representation of the first-generation APS SCU cryostat. Tubing connects the cooling channels in the magnets with the LHe reservoir.

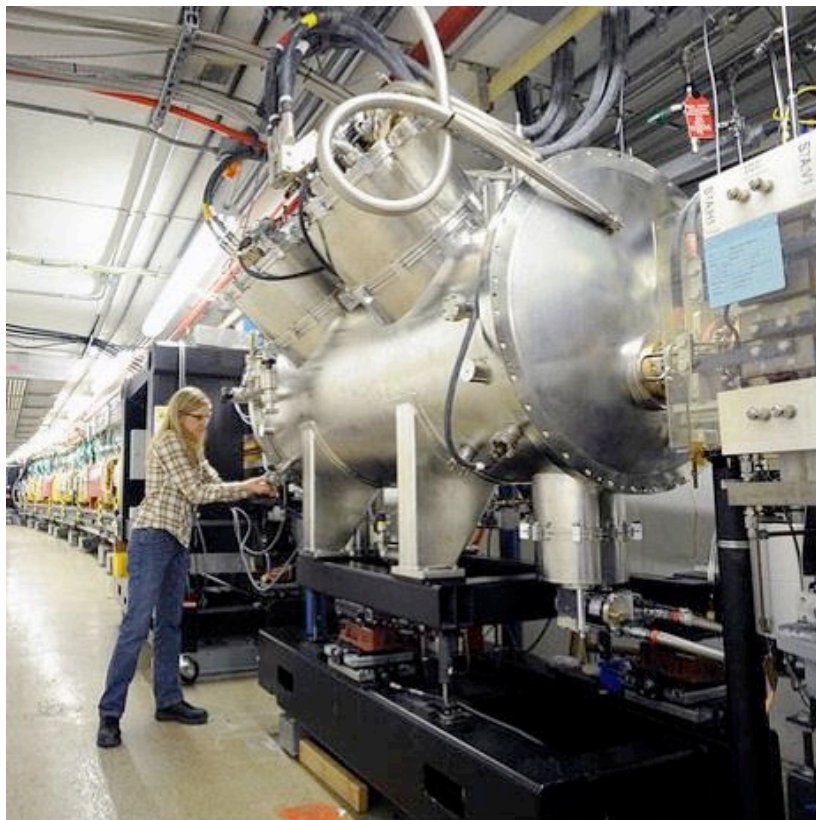


Figure 2: The first SCU installed in Sector 6 of the APS storage ring.

The cryostat couples the LHe reservoir to the magnets via tubes connecting to the liquid helium cooling channels in the magnets. The reservoir is connected to the cryocooler-based cooling system by flexible thermal links. The measured heat loads for this cryostat design are presented in Table 1 for various combinations of magnet current and storage ring electron beam heating. In all cases the heat load is less than the installed cooling power resulting in “zero boil-off” operation. In this condition the cryostat does not need to be replenished with LHe because the cooling system is able to re-condense all of the vapor generated by the combined static and dynamic heat loads. In the event of a cooling system failure the system can continue to operate. However in the absence of LHe re-condensation the cryostat would vent helium vapor, necessitating periodic LHe transfers from a portable storage dewar. So far this operating mode has not occurred due to the reliability of the system. Two SCUs of this design are currently in operation at the APS [2, 3].

Table 1: Measured heat loads for various SCU operating conditions.

Magnet Status, Beam Chamber Heat Load	4.3 K [W]	Inner Shield [W] at 10 K	Outer Shield [W] at 34 K
0 A, 0 W on beam chamber	0.61	1.46	60.2
500 A, 0 W on beam chamber	0.61	<12.5	63.2
500 A, 10 W on beam chamber	0.61	<12.5	80.9
500 A, 20 W on beam chamber	0.61	21.3	87.4

2.3.3 Second-Generation APS Cryostat

To meet the need for a more compact design, a second-generation cryostat was developed which included in addition to a smaller overall diameter a number of changes resulting from a value-engineering process [4]. This resulted in reduced cost and an overall increase in excess refrigeration power from the cooling system. The new design is represented in Figures 3 and 4 while Figure 5 shows the device installed in the APS storage ring. Major changes included elimination of the 20 K thermal shield and an optimized cryocooler arrangement.

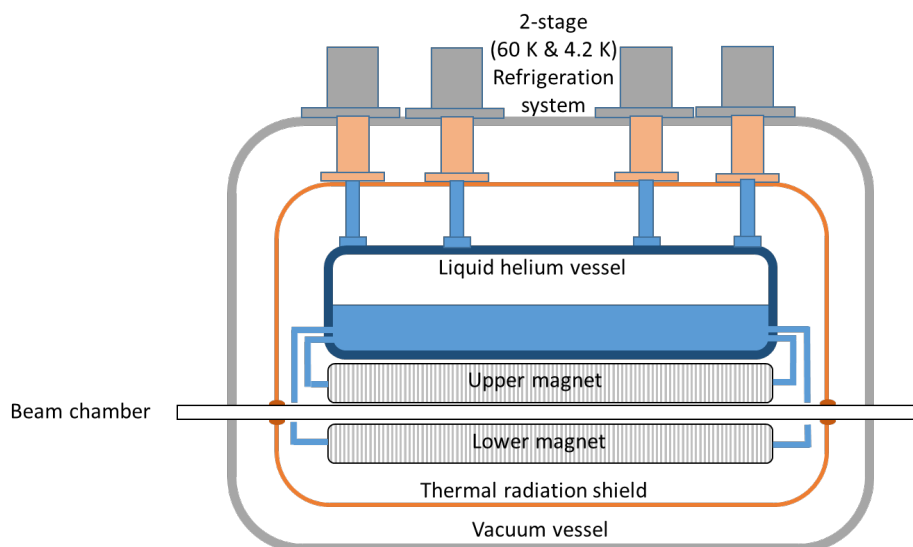


Figure 3: Graphical representation of the second-generation APS SCU cryostat and cooling system.

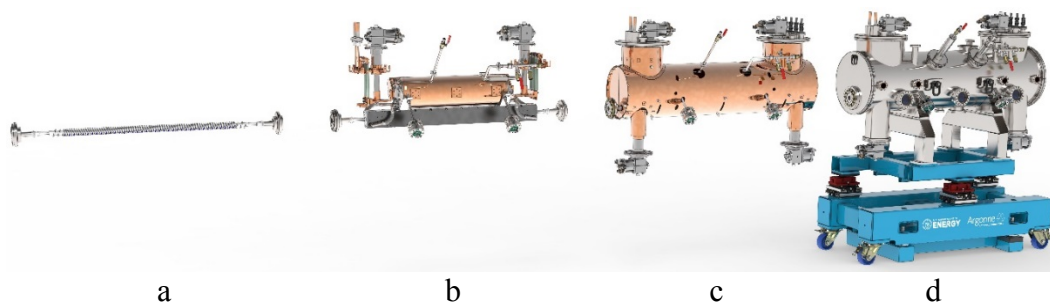


Figure 4: Exploded view of the second-generation cryostat showing beam vacuum chamber (a), cold mass (b), thermal shield (c), and complete assembly (d).



Figure 5: The second-generation SCU installed in Sector 7 of the APS storage ring.

The complete cryostat assembly including all subsystems was modeled in PTC Creo Parametric 3.0 over a six-month period. All part features were represented sufficient to describe the design. For the main cryostat components (vacuum vessel, thermal shield, and LHe reservoir) a specification document was generated to provide additional information establishing global tolerances, finishes, production techniques, and inspection/test requirements including leak checks. This document together with the CAD data for the main components (in .stp file format) constituted a procurement package which was competitively bid and awarded in the fall of 2016. The award contract included as a deliverable the creation of detail drawing packages for each component. Drawings were submitted, iterated upon, and approved prior to fabrication start.

Other subsystem components including cryocooler/current lead turrets, support & alignment systems, magnets, and beam vacuum chamber were detailed in-house and procured as build-to-print contracts in parallel with the main component contract. Value engineering of many cryostat subsystems resulted in reduced complexity and cost compared to the original design. The cryostat was ready for cold testing without the

magnet by late February 2017. Figure 6 shows pictures of selected subsystem component assemblies.



Figure 6: (left) comparison of original SCU vacuum vessel with smaller 2nd-generation vessel; (right) detail of corrector magnet current lead assembly.

The assembled cryostat (without magnet) was put through a series of engineering runs involving multiple thermal cycles between March and June 2017 to evaluate cryogenic performance and implement necessary corrections. This substantial commissioning/test window was made possible by the timely delivery and acceptance of the cryostat components and took place while magnet development, fabrication and testing were underway.

Early tests established a cool-down time of about thirty hours compared to seventy hours required for the original design. The shorter cool-down time is primarily due to improved contact between the refrigeration system and the cold mass. Figure 7 shows the cool-down curve for the second-generation design.

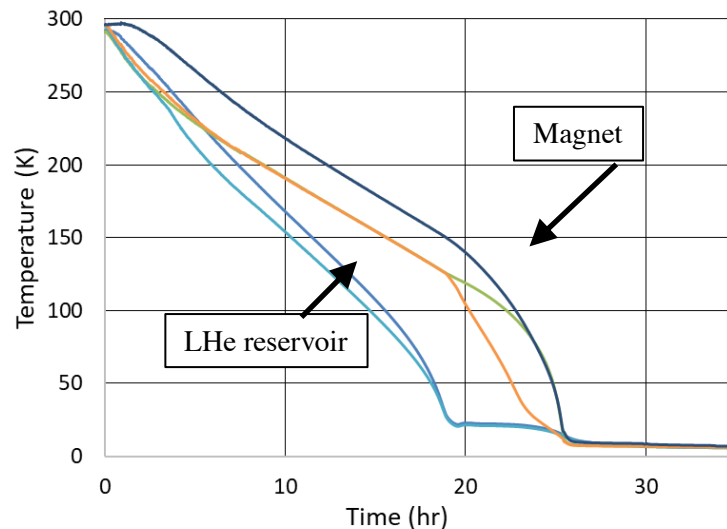


Figure 7: Cool-down curves showing cooling rates for selected temperature sensors on the LHe reservoir and the magnet assembly. Once temperatures reach the 5 K range, LHe is transferred to the reservoir to complete the cooldown process.

Zero-boil-off operation at a stable SCU operating temperature of 4.2 K can be regulated as long as there is some amount of excess cooling capacity. In this case, a trim heater is energized to match the heat load with the cooling power. However in order to

reach the operating temperature of 4.2 K, the base temperatures of the cryocoolers must operate at about 3.6 K due to thermal link conductances, contact resistances, and LHe re-condensation efficiency in the reservoir. Cryocooler load mapping on an instrumented test stand indicated a per-unit cooling power of about 0.7 W at 3.6 K. The second-generation device with four 4K cryocoolers therefore provides a total available cooling power of 2.8 W. With a measured trim heater power of 1.5 W at stable 4.2 K operation, the resulting system static heat load is 1.3 W.

During the engineering runs, initial cool-down reached only 5-7 K at the reservoir and magnet, respectively. During operation it was noticed that two cryocoolers had reached 2.7 K, indicating that they were providing negligible cooling power whereas the other two cryocoolers plateaued at the expected 3.6 K. This explained some of the imbalance between heat load and cooling power, but not all. Further investigation after warmup revealed gaps in the radiation shield which accounted for a large fraction of the excess heat load contributing to the elevated equilibrium temperature. Follow-on cool-down/warmup cycles addressed both the higher-than-expected heat load and the lower-than-expected cooling power. The former was dealt with by a combination of improved assembly technique and a re-design of the cold mass thermal support system while the latter was traced to high-impedance conduction paths between the cryocoolers and the cold mass.

Cryostat testing also included studies of system response to a simulated magnet quench. In operation the SCU magnet can release several kJ of stored energy to the system on a quench, depending on the particular magnet design. Heaters mounted to the cold mass delivered seven kJ of energy to the system over about ten seconds – sufficient to replicate the long-term system response although the peak pressure in the LHe reservoir was somewhat less than estimated. Figure 8 shows the pressure and temperature response to the simulated quench.

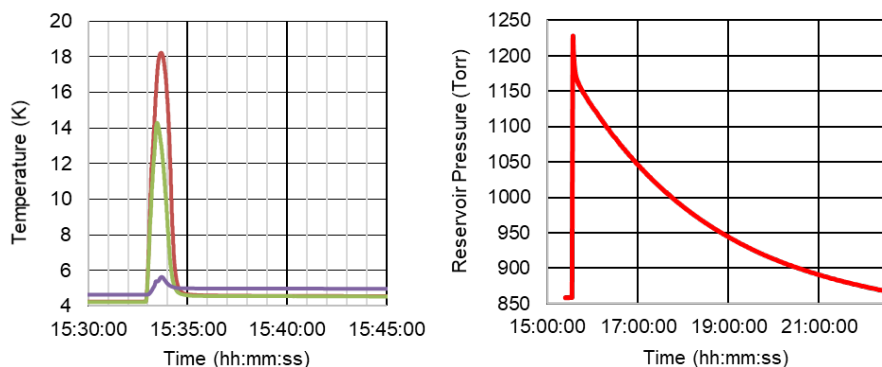


Figure 8: System temperature (left) and pressure (right) response to a simulated 7 kJ magnet quench event. System equilibrium pressure prior to the event was about 850 Torr. The system did not vent helium during this event.

2.3.4 SCU Cryostats for FELs

Cryostat concepts exist to support SCUs in an FEL application. Here the SCUs are arrayed in a contiguous string and a revised cryostat design involving multiple SCU magnets in a single cryostat is cost-effective. Since the cryostats follow one after another, the cooling system may favor a centralized cryoplant and cryogenic distribution system rather than many discreet cryocoolers. The distribution system may be either internal or

external to the cryostats. The choice depends on the relative importance of cost, packing factor (active vs. physical length between undulators), and maintainability among other factors. Figures 9 and 10 show concepts for a “minimally segmented” (internal distribution system) cryostat concept similar to that used for the superconducting RF cryomodules in the XFEL at DESY and the LCLS-II at SLAC. This strategy may be compared to a “fully segmented” layout where each cryostat is isolated from its neighbors with independent insulating vacuum spaces and an external distribution system supplies refrigeration to each cryostat via removable transfer tubes. The latter concept is typically higher cost and has a lower packing factor than minimal segmentation. However it allows rapid swap-out of a failed cryostat whereas minimal segmentation requires a thermal cycle of the entire SCU array in order to replace any individual cryostat.

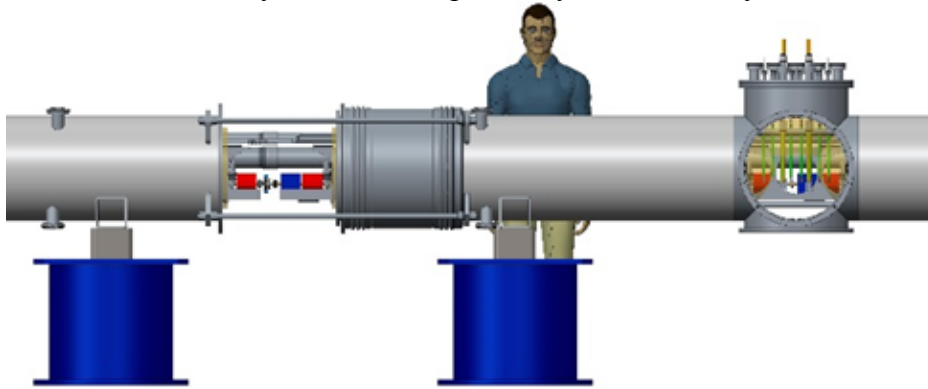


Figure 9: Concept representation of multiple SCU cryostats connected in a minimally-segmented FEL array. The inter-cryostat vacuum vessel spool is shown in the retracted (assembly) position.

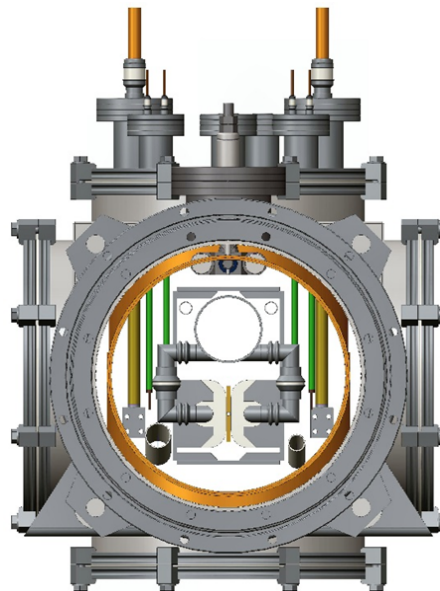


Figure 10: End-section view of a minimally-segmented SCU cryostat showing horizontal-gap planar magnets packaged with internal helium cryogenic distribution.

For FEL applications, the compact nature of SCU magnets relative to permanent magnet technology opens the possibility of multiple FEL x-ray sources within a common cryostat. The concept is shown in Figure 11.

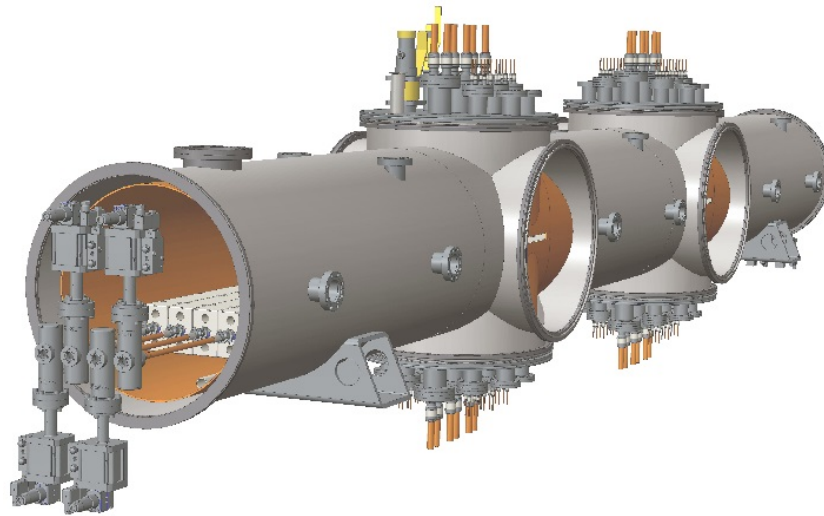


Figure 11: Concept for four independent FELs housed in a single cryostat.

2.3.5 Cooling Systems

Cooling system choice depends on the heat load and operating temperature requirements. Cryocoolers with cooling powers of 2 W at 4.2 K are available and the technology continues to advance. The portable nature of the cold head (mounted on the cryostat) and compressor package (located nearby and connected to the cold head with pressurized helium gas lines) is a good match for individual SCUs in a storage ring application. Depending on the size of the storage ring and the number of SCU insertion devices, a central cryoplant/cryogenic distribution system may provide an economic advantage over cryocoolers in terms of wall plug power and maintenance cost.

For FEL applications a small cryoplant (example shown in Figure 12) is an attractive option for either a minimal or fully segmented SCU array. Advantages include reduced operating cost and the ability to operate the magnets at temperatures below what is attainable with cryocoolers to reach higher operating current and magnetic fields. This is achieved by adding a sub-atmospheric stage to the standard helium refrigeration cycle using cold compression or warm vacuum pumping. Operating temperatures below the lambda point (2.17 K) are possible and have been the design choice for superconducting RF cryomodules in the latest FELs.

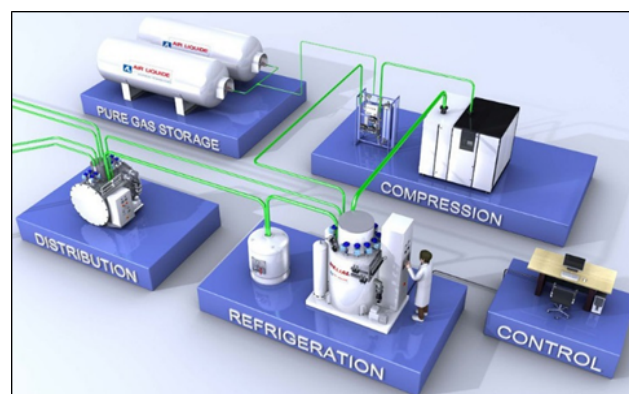


Figure 12: A small helium refrigerator system (from the [Air Liquide](#) website).

2.3.6 Alignment Systems

Alignment of SCUs requires precision in both position adjustment and measurement. Development efforts include precise (<10 micron) external adjustment capability for the magnet cold mass with respect to the cryostat when the system is at 4.2 K along with sub-5-micron laser displacement-based position measurement capability. These requirements are particularly important for multi-undulator-magnet cryostats where magnet-to-magnet alignment at the 5-micron level is desirable. Multi-magnet alignment to a common rigid cold mass support is one design option although independent magnet supports with external (or internal) precision adjustment capability are a potential alternative.

2.3.7 Beam Vacuum Chambers

In a storage ring application, SCU magnets must be screened effectively from electron beam- and/or x-ray-induced heating. An independently cooled beam vacuum chamber provides an adequate screen for planar SCUs. However a helical SCU is vulnerable to x-ray heating caused by the bending-magnet (BM) beam line immediately upstream. The vulnerability arises due to the helical magnet core design which completely envelopes the beam vacuum chamber. This heat source can be mitigated by implementing beam orbit correction to steer the BM x-ray fan away from the helical SCU magnet. For the planar SCU geometry, there is no magnet exposure along the horizontal plane of the electron beam orbit (see Figure 13).

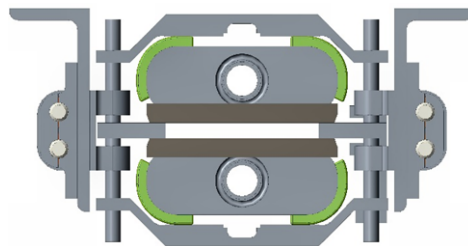


Figure 13: Cross-section of planar magnet pair showing magnet cores with helium cooling passages, pole pieces, gap separator system, and magnet support system. Particle beam vacuum chamber is not shown.

2.3.8 References

1. E. Bekhtenev, S. Khrushev, E. Kuper et al., "A multipole superconducting wiggler for Canadian light source," *Physics of Particles and Nuclei Letters* **3** Suppl. 1, S16 (2006).
2. Q. Hasse, J. Fuerst, Y. Ivanyushenkov et al., "Fabrication and Assembly of a Superconducting Undulator for the Advanced Photon Source," *Advances in Cryogenic Engineering*, AIP Conf. Proc. **1573** 392 (2014).
3. J. Fuerst, C. Doose, Q. Hasse et al., "Cryogenic Performance of a Cryocooler-Cooled Superconducting Undulator," *Advances in Cryogenic Engineering*, AIP Conf. Proc. **1573** 1527 (2014).
4. J. Fuerst, Q. Hasse, Y. Ivanyushenkov et al., "Cryogenic Testing and Initial Performance of a Helical Superconducting Undulator at the APS," in Proc. 9th Int. Particle Accelerator Conf. (IPAC'18), Vancouver, BC, Canada, paper TUPMF007, 1260-1262 (2018).

2.4 SCU Activities in the UK

Jim Clarke, Clive Hill, Alex Hinton, Kiril Marinov, Ben Shepherd, Mark Surman,
Neil Thompson; STFC Daresbury Laboratory, Warrington, UK
Vicky Bayliss, Josef Boehm, Tom Bradshaw, Simon Canfer, Mike Courthold,
Ben Green, Tim Hayler, Phillip Jeffery, Craig MacWaters, Anna Orłowska;
STFC Rutherford Appleton Laboratory, Didcot, UK
Steve Milward, Diamond Light Source, Didcot, UK
Mail to: jim.clarke@stfc.ac.uk

2.4.1 Introduction

Superconducting undulators promise higher peak fields on axis than any other technology but they are still not a mainstream solution for 3rd or 4th generation light sources. A collaboration within the UK from STFC (Daresbury and Rutherford Appleton Laboratories) and Diamond Light Source (DLS) are actively working on SCUs for both storage rings and free electron lasers (FELs). Almost ten years ago we successfully built and tested a 4m long helical undulator for the ILC positron source [1] and since then we have developed the design of a short period, narrow aperture, planar superconducting undulator which is currently at the prototype stage. More recently we have focussed our attention on the optimisation of SCUs for FELs and have started the development of a helical SCU solution. This report will describe the main SCU activities within the UK and the status of both the planar and helical concepts.

2.4.2 Planar SCU Activities

2.4.2.1 *Parameters and Design Choices*

The key parameters of the planar undulator have been developed closely with DLS to ensure that the output of the undulator is closely matched to the user science needs and that installation into a modern storage ring facility can be achieved with little disruption to the existing operational performance. In particular the magnet gap has been determined by ensuring that the new fixed gap aperture set by the undulator is equivalent to the existing lowest fixed gap aperture currently installed at DLS. The current limiting fixed gap vertical aperture is 8 mm over a 5 m long straight section. Scaling this down for a 2 m long magnet installed in the centre of a 5 m straight defines the vertical aperture to be 5.4 mm. This should ensure that the impact on the operation of DLS is negligible in terms of reduced aperture to the electron beam. The selected optimum undulator parameters are summarized in Table 1.

Despite the clear advantages of superconducting technology in the generation of very high magnetic fields, the generation of a relatively modest field (1.25 T) in a magnet with 15.5 mm period and magnet pole gap of 7.4 mm using this technology is extremely challenging. The SC material must be operated close to the quench limit to achieve these fields, leaving little safety margin. We have made a number of design choices in order to try to ensure that the undulator will achieve the design field whilst simultaneously maximising the safety margin.

Table 1: Undulator parameters.

magnet length	~2.0	m
period	15.5	mm
peak field on axis	1.25	T
K	1.8	
required phase error	<3	°
magnet pole gap	7.4	mm
vertical beam aperture	5.4	mm
SC material	NbTi	
beam tube temperature	12 – 16	K

The first design choice we have made is to provide an intermediate temperature (12 to 16 K) vacuum vessel for the electron beam. This vessel will be able to cope with the anticipated beam heating due to resistive wall wakefields and any uncollimated synchrotron radiation from the upstream dipole. This vessel will be thermally isolated from the undulator magnet with no direct points of contact allowed. A major consequence of this choice is that a full allowance of 2 mm has been allowed for between the vertical beam aperture and the magnet pole gap to provide space for the vacuum vessel walls and thermally isolating vacuum gap.

The second design choice is that we aim to construct the magnet to within very challenging engineering tolerances in order to remove any requirement for magnet shimming. Numerous shimming proposals have been made for similar superconducting undulators but they all tend to have a negative impact in terms of reducing the peak field on axis or adding substantial complexity to the cryomodule. We have carefully assessed the engineering tolerances which are required in order to maintain the phase error to within $\sim 3^\circ$ and we have based our design on achieving these values.

Significant magnet modelling has been carried out during this project in order to compare the possible alternative geometries, materials, and winding arrangements. These studies concluded that rectangular NbTi wire was the optimum choice for the undulator in terms of operating margin and ease of fabrication. Nearly fifty 3D models have been simulated using Opera magnet modelling software covering a range of periods from 11 to 15.5 mm and magnet pole gaps from 3 to 10 mm. The peak on-axis field, B_{y0} , for all these models has been established at a fixed operating margin for the SC wire of 20% (i.e. the wire operates at 80% of the short sample limit) and at 4K. An empirical equation has been fitted to our modelling results to help with estimating the possible peak fields at intermediate gap and period values as a function of undulator period, λ_u , and magnet gap between the poles, g [2].

$$B_{y0} = (0.3282 + 0.0678\lambda_u - 1.053 \times 10^{-3}\lambda_u^2 + 5.85 \times 10^{-6}\lambda_u^3)e^{-\pi\left(\frac{g}{\lambda_u}-0.5\right)}$$

2.4.2.2 *Prototype Construction and Testing*

The magnet former is an essential component for the development of the SCU. The current design utilizes a solid steel core with machined grooves; this approach does not suffer from the accumulated tolerances that you might expect from a piece part assembly, it relies on the uniformity of the groove geometry and period to be machined to within a profile tolerance of 20 μm . The groove walls are coated with Isopon to provide electrical isolation between the coil winding and the low carbon steel former.

Several prototype magnets have been produced to assess the design and different manufacturing processes; these prototypes began with 4-coil magnets and moved on to full 36-coil production magnets; the prototyping work covered the formers' geometric precision both with the steel work and Isopon coating, the winding scheme, the resin impregnation and electrical breakdown tests. Magnetic measurements of the first completed 36-coil magnets are presented here. The results come from a set of two tests; firstly Hall probe measurements to record the magnetic field map of the magnet and to determine the critical current, secondly tested with beam at 25 MeV in CLARA [3] (Compact Linear Accelerator for Research and Applications) at Daresbury, with the SCU generating light in the infra-red (IR) region (~ 1.3 to $7 \mu\text{m}$ depending upon SCU field level and electron energy utilized) and detected using the diagnostic system previously used for the ALICE (Accelerator and Lasers in Combined Experiments) FEL [4]. A successful demonstration with beam proving that there is negligible beam heating to the 4K magnet, that the magnet build quality is sufficient, and that the phase and trajectory errors are small. Details of the prototypes, and the development from the first 4-coil magnets to the current production magnets, are presented here.

There are multiple design choices for magnet formers and many schemes were debated from assemblies to solid core designs with just as many manufacturing techniques considered. The aim was to achieve the best uniformity of groove geometries for the positioning of the wire stack; this precision is required in order to achieve the best field quality. The final decision was to proceed with the solid core design, as shown in Figure 1.

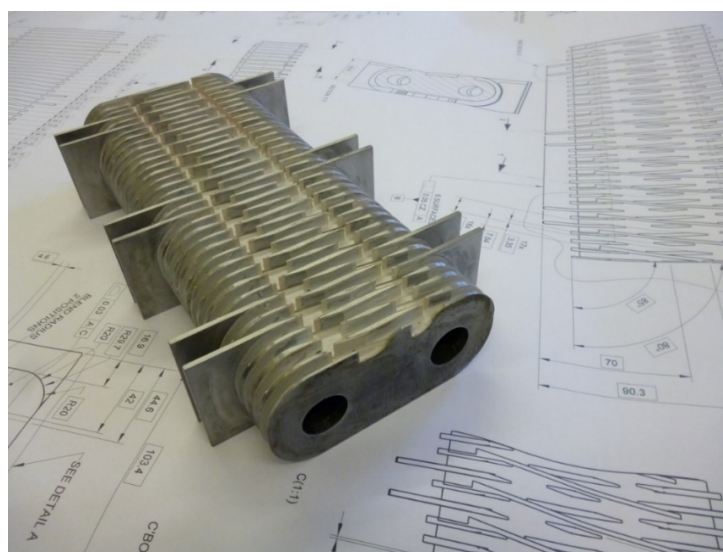


Figure 1: A 300 mm long steel former.

The solid core design is made out of 1006 low-carbon steel. All the pole grooves are machined precisely from the same reference plane to secure the period of the undulator. The groove position and geometry are defined by a $20 \mu\text{m}$ profile tolerance as shown on the manufacturing drawing. The width and depth of the grooves have been determined by the prototyping work, which involved sectioning magnet formers and inspecting the cross section of the superconducting wire stacks for uniformity and fit.

Many lessons were learnt in the manufacture of the early formers. The metrology results led to the development of three functional datums, the consideration of how the

datums relate to the magnets assembly on the support beam, and their corresponding geometric tolerances.

After the manufacture and metrology of the steel former the grooves are filled with Isopton, which is a car body filler but here is acting as an insulator. The Isopton is then partly machined away to create a new groove. The layer of Isopton acts as an insulator which makes the winding process more reliable from a short circuit to ground point of view. The period of the steel grooves is generally to within a $20\ \mu\text{m}$ profile tolerance. However, the Isopton grooves did not typically sit central to the steel groove, probably due to the difficulty in re-establishing datums in the secondary machining operation. Typically, there should be a layer of Isopton on either side of the groove with a thickness of $0.1875\ \text{mm}$; this was more often $0.140\ \text{mm}$ on one side and $0.235\ \text{mm}$ on the other side. In addition to this, the side of the groove which bore the thin or thick layer flipped halfway along the former, this was indicative of machining the former in two steps. Because of the limited reach of the machines stub arbour it was only possible to machine halfway down the total length of the former, at this point the former had to be turned over on the machine bed to machine the second half. This offset in insulation thickness does not affect the periodicity of the undulator to first order since this is set by the former itself. Rather, it affects the exact position of the wires within the grooves which is less critical. The flatness of the pole heights on both magnets are to within $38\ \mu\text{m}$.

Magnetic measurements were used to confirm the precision of the core manufacturing, winding and potting processes. The magnetic measurements were undertaken using a warm guiding tube approach [5]. The warm-bore measurements limited the operational current of the undulator to $250\ \text{A}$. Without the warm-bore device the magnet operates reliably at a minimum of $340\ \text{A}$.

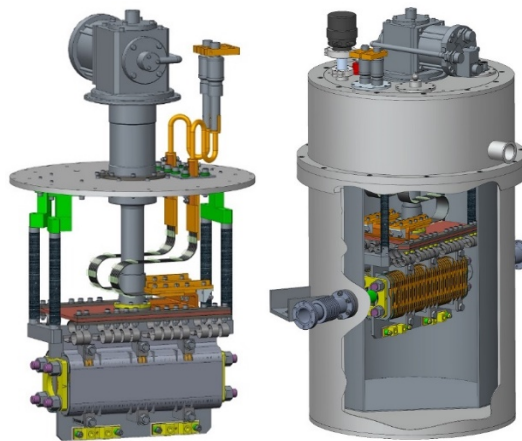


Figure 2: The superconducting undulator mounted inside the cryostat.

2.4.2.3 *Prototype Test with CLARA*

To further verify the performance of the planar SCU, it was installed on STFC's electron test facility, CLARA, which is located at Daresbury Laboratory. Once CLARA phase 2 is completed, it will provide a $250\ \text{MeV}$ "FEL-ready" beam into a user exploitation area FEBE (Full Energy Beam Exploitation) as well as leaving space for a planned Phase 3 FEL test facility. The present stage of CLARA provides a $50\ \text{MeV}$ electron beam to a user exploitation area.

The SCU team made a successful application for CLARA beam time. The experiment was installed on CLARA using a purpose-built beam line, and operated for two weeks in Mar 2019.

The SCU beam line was designed with two primary purposes: to protect CLARA from the SCU, and to characterize the IR beam produced by the interaction of the CLARA beam with the undulator. The protection was necessary due to the difference between CLARA's stringent vacuum requirements (typically around 10^{-8} mbar), and the vacuum level inside the SCU (around 10^{-6} mbar, increasing at higher current or in the event of a quench) since our prototype SCU has no internal beam vacuum chamber. The materials used to insulate the SCU windings were a large potential source of contaminants from which CLARA had to be protected. With this in mind, the beamline contained two thin foils inside manual valves which the electron beam could pass through but which would keep the two vacuum regimes well separated. The SCU itself is housed in a cryostat and conduction cooled to 4K using a cryocooler. The field direction is horizontal and the beam undulates vertically. YAG screens are located just before and after the SCU to check the beam position.

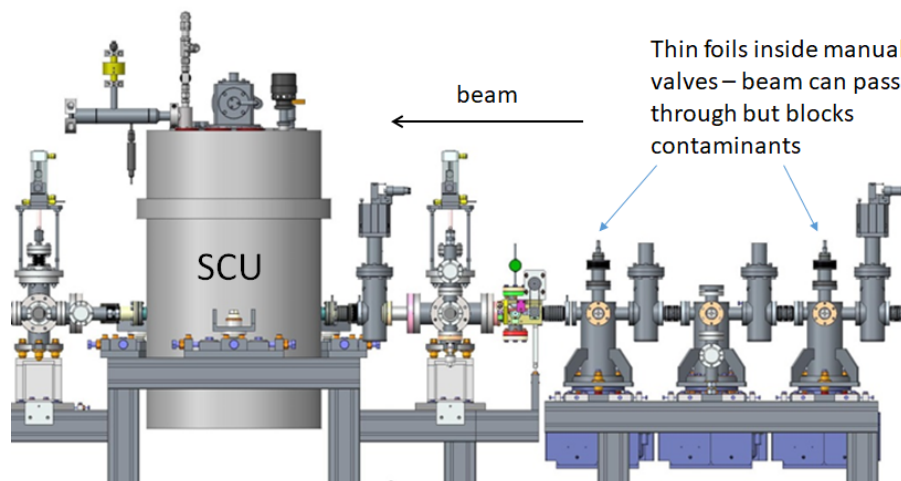


Figure 3: Layout of the SCU beamline on CLARA. The beam direction is right to left.

After the electron beam passed through the SCU, it was deflected by a dipole. The photon beam continued through a diamond window to the IR diagnostics station. This consisted of an MCT detector to provide a raw signal, and an IR spectrometer to measure the spectrum produced. The wavelength of light produced was calculated to be between $1.3\text{-}7\ \mu\text{m}$ depending on the current in the SCU and the energy of the beam, and the detectable range of the IR detection system was wavelengths above $2.5\ \mu\text{m}$.

Construction of the beamline took place offline away from the CLARA accelerator hall. The SCU was delivered to Daresbury from RAL, cooled down to 4K, and the alignment checked using a HeNe laser. Due to thermal effects, the alignment was slightly different when cold and the baffles inside of the cryostat needed to be enlarged to ensure the beam could pass through the undulator.

The beamline was then installed on CLARA, cooled down, and the vacuum pressure reduced to its operating level. The electron beam passed through the foils in the beamline without any measurable effect, and through the undulator in the powered-off state. There were some issues when powering the SCU – at low excitations, the PSU stability was somewhat reduced, and this had the effect of triggering ‘false quenches’ within the

quench detection electronics. This was mitigated by bringing a ‘reset button’ into the control room, which meant that a false quench reset could be performed without having to go into the accelerator area.

When ramping up the SCU, a large kick was imparted to the electron beam even at low excitations. This could not be mitigated using the existing correctors on CLARA; an additional electromagnetic corrector was placed just before the SCU, and in addition a fixed strength permanent magnet corrector was added at the entrance to the SCU. These extra correctors enabled the beam to be transported through the SCU up to a level of around 200A. However, it was clear that a large field offset was present. This effectively curtailed the experimental programme, as the electron trajectory was not sufficiently straight inside the SCU to produce a detectable IR beam.

Following the experimental run, further electromagnetic modelling was carried out to determine the cause of the field offset. It was traced to the ‘wings’: features on the sides of the undulator former that rest on slip gauges to precisely control the undulator gap. These wings are mounted in pairs a period apart, and consequently there is ‘leakage’ of field at the sides of the undulator always on the same pole polarities, contributing to an overall on-axis field offset. The wings had been previously included in the model, but the symmetry of the model meant that the field offset did not show up. A maximum field integral of around 20 T.mm was inferred from the beam position on the upstream and downstream YAGs. Note that the field integral reduces at higher currents due to saturation in the wings.

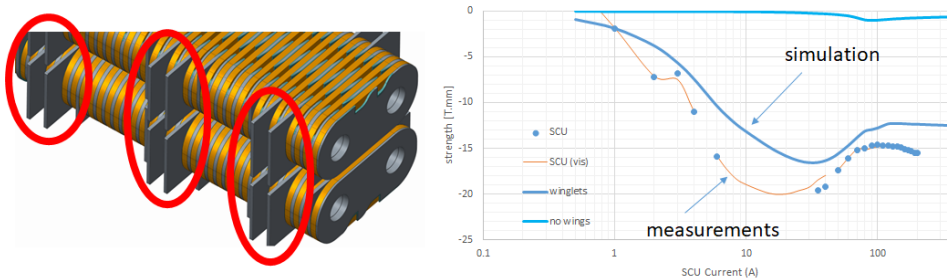


Figure 4: Drawing of the SCU showing the ‘wings’ (left), and a comparison of the field integral measured via the CLARA experiment with the electromagnetic simulation of the SCU. The blue points and orange line are the measured field integrals calculated from beam positions at the YAG screens; the dark blue line is the simulation including wings; and the light blue line shows the simulated field integral with no wings present.

This experiment was the first-ever test of an in-vacuum SCU on an operational accelerator facility. Despite the setback of not being able to measure any IR radiation produced by the undulator, we have gained extremely valuable experience in operating a superconducting undulator on an accelerator. The vacuum performance of the SCU was very good; the beamline worked as designed to protect CLARA from any contamination; the control and quench protection systems were verified. Despite the narrow gap, intense beam and likely beam loss inside the vessel, the SCU operation was very stable and no beam-induced quenches were observed.

2.4.2.4 Next Steps

Mitigation strategies to reduce the field offset and make the SCU more transparent to the electron beam have been considered. The agreed strategy was to fix additional ‘wings’ to the sides of the SCU formers on the alternative polarity poles. This ensures a more

even distribution of flux through the magnet, and was estimated to bring the field integral down to the 2-3 T.mm level.

After the modifications, as described above, field measurements were performed on the cold magnet with the modifications in place. A Hall sensor was moved between the two halves of the undulator coil bodies by a motorized actuator. The travel distance of the actuator was not sufficient to cover the full extent of the magnet, hence the difference of signal at the beginning and the end of the field trace in Figure 5. The small bias field is barely noticeable, but still present, and will be set to zero by an external Helmholtz-type coil arrangement around the outside of the cryostat.

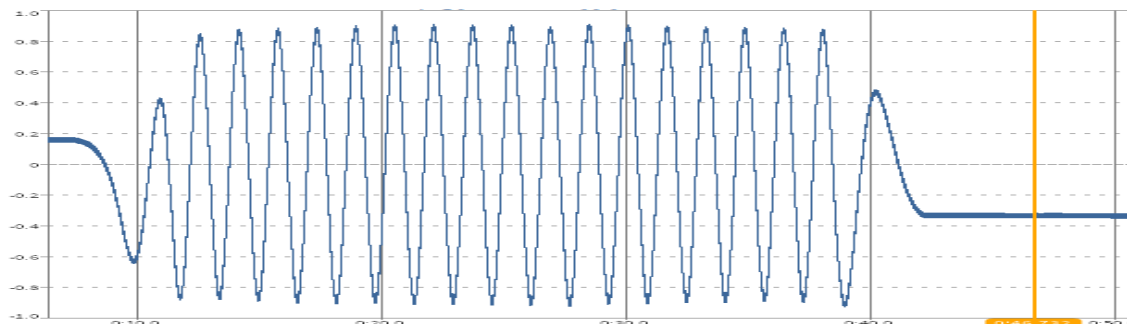


Figure 5: Magnetic field profile of the planar SCU measured at 200A.

Once the bias field in the SCU prototype has been removed, an application will be made to re-run the experiment during the third CLARA user run in late 2020.

2.4.3 Helical SCU Activities

2.4.3.1 *Motivation for Helical*

The motivation for using a helical design for a FEL, rather than a planar design, is that for two reasons the coupling between the electron beam and radiation is stronger. Firstly, we consider the electron longitudinal motion. In a planar field the electrons move transversely in a sinusoidal trajectory. This means that there is an oscillation in the longitudinal component of their velocity, and hence in the electron phase with respect to the co-propagating light. This oscillation, or ‘dephasing’, degrades the microbunching process upon which the FEL depends, and this degradation increases for higher K values. However, in a helical field, the electrons move in a helical trajectory with constant longitudinal velocity so the relative electron/light phase is constant and the microbunching process is not degraded. Secondly, we consider the electron transverse dynamics. In the planar field the transverse electron acceleration is not constant, and the electrons only experience the maximum magnetic field at two positions per undulator period. In a helical field the electrons experience the maximum transverse acceleration constantly, and hence the photon emission is stronger.

2.4.3.2 *Magnet Modelling*

The magnet modelling work for the helical undulator is still very much in the exploratory phase. A design will be produced for a full-length undulator module suitable

for installation in an FEL facility, including components to be installed between the modules such as phase shifters, quadrupoles, correctors and diagnostics. Following this design work, a short prototype undulator will be built and tested.

The undulator parameters will be set so that the full-scale undulator is capable of producing 8-16 keV photons at the proposed CompactLight facility [6], where the electron beam energy is set at 5.5 GeV. A helical undulator with parameters in the range $\sim 4\text{-}5$ mm gap and $\sim 11\text{-}13$ mm period is under consideration. Further studies to complete the magnet specification are ongoing and will continue over the next few months.

2.4.3.3 *Open Questions*

At this early stage of the project, there are several unresolved issues around the design of the helical SCU. Some of these issues are listed below.

- **Field quality.** The errors on the peak field should not contribute significantly to degradation of the FEL light output. This sets a constraint on $\Delta K/K$ of $\sim 10^{-4}$. The trajectory straightness is also important and to limit the loss in FEL output power compared to the ideal case to $\sim 10\%$ needs to be maintained to within ~ 5 μm down the length of the undulator.
- **Wire choice.** This is clearly critical for estimating the operating point of the undulator. Insulating coatings must be considered as well, to limit outgassing rates in order to preserve low vacuum pressures.
- **Cryogenic system.** It may be more efficient for an FEL facility to maintain a central cryoplant and a single integrated cryostat for multiple undulator modules.
- **Bore material.** This has an impact on wakefields, and assembly of the steel core of the undulator must be considered.
- **Magnetic measurements.** Small Hall probes that operate at low temperatures are required to map the field in both transverse directions. Pulsed-wire or stretched-wire techniques could be useful for integral measurements.

2.4.4 **Conclusion**

Our UK collaboration has over ten years' experience in developing innovative superconducting undulator technology. We have been working for several years now in developing a planar SCU, and this has culminated in the production of a prototype and the first-ever installation of an in-vacuum planar SCU on an operational accelerator. Modifications to our prototype are ongoing and we plan to run another experiment on CLARA in 2020.

SCUs have great potential for use on future FEL facilities. STFC is uniquely well-placed to realize this potential; our research group has the world-leading experience and skills to design and build the next generation of undulators ready to install on a future light source. Our programme is now expanding to also include the development of a helical SCU specifically designed for an X-ray FEL.

2.4.5 **References**

1. D. J. Scott et al., "Demonstration of a High-Field Short-Period Superconducting Helical Undulator Suitable for Future TeV-Scale Linear Collider Positron

- Sources”, *Phys. Rev. Lett.* **107**, 174803 (2011).
2. F. Nguyen et al, “XLS Deliverable D5.1: Technologies for the Compact Light Undulator,” XLS-Report-2019-004, 2019.
 3. J. A. Clarke et al., “CLARA Conceptual Design Report,” *JINST*, **9(05)** T05001 (2014).
 4. N. R. Thompson et al., “First lasing of the ALICE infra-red Free-Electron Laser,” *Nucl. Instrum. Meth. A* **680** 117-123 (2012).
 5. Y. Ivanyushenkov et al., “Development Status of a Magnetic Measurement System for the APS Superconducting Undulator,” in *Proc. PAC’11*, New York, NY, USA, Mar.-Apr. 2011, paper TUP243, pp. 1286-1288 (2011).
 6. G. D’Auria et al., “The CompactLight Design Study,” in *Proc. IPAC’19*, Melbourne, Australia, May 2019, pp. 1756-1759 (2019) doi:10.18429/JACoW-IPAC2019-TUPRB032

2.5 Practical Superconducting Materials for High-Field Undulators

Ibrahim Kesgin, Yury Ivanyushenkov and Efim Gluskin

Mail to: ikesgin@anl.gov

Advanced Photon Source, Argonne National Laboratory,
9700 S Cass Ave, Lemont, IL 60439

2.5.1 Introduction

Undulators are the primary sources for the x-ray radiation in modern light sources (SRs) and as amplifiers of radiation, they also constitute one of the most critical elements for free electron lasers (FELs). Undulators force relativistic electrons to follow a sinusoidal-like motion in the periodic magnetic field with an amplitude of B_0 . As a result, electrons emit powerful radiation concentrated in a narrow angle along their trajectory. The undulator radiation flux depends directly on the on-axis field value, B_0 . Hence, the pursuit for stronger magnetic fields in undulators is important.

Attempt to build superconducting insertion devices started in late 1970s. A comprehensive review of the SCUs and superconducting wigglers (SCWs) can be found in [1]. A comparison of two competing technologies, permanent magnet undulators (PMUs) and SCUs, are also reported in [2]. Over the past decade, SCU technology has been significantly developed. To our knowledge, currently, there are four SCUs in operation at SR sources worldwide: Three at Argonne National Laboratory's Advanced Photon Source and one at the Karlsruhe Institute of Technology (KIT). All these devices are using NbTi superconducting wire to build electromagnets that are designed and assembled as undulators. In order to operate them at low (around 4 K) temperature, these undulators are housed in cryostats. The ANL's cryostat vacuum system is separated from the storage ring vacuum system by a vacuum chamber that is embraced by the SC undulator magnet. The SCU vacuum chamber consumes about 2 mm of the undulator aperture; nevertheless, it has been experimentally proven that for the undulator period starting at 15 mm and for the same beam stay clear apertures, NbTi-based SCUs provide stronger on-axis magnetic field as compared to most advanced cryogenically-cooled in-vacuum undulators (CIVUs) [2]. While such CIVUs represent the limit for permanent magnet undulator technology, SCUs have an obvious potential beyond the NbTi-based devices.

SCUs have a decided advantage in the strength of the magnetic field that leads to implementation at the storage ring and potentially free-electron-based light sources with shorter periods, and results in more efficient use of storage ring straight sections and free-electron-laser undulator tunnels. Short-period undulators call for a small undulator gap, and that could result in significant radiation damage in magnetic structure. There are several indications that SCUs would tolerate a harsh radiation environment better than CIVUs. Since SCUs do not require a complicated and bulky mechanical structure to control the strength of the magnetic field, they could be made quite compact with one cryostat accommodating multiple undulator lines. And, although the SCU vacuum chamber consumes part of the magnetic gap, it pays back by being a cryogenic pump in the storage ring straight section or FEL undulator line vacuum system.

Given these advantages, a quest to increase the undulator field, B_0 , beyond the current NbTi based devices, and to aim for SCUs with a period as small as 10 mm while

maintaining the same undulator parameter as for NbTi SCUs represents very challenging, but highly rewarding goal. It is well-known that NbTi has reached its limits of its critical superconducting parameters and any performance increase, in terms of achievable B_0 , will be only incremental. A different type of superconducting material has to be deployed in order to have a transformative increase in the B_0 . Below is a summary of the potential practical superconductors that can be used in high field SCU applications.

2.5.2 Practical Superconducting Materials for SCUs

The greatest interest in superconductors is due to their extreme current carrying capacities, which allow generation of high magnetic fields in space-constrained applications. The three parameters that define the critical boundaries in superconductors are critical temperature, T_c ; critical field, B_c ; and critical current, J_c (Figure 1). These parameters define the position of a critical surface with coordinates T , J , and B . Exceeding one of these parameter results in a phase transformation from superconductive to normal state and destroys the superconductivity. Therefore, it is desirable that the specified critical parameters be the higher values.

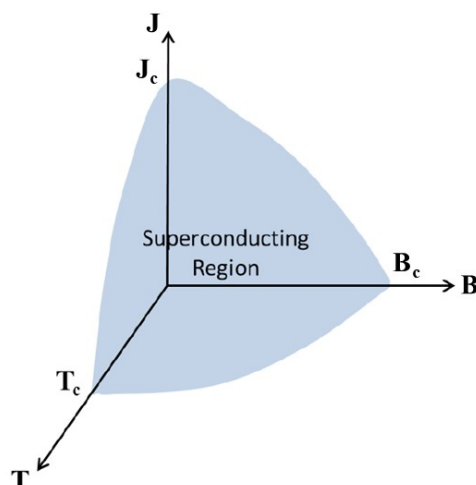


Figure 1: Critical boundaries that limit superconductivity.

In parallel to NbTi-based SCU developments, the performance of superconducting materials has advanced significantly and several practical superconductors have become strong candidates for use in undulator technology to further increase the B_0 . Table 1 summarizes critical parameters for these practical superconductors with their cost aspects.

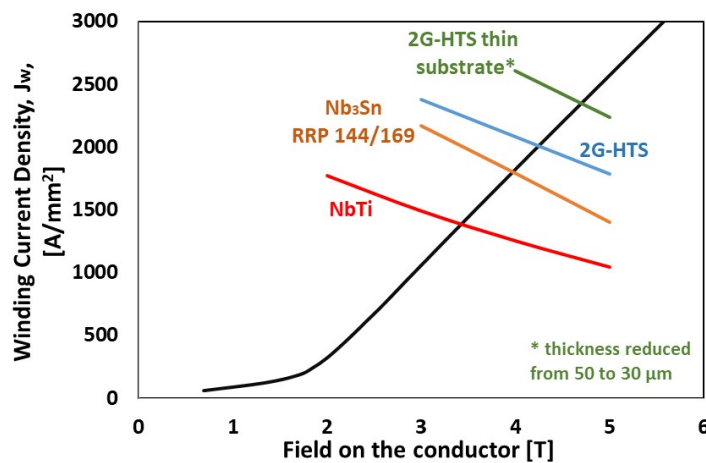
All currently operating SCUs use NbTi superconducting wire. Other potential candidate materials are niobium-tin (Nb_3Sn) and second-generation $\text{YBa}_2\text{Cu}_3\text{O}_{7-x}$ (yttrium barium copper oxide, YBCO) based (x is for oxygen concentration) high temperature superconducting materials. First-generation $\text{Bi}_2\text{Sr}_2\text{CaCu}_2\text{O}_{8+x}$ (bismuth strontium calcium copper oxide, BSCCO) based high temperature materials have been around for quite some time, and new classes of materials, namely iron-based and magnesium diboride superconductors, have also been recently discovered. However their performances are well below the NbTi level and will not be covered here. In addition, uniform long length iron-based conductors are not yet commercially available.

Table 1: Relevant parameters for practical superconductors.

Material	Critical Temperature, T_c [K]	Upper Critical Field, H_c [T]	Cost*, [\$/m]
NbTi	8	13	0.5-1
Nb ₃ Sn	18	23	6-10
BSCCO	90	89	60-90
YBCO	95	110	40-70
MgB ₂	40	32	5-15

*As of 01/01/2019

Figure 2 provides a comparison of winding current density, J_w , defined as I_c divided by the winding groove area, versus on-conductor field values in an undulator load line for different materials. J_w is an engineering parameter and a perfect tool for comparing performances of different superconductors. NbTi is a well-established technology with a J_w of ~ 1400 A/mm² at ~ 3.5 T. Nb₃Sn is mainly used for high-field magnets with a T_c of 18 K and an upper critical field in excess of 25 T offering a J_w of ~ 1800 A/mm² at ~ 4 T. 2G-HTS coated conductors offer an attractive opportunity to realize the next phase of undulator technology with a J_w of more than ~ 2000 A/mm² ~ 4.3 T. Its higher transition temperature, 90 K, also offers various opportunities for simplified undulator cryogenic systems. This could potentially reduce the cost of the overall device and make it more attractive to end users. The generated undulator field is roughly proportional to J_w , which means increasing J_w will directly translate to a higher B_0 at a similar rate.

**Figure 2:** Winding current densities, J_w , for various superconductors in an undulator load line.

The insulated wire diameters of 0.753 mm and 0.73 mm were used for NbTi and Nb₃Sn, respectively. An HTS tape cross section of 4 mm by 0.094 mm was used in the calculations.

In the following sections, the details of each of these selected superconducting materials will be presented along with performance comparisons in terms of achievable J_w values obtained from either real operating devices or short prototype magnets. An outlook will be provided considering their future performance projections based upon ongoing research activities, which will be a road map for future high field SCUs.

2.5.2.1 Niobium Titanium (NbTi)

As with the other accelerator magnets, NbTi has been the workhorse for SCUs. It was first used in the late 1970s [3-7], but the pace of effort slowed after simultaneous demonstrations in the early years of its development. Most of the early works were focused on the SCWs and, with recent more challenging user requests, interest in SCUs has revived. NbTi-based SCUs are operating at KIT [8]. Two planar 1.1 m-long undulators and one 1.2 m-long helical undulator are also operating at the APS [9] and longer magnets (~2m) for the APS Upgrade are being designed and currently in fabrication. Recently developed NbTi-based SCUs and their performances are compared in Table 2.

Table 2: NbTi-based SCU parameters and performances at 4.2 K.

Period and undulator lengths in mm, [Ref.]	Conductor dimensions [mm]	Max training current [A]	Number of turns	Winding groove area [mm²]	Max $\sim J_w$ [A/mm²]
18, 1100, [10]	0.643	541	53	21.8	1315
16, 330, [11]	0.753	782	39	22.3	1365
20, 154, [12]	0.76	577	113	65	1000
15, 1550, [8]	0.54×0.34*	175	91	16.7	950
16, 800, [13]	0.6+ins	400	83	28.9	1150

*Rectangular conductor

Fabrication of NbTi wire starts with preparation of the ingots. With multiple iterations of the extrusion/drawing process, it is formed to its desired final shape and dimensions. It is a ductile alloy and the process is well-controlled. The round nature of NbTi wire, (there is also a rectangular option) is ideal for undulator winding. A cross section of a NbTi undulator winding is shown in Figure 3 along with an SEM image of individual 75- μm NbTi filaments. This particular magnet has 39 NbTi turns inside a winding groove. The wire is used as received from the manufacturer and does not require any high temperature heat treatment. Most of the NbTi-based undulators developed were continuously wound, layer-by-layer transitions from one winding stack to another by using a 180° turn to eliminate the resistive joint. SCUs are cooled both with cryogen at the APS and in a cryogen-free environment at the KIT. The NbTi SCU magnets are self-protected and generally do not require any active quench detection and protection system (QDPS). NbTi is a very well-established and mature technology; however, as can be seen in Table 2, the maximum achievable J_w is ~ 1400 A/mm². Since it has reached its material limits, there is not much research being focused on increasing NbTi performance, and it is unlikely that this material will offer a significant boost in achievable B_o in the future than it offers now.

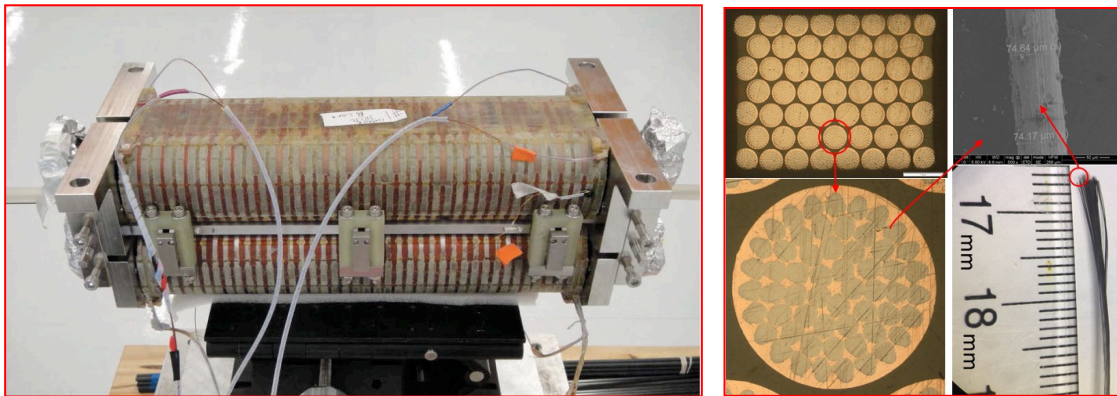


Figure 3: A picture of NbTi SCU magnets in the assembly (left) [11] and cross-sectional cut out section (right) showing NbTi turns inside an undulator winding groove, individual NbTi wire, filament bundle, and an SEM image of a $\sim 75 \mu\text{m}$ filament.

2.5.2.2 Niobium-Tin (Nb_3Sn)

Nb_3Sn has been used for high-field magnets. The ITER cable-in-conduits and various NMR magnets also have been fabricated using Nb_3Sn cables or strands. It is the second most widely explored material after NbTi. Like NbTi, Nb_3Sn is prepared as a billet and drawn into its final shape and dimensions. The three most common methods used in Nb_3Sn fabrications are described below.

- (i) Bronze-processed conductors are fabricated very similar to NbTi. Holes are drilled in a bronze (Cu,Sn) ingot and Nb filaments are inserted (Figure 4a). A superconducting filament size of about $2 \mu\text{m}$ can be achieved and is ideal for AC applications, but the critical current densities are low—comparable to NbTi—due to the limited Sn content.
- (ii) Powder in tube (PIT) is another manufacturing technique where a powder, usually Nb,Sn, is inserted in Nb tubes (Figure 4b). Here the problem is the big filament diameter as well as the homogeneity over long lengths.
- (iii) Internal tin (IT) processed conductors have a higher Sn level, and thus higher Nb_3Sn total cross section areas can be achieved with this technique. In IT process, a Sn core is surrounded by Nb rods in a Cu matrix (Figure 4c). The filaments in a sub-element grow together during the reaction process resulting an effective filament size equal to the size of the sub-element ($60 \mu\text{m}$); this is, for example, a problem for both AC applications and stability against flux jumps. In high J_c wires, also called distributed-barrier IT, the individual filaments have their own barrier layer [restacked-rod process (RRP) developed by Bruker-OST] offering higher J_w .

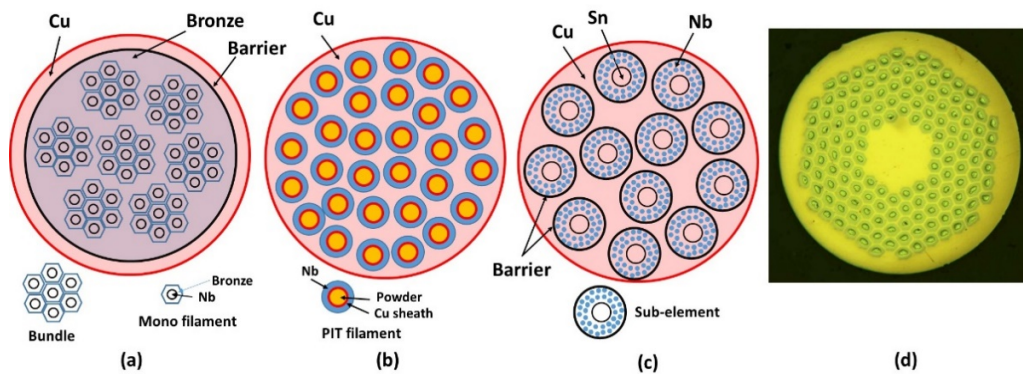


Figure 4: Sketches (not to scale) of the Nb_3Sn conductor manufacturing techniques: (a) Bronze process, (b) powder-in-tube (PIT), (c) internal tin (RRP) (d), an actual microscope image of a reacted RRP 144/169 strand.

Common to all of these manufacturing techniques is the need for a wind-and-react (W&R) process: A wire is wound into the desired magnet shape followed by a high-temperature annealing step in which the superconducting phase forms. As received wire contains unreacted Nb and Sn rods and Nb_3Sn phase forms after a high temperature reaction process. The resulting superconducting wire is very brittle and sensitive to mechanical strain that degrades the performance significantly. This is the reason why the wire typically cannot be wound after the reaction steps, though large applications might pursue that path. The reaction temperature is at $650\text{ }^\circ\text{C}$ and the magnet operates at $269\text{ }^\circ\text{C}$ below zero. The temperature span is about $1000\text{ }^\circ\text{C}$ and this makes the magnet design very challenging. The metallurgy is also complex, and performance depends on the uniformity of the heat treatment (HT) cycle. The parameters that affect the performance of the magnet are the temperature and duration of the heat treatment. The magnets are filled with an inert gas or are in vacuum during the HT process. A typical HT cycle is shown in Figure 5.

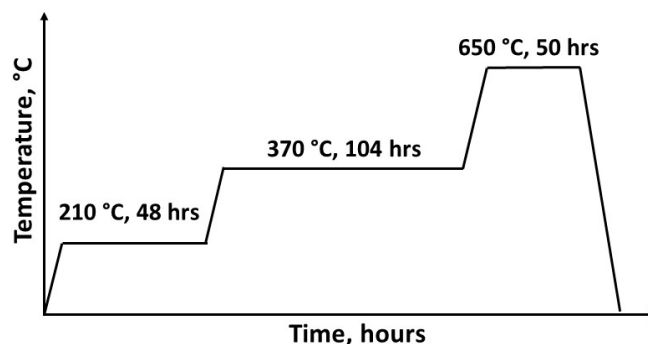


Figure 5: A typical heat treatment cycle for ANL's Nb_3Sn SCU magnets.

One of the biggest problems for the Nb_3Sn magnet technology is conductor stability. The magnetic field penetrates into the superconductor as quantized vortices and they move. This motion dissipates energy and if it exceeds a certain level, it induces quench, a portion of the superconducting wire becomes non-superconducting. Such an event is

acceptable during the training of a magnet and is actually part of the magnet fabrication. However, flux jumps in Nb₃Sn wire can sometimes make the training process very complicated and can prevent the magnet from reaching its design current level; this is referred to as magnetic instability. For this reason, using the optimal heat treatment of the wire to achieve the highest performance is not necessarily the most practical method to use in the construction of superconducting magnets. Other aspects must be considered. There are two major parameters that affect the stability of a conductor: residual resistivity ratio (RRR) and the filament or sub-element size. According to analysis provided in [14], the minimum sub-element size has to be 36 μm or less for stable operation in SCU applications. Higher RRR values are also desired since in the event of a flux jump, the dissipated energy can be removed more efficiently and thermal runaway can be prevented. Currently, the state-of-the-art RRP conductor is a good choice for the undulator applications and offers perfect combination of J_w , RRR and filament diameter, thus allowing stable operation and increased B_0 .

In the event of a quench, the current flowing in the super-conductor is transferred to the copper matrix making the copper current density extremely high, and if the energy in the magnet is not safely extracted, detrimental consequences can occur. An active protection scheme with proper dump resistor seems to be adequate to protect these magnet. However, coil-to-ground insulation must to be designed carefully to prevent shorts, and it needs to withstand the high voltage that forms during the quench.

The potential of Nb₃Sn has been realized, and there have been quite substantial efforts to establish a superconducting undulator technology. Many short Nb₃Sn undulator model magnets (prototypes) have been built and tested, but none of those efforts has resulted in a functional device. A summary of engineering current densities and undulator structures is provided in Table 3. Efforts at LBNL [19, 20], NHMFL [17], and ANL [16] highlighted the Nb₃Sn wire's potential. Most of these efforts were limited to short prototypes, less than 10 periods. Some of them suffered from magnetic instabilities and did not reach the desired current levels. LBNL attempted to scale the short prototype models to 1.5-m lengths. Recently, ANL has also revived the Nb₃Sn effort. The APS first started with short model magnets to develop the technology [18] and recently scaled the short model magnet to a 0.5-m-long intermediate length. A picture of APS's 0.5-m-long magnet is shown in Figure 6.

Table 3: Nb₃Sn-based SCU parameters and performances at 4.2K.

<i>Period and undulator lengths in mm, [Ref.]</i>	<i>Conductor dimensions [mm]</i>	<i>Max training current [A]</i>	<i>Number of turns</i>	<i>Winding groove area [mm²]</i>	<i>Max $\sim J_w$ [A/mm²]</i>
19, 1500, [15]	0.6+ins	790	56	24.2	1800
14.5, 100, [16]	0.8+ins	1725	23	20.6	1900
15, 80, [17]	0.8+ins	1500	23	23	1500
18, 84, [18]	0.73	1150	46	29.4	1800



Figure 6: ANL's 0.5-m-long Nb₃Sn model (prototype) magnet after the reaction and epoxy impregnation.

2.5.2.3 *Second-Generation High-Temperature Superconductors (2G-HTS)*

Second-generation high-temperature superconducting (2G-HTS) materials offer an alternative to the traditional Nb-based superconductors and have the potential to further increase the B_0 . This potential has been realized and multiple attempts were made in short prototypes. Laser ablated [21] or lithography etched [22] tapes were stacked in these demonstrative models and the generated field was measured. A more generic approach was taken in later studies [23-25], which also highlighted the 2G-HTS tapes' potential.

Manufacturing 2G-HTS tapes is quite complex, and reproducibility is a persistent unresolved problem. These conductors are fabricated layer by layer using a variety of deposition techniques. A typical architecture of a 2G-HTS tape is shown in Figure 7. Common to all, the main goal is to epitaxially grow superconducting layers onto flexible metallic substrates. This specific growth condition is very important for high-performance tapes. As the superconducting layer becomes thicker, i.e., more than 2 μm , the non-epitaxial growth deteriorates performance, and the thicker layer does not contribute to the current carrying capacity. This problem has been recently overcome using advance deposition techniques in research scale samples [26, 27] with ongoing scaling up efforts. It is important to note from the tape architecture that only a small fraction of the entire thickness carries the current (only 2-3 %) whereas this ratio is about 50% for the Nb-based superconductors. Regardless, the I_c value of manufacturing-scale 2G-HTS tapes that are currently commercially available carries large enough current, and the overall J_w still outperforms that all of competing materials.

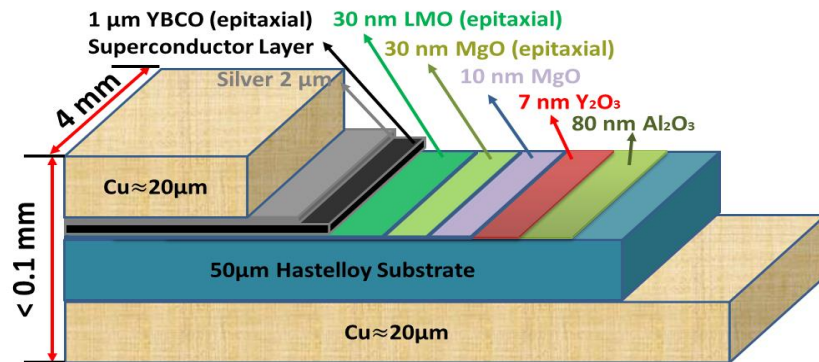


Figure 7: Typical architecture of the tape-shaped 2G-HTS (YBCO) coated conductors. Note that the thickness-to-width ratio is not drawn to scale. Only 1-2 % of the entire cross section is superconducting (shown in black).

Table 4 summarizes the results for short 2G-HTS prototypes. A major obstacle in realizing the 2G-HTS potential arises from transferring the well-established magnet technologies developed for Nb-based wires to the tape-shaped conductors. In particular, due to their large aspect ratio (width versus thickness, $4 \text{ mm} \times 0.1 \text{ mm}$) the tapes tolerate only small side-bending (bending within the plane of the tape); furthermore, normal bending is typically limited to bend diameters larger than 11 mm in order to avoid irreversible degradation of the critical current. Therefore, the traditional continuous winding approach is, in most cases, not feasible with 2G-HTS conductors.

Table 4: 2G-HTS-based SCU parameters and performances at 4.2K.

<i>Period and undulator lengths in mm, [Ref.]</i>	<i>Conductor dimensions [mm × mm]</i>	<i>Max training current [A]</i>	<i>Number of turns</i>	<i>Winding groove area [mm²]</i>	<i>Max $\sim J_w$ [A/mm²]</i>
16, 68, [23]	4×0.1	420	30	18	700
18, 32, [28]	4×0.1	545	55	22	1360
17.4, 90, [29]	4×0.1	800	40	16	2000
17.4, 90 [ANL]	4×0.1	875	50	20	2150

The very first short 2G-HTS SCU prototype was produced by Babcock Noell GmbH, now Bilfinger [23]. The prototype was 4 period long and the achieved J_w value was very low (see Table 4). Later, ANL developed this approach further and fabricated a two-period undulator with resistive joints. The achieved J_w value was at a level similar to the NbTi wire. While this exercise significantly helped the technological developments, it also revealed unresolved challenges related to winding tape-shaped conductors, the large number of resistive joints, and conductor delamination [30]. ANL recently introduced an approach that is viable and scalable and enables the continuous winding—no resistive joints—of tapes into a sequence of alternatingly poled windings in the undulator [31]. A partial interlayer insulation scheme was introduced to maintain the maximum J_w in the parts of the magnet facing the beam pipe [29].

Using ANL's method [31], a short model magnet was fabricated and is shown in Figure 8. The short model magnet has 11 poles and is dry wound using high-performance 2G-HTS tape obtained from SuperPower, Inc. A current value of 800 A [29] was reached

on this prototype. Using the same method, a second short prototype magnet was later fabricated that reached 875 A; this was limited by the power supply. Nevertheless, this current corresponds to a J_w of ~ 2150 A/mm². It is important to note that there is a steady increase in the J_w and these levels are higher than both Nb₃Sn and NbTi.

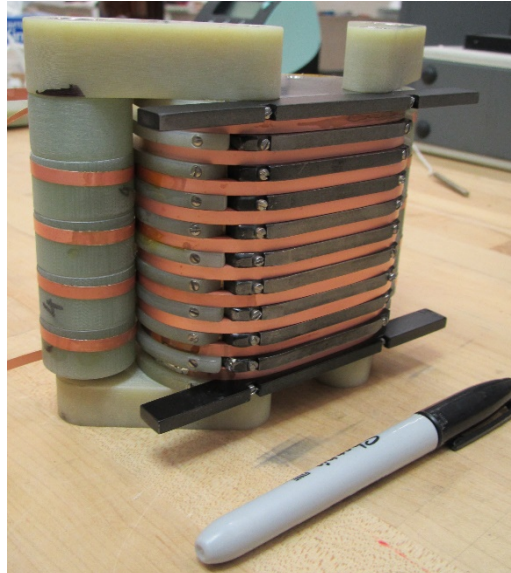


Figure 8: ANL's 2G-HTS wound short model (prototype) undulator magnet. It has 5 periods with a period length of 17.4 mm.

In addition to improved undulator performance, an important benefit arises from the high-transition temperature of the 2G-HTS conductors, which enables operation at a temperature higher than 4.2 K, thereby making possible the use of cryogen-free cryostats, and enabling the use of a less complex and cheaper cooling system than what is currently required for NbTi magnets.

The remaining challenges related to 2G-HTS technology that impede its full adaptation to SCU technology are as follows. Quench detection and protection requirements are different from the Nb-based superconductors, and proper solutions need to be developed. Since the normal zone propagation velocity is one to two orders of magnitude slower in 2G-HTS tapes than in Nb-based superconductors, to avoid damage of the HTS tape, quench detection in an HTS magnet needs a fast response time with a smaller quench detection voltage threshold. Current must decay fast without damaging the conductor and without exceeding the safe voltage limits. Also the shielding current induced field errors can be a potential problem for an SCU device that increases the phase errors. Remedies for removing these errors are proposed, which could be applied to the undulator magnets. Delamination is also a long-standing problem. This weak mechanical behavior causes damage to the magnets. Currently, available piece-length conductor is limited, but efforts show that this will be resolved in a few years as the companies have made significant progress over the past couple of years. It is feasible to expect production of reasonable long-length conductors, suitable for an undulator magnet, with uniform properties, soon. 2G-HTS tapes offer unique features to undulator technology; however, these problems need to be addressed before this technology is used in a fully functional device.

2.5.3 Conclusion and Outlook

Over the last decade SCUs have been designed and fabricated using NbTi superconductors. These devices successfully and reliably operate at 3rd generation light sources around the world. Such encouraging results call for future development of SCUs with higher B_0 and smaller period lengths, about 10 mm, which in turn requires deployment of different superconducting wires or tapes with higher J_w s.

One such material, Nb₃Sn, is mainly used for high-field magnets such as NMR and also is considered a front-runner candidate for future accelerator magnets such as the Future Circular Collider (FCC). These future projects demand further improvements on the current Nb₃Sn technology [32]. Developments on the performance increase are very promising [33, 34] and might potentially increase the J_w to even higher levels. Once a functional device is demonstrated, further optimization of both Nb₃Sn wire and SCU magnet technology could make significant performance increase. Recently APS has begun extensive effort toward developing a Nb₃Sn-based SCU. These technological developments are now approaching a point where a fully functional device could be fabricated and installed in the storage ring to serve user operations. It is expected to have the first Nb₃Sn undulator installed on the APS storage ring in the next two years.

Another even more rewarding direction in SCU developments is exploration of 2G-HTS technology for SCU magnets. Current performance of 2G-HTS tapes already exceeds the Nb-based superconductors, and further improvements in J_w of commercial 2G-HTS tapes can be achieved by geometrical and microstructural modifications. For instance, thinner substrate tapes (by about 20%) are now commercially available and they can substantially increase the J_w about 60% over NbTi wires (Figure 2). In addition, thicker 2G-HTS films have been grown with the linear I_c increased up to a thickness of about 4 μ m. Such an increase doubles the J_w value and brings unprecedented opportunities in SCU technology. It is important to note that the Nb-based materials are likely approaching their limits, and their performance levels are falling substantially below than those of the 2G-HTS materials. There is a continuous improvement in 2G-HTS technology, and it seems inevitably that this technology will be the main driver for future technologies. With improvement of the weak mechanical properties and advancements in production quantity of 2G-HTS tapes, reaching record high fields at 10 mm and smaller periods could be a breakthrough in the undulator technology.

SCUs represent the cutting edge in undulator technology. They have the potential to bring flexibility in adopting new magnet geometries and, in combination with deployment of high J_w superconductors, would improve the efficiency and versatility of light sources. There is a strong chance that in the future SCUs will dominate in SR- and FEL-based light sources.

2.5.4 References

1. E. Gluskin and N. Mezentsev, "Superconducting Wigglers and Undulators," in *Synchrotron Light Sources and Free-Electron Lasers: Accelerator Physics, Instrumentation and Science Applications*, E. Jaeschke, S. Khan, J. R. Schneider, and J. B. Hastings Eds., Cham: Springer International Publishing, 2019, pp. 1-51.
2. J. Bahrtdt and E. Gluskin, "Cryogenic permanent magnet and superconducting undulators," *Nucl. Instrum. Methods A* **907** 149 (2018).
3. L. R. Elias, W. M. Fairbank, J. M. J. Madey, H. A. Schwettman, and T. I. Smith,

- “Observation of Stimulated Emission of Radiation by Relativistic Electrons in a Spatially Periodic Transverse Magnetic Field,” *Phys. Rev. Lett.* **36**(13) 717 (1976).
4. L. R. Elias and J. M. Madey, “Superconducting helically wound magnet for the free-electron laser,” *Rev. Sci. Instrum.* **50**(11) 1335 (1979).
 5. A. S. Artamonov et al., “First results of the work with a superconducting “snake” at the VEPP-3 storage ring,” *Nucl. Instrum. Methods* **177**(1) 239 (1980).
 6. D. A. G. Deacon et al., “Gain Measurement on the ACO Storage Ring Laser,” *IEEE Trans. Nucl. Sci.* **28**(3) 3142 (1981).
 7. M. Bazin, Y. Farge, M. Lemonnier, Y. Petroff, and J. Perot, “Design of an undulator for ACO and its possible use as free electron laser,” *Nucl. Instrum. Methods* **172**(1/2) 61 (1980).
 8. S. Casalbuoni et al., “Characterization and long term operation of a novel superconducting undulator with 15 mm period length in a synchrotron light source,” *Phys. Rev. Accel. Beams* **19**(11) 110702 (2016).
 9. Y. Ivanyushenkov et al., “Status of the Development of Superconducting Undulators at the Advanced Photon Source,” *Synchrotron Radiation News* **31**(3) 29 (2018).
 10. Y. Ivanyushenkov et al., “Development and operating experience of a 1.1-m-long superconducting undulator at the Advanced Photon Source,” *Phys. Rev. Accel. Beams* **20**(10) 100701 (2017).
 11. Y. Ivanyushenkov et al., “Development and operating experience of a short-period superconducting undulator at the Advanced Photon Source,” *Phys. Rev. ST Accel. Beams* **18**(4) 040703 (2015)
 12. S. Casalbuoni et al., “Test of Short Mockups for Optimization of Superconducting Undulator Coils,” *IEEE Trans. Appl. Supercond.* **24**(3) 1 (2014).
 13. J. Xu et al., “Development of a Superconducting Undulator Prototype at the SSRF,” *IEEE Trans. Appl. Supercond.* **27**(4) 1 (2017).
 14. A. V. Zlobin, E. Barzi, D. Turrinoni, Y. Ivanyushenkov, and I. Kesgin, “Advantages and Challenges of Nb₃Sn Superconducting Undulators,” in *Proc. 9th International Particle Accelerator Conference, Vancouver, BC, Canada, 2734-2737, WEPML025* (2018).
 15. D. Arbelaez, Private communication, 2019.
 16. S. H. Kim, C. L. Doose, R. L. Kustom, and E. R. Moog, “Development of Short-Period Nb₃Sn Superconducting Undulators for the APS,” *IEEE Trans. Appl. Supercond.* **18**(2) 431 (2008).
 17. H. W. Weijers, K. R. Cantrell, A. V. Gavrilin, E. L. Marks, and J. R. Miller, “Assembly Procedures for a Nb₃Sn Undulator Demonstration Magnet,” *IEEE Trans. Appl. Supercond.* **17**(2) 1239 (2007).
 18. I. Kesgin et al., “Development of Short-Period Nb₃Sn Superconducting Planar Undulators,” *IEEE Trans. Appl. Supercond.* **29**(5) 1 (2019).
 19. D. R. Dietderich et al., “Fabrication of a Short-Period Nb₃Sn Superconducting Undulator,” *IEEE Trans. Appl. Supercond.* **17**(2) 1243 (2007).
 20. S. O. Prestemon et al., “Design, fabrication, and test results of undulators using Nb₃Sn superconductor,” *IEEE Trans. Appl. Supercond.* **15**(2) 1236 (2005).
 21. T. Holubek et al., “Magnetic Performance of a Laser Structured YBCO Tape Suitable for Insertion Devices Technology,” *IEEE Trans. Appl. Supercond.* **23**(3) 4602204 (2013).

22. S. Prestemon et al., "Development and Analysis of HTS-Undulator Components for FEL Applications," *IEEE Trans. Appl. Supercond.* **21**(3) 1880 (2011).
23. C. Boffo et al., "Industrial experience on Superconducting Undulators," SRI-Workshop on SC Undulators, Argonne National Laboratory, Sept. 20, 2010.
24. I. Kesgin et al., "Feasibility and electromagnetic analysis of a REBCO superconducting undulator," *Superconductor Science and Technology* **29**(5) 055001 (2016).
25. I. Kesgin, C. L. Doose, M. T. Kasa, Y. Ivanyushenkov, and U. Welp, "Design of a REBCO thin film superconducting undulator," *IOP Conference Series: Materials Science and Engineering* **101** 012053 (2015).
26. G. Majkic, R. Pratap, A. Xu, E. Galstyan, and V. Selvamanickam, "Over 15 MA/cm² of critical current density in 4.8 μm thick, Zr-doped (Gd,Y)Ba₂Cu₃O_x superconductor at 30 K, 3T," *Scientific Reports* **8**(1) 6982 (2018).
27. G. Majkic et al., "Engineering current density over 5 kA mm⁻² at 4.2 K, 14 T in thick film REBCO tapes," *Superconductor Science and Technology* **31**(10) 10LT01 (2018).
28. I. Kesgin et al., "Feasibility and electromagnetic analysis of a REBCO superconducting undulator," *Superconductor Science and Technology* **29**(5) 055001 (2016).
29. I. Kesgin, M. Kasa, Y. Ivanyushenkov, and U. Welp, "High-temperature superconducting undulator magnets," *Superconductor Science and Technology* **30**(4) 04LT01 (2017).
30. I. Kesgin, N. Khatri, Y. Liu, L. Delgado, E. Galstyan, and V. Selvamanickam, "Influence of superconductor film composition on adhesion strength of coated conductors," *Superconductor Science and Technology* **29**(1) 015003 (2015).
31. I. Kesgin, U. Welp, C. L. Doose, M. Kasa, and Y. Ivanyushenkov, "Continuous winding magnets using thin film conductors without resistive joints," US Patent 10249420 Patent Appl. 2017/0162309, Apr. 2, 2019, 2017. [Online]. Available: <https://www.google.com/patents/US20170162309>
32. A. Ballarino and L. Bottura, "Targets for R&D on Nb₃Sn Conductor for High Energy Physics," *IEEE Trans. Appl. Supercond.* **25**(3) 1 (2015).
33. S. Balachandran et al., "Beneficial influence of Hf and Zr additions to Nb₄Ta on the vortex pinning of Nb₃Sn with and without an O source," *Superconductor Science and Technology* **32**(4) 044006 (2019).
34. X. Xu, P. Li, A. V. Zlobin, and X. Peng, "Improvement of stability of Nb₃Sn superconductors by introducing high specific heat substances," *Superconductor Science and Technology* **31**(3) 03LT02 (2018).

2.6 Superconducting Undulator Developments at Lawrence Berkeley National Laboratory

Diego Arbelaez, Scott Myers, Xiaorong Wang, Marcos Turqueti, Heng Pan,
Ross Schlueter, Soren Prestemon

Mail to: darbelaez@lbl.gov

Lawrence Berkeley National Laboratory

2.6.1 Introduction

Superconducting undulators have been considered for synchrotron radiation sources since the late 1970s [1]. The development of permanent magnet (PM) undulator systems by Klaus Halbach at LBNL in the early 1980s resulted in tremendous growth in PM undulators, and ushered in the era of 3rd generation storage rings. Today, most undulators installed in storage rings and FELs around the world are PM devices. However, as superconducting undulator technology has progressed, the potential of SCUs for light sources has re-emerged as they outperform PM devices over a significant range of period length and gap. Significant work has gone into the development of NbTi SCUs, and they are now operating at the Advanced Photon Source [2] in the US and at ANKA [3] in Germany. At LBNL, the main focus on superconducting undulator research and development has been through the use of the superconductor Nb₃Sn. Higher current densities can be obtained with Nb₃Sn when compared to NbTi, leading to higher magnetic field for a similar undulator configuration. For example, Figure 1 shows the expected effective magnetic field at different period lengths for NbTi and Nb₃Sn devices. However, Nb₃Sn is a brittle superconductor that must be reacted at high temperature, making the process of coil fabrication more complicated.

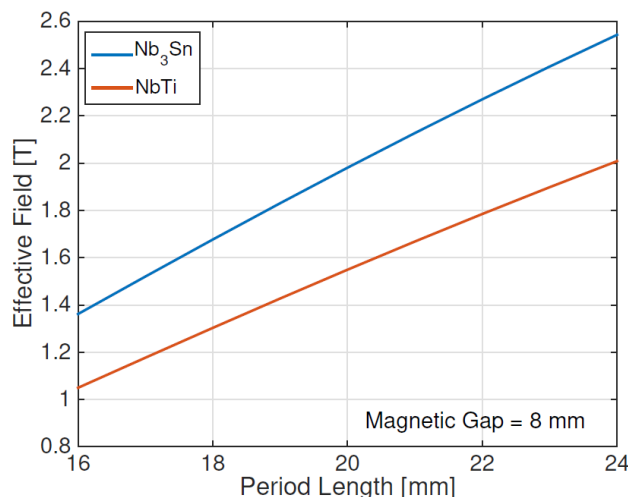


Figure 1: Calculated magnetic field strength for Nb₃Sn and NbTi undulators for different period lengths and a magnetic gap of 8.0 mm.

Initial work on short undulator prototypes at LBNL in 2007 [4] demonstrated Nb₃Sn conductors could be used at low field and high current density, as is required for undulators. An R&D collaboration between SLAC, ANL, and LBNL took place from 2014 to 2016 [5], in order to demonstrate that SCUs are viable for use in FELs. As part

of this collaboration, LBNL was responsible for fabricating a 1.5 m long Nb₃Sn undulator that is compatible with the Linac Coherence Light Source upgrade project (LCLS-II) and a novel system for correcting magnetic field errors. Table 1 shows the undulator design parameters. The test cryostat and magnetic measurement systems were developed and fabricated at ANL, along with a 1.5 m long NbTi undulator that is compatible with the LCLS-II. The Nb₃Sn undulator was tested in the ANL facility, but it did not reach its intended design field due to a low performing coil. A replacement coil was fabricated after the collaboration was complete. After reassembling the undulator with the new coil, the target current was achieved. This work will describe the Nb₃Sn undulator design, fabrication, and test results from the R&D collaboration. The novel magnetic field correction system is also presented.

Table 1: Nb₃Sn undulator parameters.

<i>Undulator Parameter</i>	<i>Value</i>
period length	19.0 mm
magnetic gap	8.0mm
maximum B _{eff}	1.83 T
number of periods	73
conductor type	Nb ₃ Sn
wire diameter	0.6 mm
current at max, B _{eff}	780 A

2.6.2 SCU Design

For the magnetic design of the periodic section, the objective is to meet the required on-axis magnetic field strength while ensuring that the operating point has sufficient margin relative to the critical surface of the superconductor. For the design of the conductor layout, the load line margin was used as the criterion for choosing the size of the coil pack relative to the period length. For the coil pack optimization, a two dimensional, one-quarter period, finite element model was created within the software package Vector Fields Opera. The model is parametric with the following key parameters: period length, magnetic gap, number of winding turns in the horizontal direction, number of winding turns in the vertical direction, and yoke height. The period length and magnetic gap are fixed for the design based on the chosen design requirements. The yoke height was chosen to be sufficiently large to avoid saturation of the steel at the center of the undulator core. The free parameters in the optimization are the number of horizontal and vertical turns in the coil pack. The coil pack size was calculated assuming that the insulation thickness is 60 μm and the turns are arranged in a close packed structure.

Figure 2 shows load line for the final coil pack design, which has eight turns and seven layers per pocket. The addition of more vertical turns gives a small further reduction in margin; however, it is at the expense of a substantial increase in the length of the wire. A reasonable solution would also be to have only five vertical turns, but this would raise operating current in the wire. At the time of the design, there were concerns about low field instabilities in the conductor so the lower operating current point that is achieved with seven vertical turns was chosen. The target field strength of 1.83 T is achieved with a current of 780 A, which is slightly less than 80% of short sample.

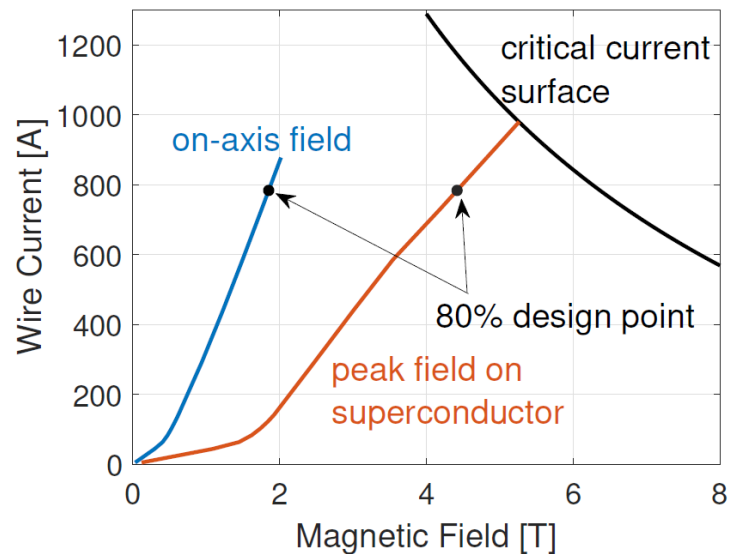


Figure 2: Load line for the Nb₃Sn undulator with the chosen coil pack configuration. The target magnetic field is achieved at approximately 80% of the short sample limit.

2.6.3 SCU Fabrication

The magnetic design is based on a solid low carbon steel mandrel structure into which grooves are machined to accommodate the coils. The result is a single structure that provides all of the magnetic and structural characteristics of a half-undulator. Figure 3 shows the mechanical design of the undulator. The left side of Figure 3 shows the single-piece mandrel, the end section where the Nb₃Sn wire is spliced to a NbTi cable, and a decoupled end-kick corrector. A secondary corrector coil is wound into the first and last pocket of the undulator to compensate for distributed field effects that are present across the gap. The leads for these correctors are also shown in the joint section in Figure 3. On the right picture, the winding reversal scheme is shown. Roll pins are pressed into the side of the undulator cores to capture the wire as the winding direction is reversed from pocket to pocket.

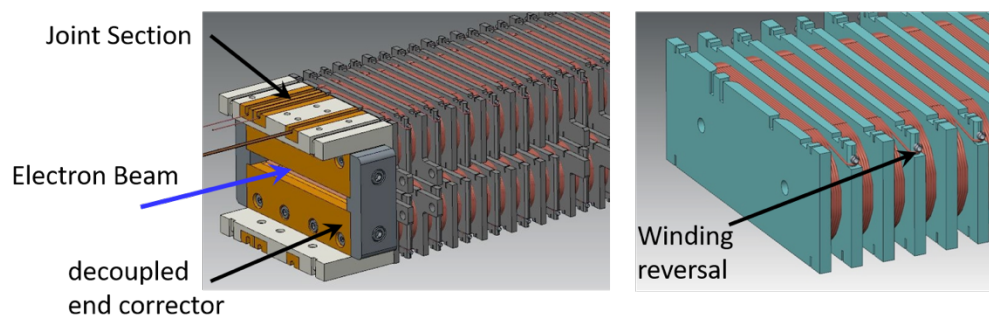


Figure 3: The mechanical design of the undulator incorporates the single piece mandrel, the end correctors, and the joint section where NbTi leads are soldered to the Nb₃Sn wire.

The figure on the right shows the turn-around scheme for reversing the winding direction from pocket to pocket.

Figure 4 (top) shows the undulator core after machining. Coordinate Measuring Machine (CMM) measurements showed that the stringent tolerances that are required to achieve high field quality are met. In order to ensure that the electrical integrity of the coil is maintained after a quench, an electrically insulating coating on the magnet cores is desirable. Since the coils must go through a high temperature heat treatment, this sets a restriction on the materials that can be used for the coating. After several trials of different possible insulations, a plasma spray coating of Aluminum Oxide was selected. The uniformity of the coating during the trials was verified with CMM measurements in order to ensure that it would not have a significantly detrimental effect on the field quality. Figure 4 (bottom) shows the undulator core after the insulation was applied.

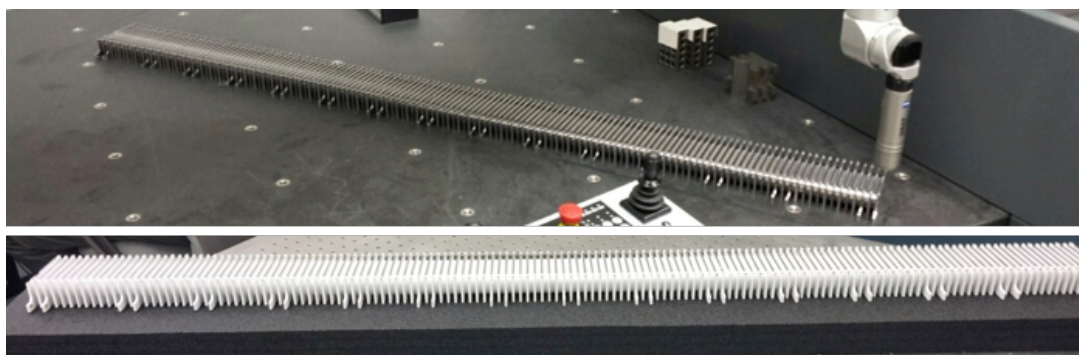


Figure 4: The machined mandrels were measured on a CMM to ensure that they meet the stringent manufacturing requirements. An electrically insulating Aluminum Oxide coating was applied to mandrels before winding (bottom).

The half-undulator is wound from a single continuous length of wire with alternating wire directions in neighboring coil packs. A rod and restack process (RRP) wire from Oxford Instruments Scientific Technology (OST) with a diameter of 0.6 mm and filaments that are less than 40 μm in diameter is used in order to avoid low field instabilities. Short sample measurements on the wire showed that the conductor is stable for currents exceeding 1300 A. Insulation in the form of an S-glass braid with a thickness of 55 μm was used to electrically isolate the wire. Several braiding trials, in collaboration with New England Wire, were performed in order to obtain this thin yet robust braid insulation.

The coil processing involved the winding of the conductor on the steel core followed by a heat treatment at 650 $^{\circ}\text{C}$. Figure 5 (top) shows the winding machine that was used to accurately place the windings in each groove of the undulator. Each pocket contains 56 turns, and a total of 1.6 km of wire are used for each undulator half. Following the winding, the coil is placed in special tooling for the heat treatment. Figure 5 (lower left) shows the coil and tooling assembly inside of a retort, which is used to ensure that a high quality inert atmosphere is maintained during heat treatment. The assembly tooling was carefully designed in order to minimize the distortion of the coils during heat treatment. Once the heat treatment is complete, NbTi lead cables are soldered at the ends of the undulator coil and the coil is impregnated with epoxy, as shown in Figure 5 (lower right).

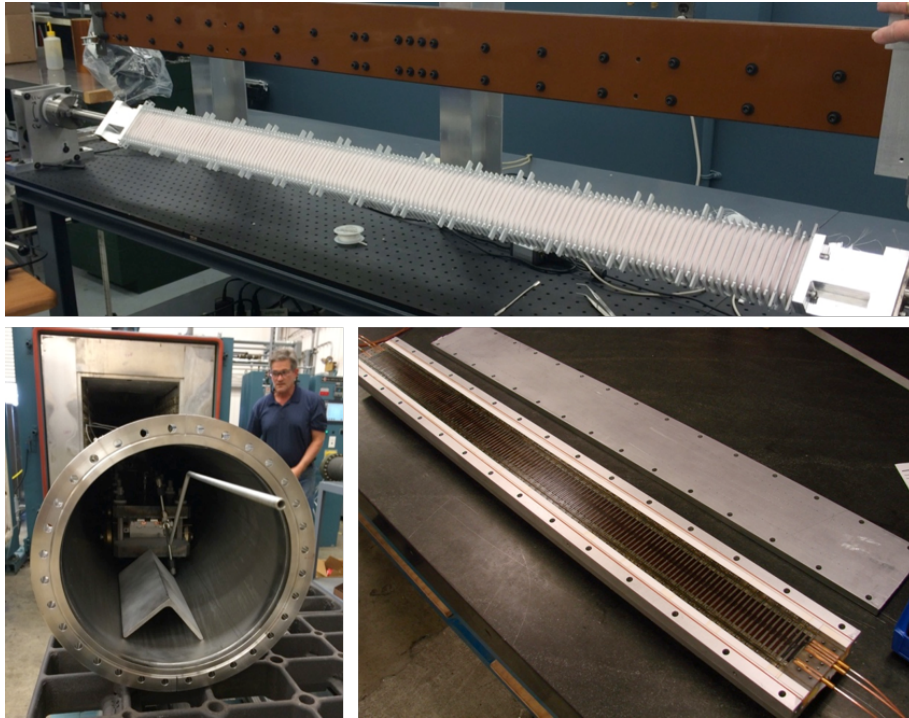


Figure 5: The coil fabrication process includes the precise winding (top), heat treatment (lower left), and epoxy impregnation (lower right).

After fabrication, the individual coils were first tested in a vertical liquid helium dewar and trained close to the operating current. Once testing of the individual coils was complete, the system was assembled for testing in the ANL cryostat. The undulator was designed in order to have a seamless integration into the ANL test cryostat. Special cooling plates were designed to integrate with the liquid helium transfer system of the cryostat. The undulator is cooled through these plates, making the thermal interfaces critical in order to meet the cryogenic performance requirements. The plates are segmented in order to minimize the effect of thermal contraction between the different materials, and they are thermally connected to a liquid helium pipe with flexible copper links. Indium strips were added between the bare steel poles on the back of the magnet cores and the copper plates in order to ensure proper thermal contact. Figure 6 shows the full undulator assembly including the two undulator coils, the cooling plates, the gap spacers, the decoupled end correctors, and the undulator vacuum chamber.

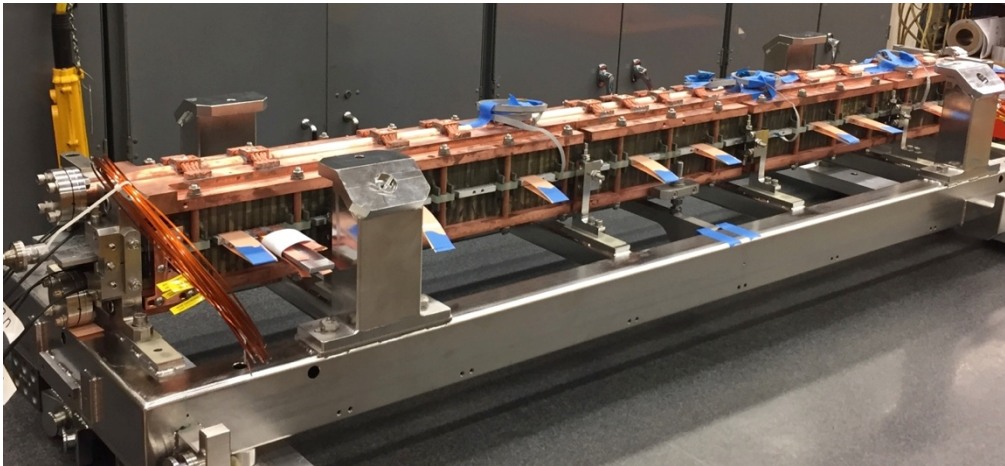


Figure 6: The full magnet assembly consists of the two undulator coils, gap spacers, cooling plates, clamping rods, and end correctors.

2.6.4 Magnet Training

After fabrication, the individual cores were tested in a vertical liquid helium dewar. The first undulator coil had a first quench at 696 A and reached 766 A after two quenches before the testing was stopped. The second undulator coil reached a peak value of 729 A after 80 quenches. It is not completely clear why such a vastly different training behavior was seen between the two coils, but it is suspected to be due to different epoxy impregnation temperatures. The two coils were assembled and sent to ANL for testing in the measurement cryostat. During the test, it was found that the current could not go beyond 535 A due to consistent quenching in coil 1. The magnetic measurements were performed at a maximum current of 500 A, and the test was stopped since the target current was not achieved. After transporting the undulator back to LBNL, a new coil was fabricated (coil 3) and the undulator was reassembled with coils 2 and 3. Coil 3 was first trained in single coil configuration to 766 A after 45 quenches. The two coils were then powered in the full undulator mode (i.e., coils powered in series) and the target current was reached after 27 quenches. Figure 7 shows the training quench current for the full undulator assembly with coils 2 and 3. This demonstrated the successful operation of the undulator in terms of achieving the target current.

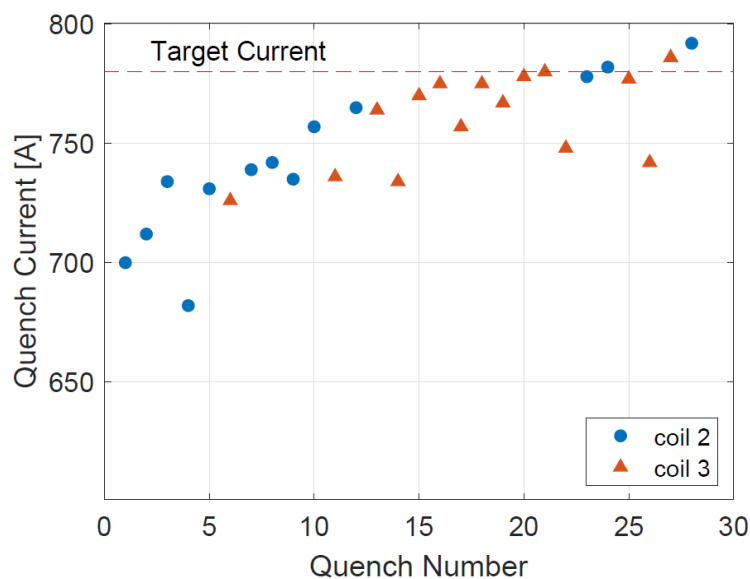


Figure 7: After individual coil training, the full undulator assembly required 27 quenches to reach the target current. This test was performed in a vertical LHe dewar at LBNL.

2.6.5 Magnetic Measurements

Figure 8 shows the measured magnetic field of the Nb₃Sn undulator at a current of 500 A in the ANL cryostat. For this configuration the on-board end correctors are powered to a current of 2.5 A, and the decoupled end correctors are not used. The measurements were performed using the Hall probe system. The first integral is derived directly from the Hall probe data without corrections from the stretched wire coil. The second integral is corrected numerically to remove the first integral offset inside the undulator. This error component can be corrected with the decoupled end correctors, however, they were not energized at this time. The field measurement results demonstrate that reasonable electron trajectories can be achieved with Nb₃Sn undulators.

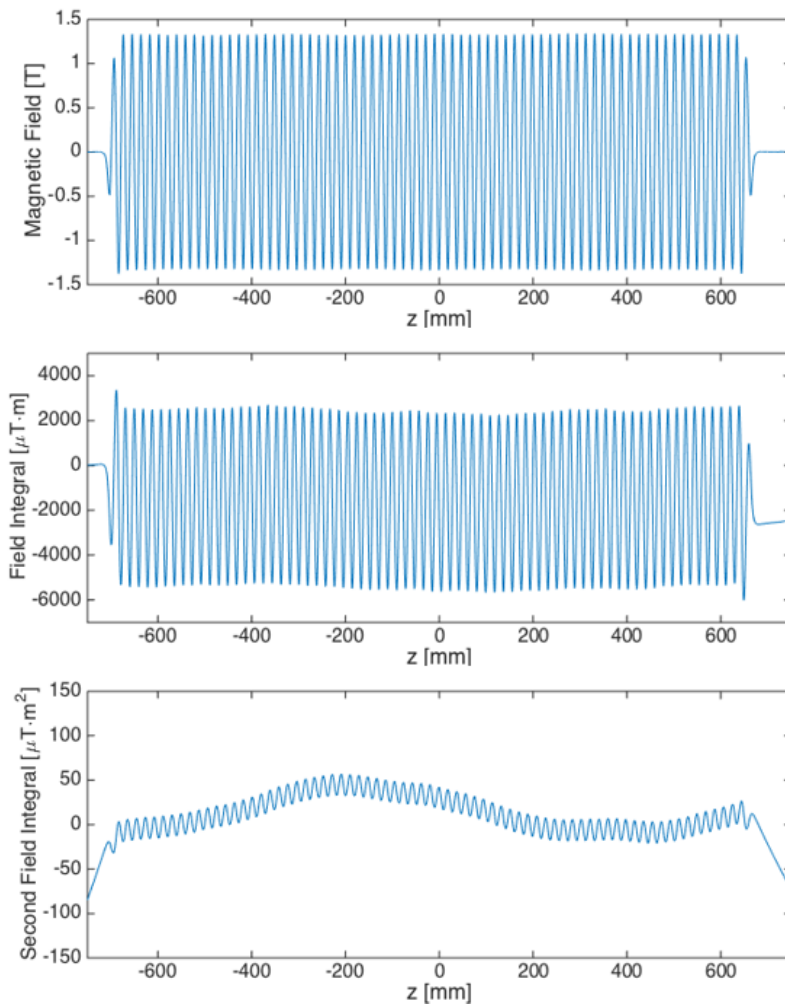


Figure 8: Magnetic field measurements were performed at a current of 500 A in the ANL measurement facility. These measurements demonstrate that reasonably good field quality (without any corrections) can be obtained with Nb₃Sn superconducting undulators.

2.6.6 Local Field Error Correction System

For superconducting undulators, in order to reduce magnetic field errors, much of the focus is placed on accurate winding methodologies and machining processes (e.g., [2]). Nevertheless, for long devices, correction methods may still be necessary depending on the allowed tolerances for the electron trajectories and phase errors. In a superconducting undulator, typical correction methods include a variety of on-board and decoupled end correctors, for example, as shown in [2]. Here, a novel method is presented for trajectory correction and phase correction in the periodic section of the undulator. Different methods to correct local field errors have been previously proposed by several researchers. For example, the use of passive shim coils [6] and methods where the iron pole geometry is modified [7]. Active methods have also been proposed that combine trim coils [8] and active switching networks [9] in order to perform in-situ corrections of errors at specific locations in a device. This concept was first pursued using the high temperature superconductor YBCO in [10]. The use of YBCO has the advantage that the

superconductor is available in the form of a thin tape and it is readily available from commercial sources. In this work a method is presented where YBCO tapes are patterned into single-turn coils that can be actively switched using heaters. This allows for in-situ correction of errors at desired locations along the length of the undulator.

The tuning scheme presented here uses single-turn coils and superconducting switches in order to correct the magnetic field at specific locations along the periodic section of the device. All of the single-turn coils are wired in series such that, when activated, the current through all coils is the same. The coils can be activated by using heater switches that divert the current from a bypass path to the individual single-turn coils. Therefore, the correction is performed with a single variable current source and variable on/off single-turn coils that can be activated at the desired locations along the length of the device. This type of concept has the advantage that it can be used to tune the undulator in-situ while magnetic measurements are performed on the device.

A switching scheme that uses YBCO tapes with resistive joints and active heaters has been developed for the tuning of the undulator prototypes. Figure 9 shows a diagram of this concept, which includes the main tape, the soldered single-turn coil tapes (low resistance joints), and the switching heaters. As is shown in the figure, when the heaters are off the current bypasses the single-turn coils since the top path is superconducting. Once a heater is turned on, a majority of the current (>99%) now goes through the single-turn coil for undulator field correction. This is the case since the resistance of the top path in the normal state is much higher than the resistance of the joint between the two soldered tapes.

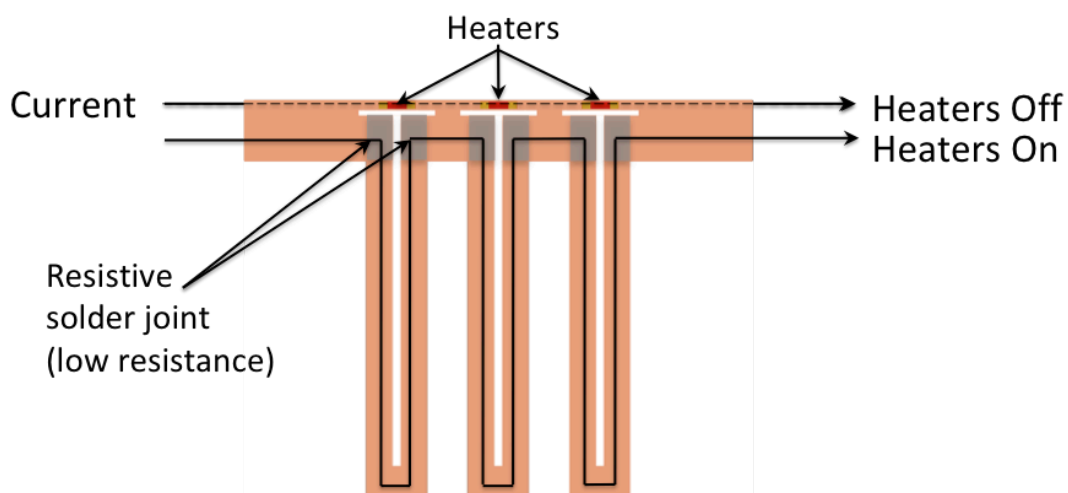


Figure 9: A field correction method has been developed that uses YBCO current loops that are centered on the undulator poles, to modify the local field of the undulator. Heaters are used to turn the correction on at desired loops along the length of the device.

In order to incorporate the correction system for the undulator test, the YBCO correctors must be attached to the vacuum chamber. A vacuum bag process was used in order to ensure an even surface after adhesion with a thin glue line. The corrector system added approximately 0.2 mm to each side of the vacuum chamber. Figure 10 (left) shows the segments, which were fabricated using lithography and etching to generate the loops, soldering to adhere the heaters and create the low resistance electrical connections, and laser cutting to separate the ends of the current loops. The segments were subsequently

wired with the flexible circuit boards (middle) and adhered to the surface of the vacuum chamber (right).

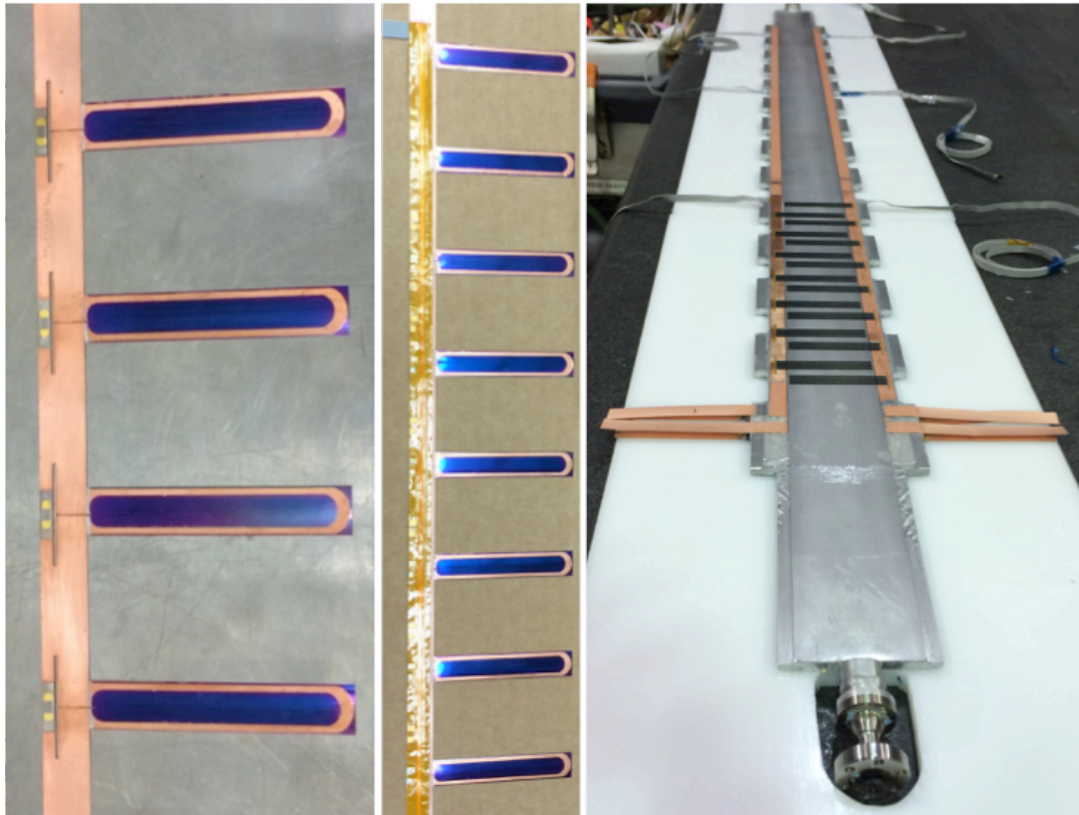


Figure 10: The local correctors are adhered to the vacuum chamber surface with epoxy, using a vacuum bag process.

Figure 11 (top) shows the magnetic field generated due to the activation of six correctors along the length of the device at 100 A. The shaded area represents the locations where correctors were available. Due to some fabrication issues and time constraints, the correctors were applied to the first and last third of the vacuum chamber, and they were only present on one side of the chamber. Therefore, the correctors were only available over two-thirds of the device at one-half of their nominal strength. The bottom graphic in Figure 8 shows the change in phase error obtained from the applied corrections. It can be seen that even with the limited location and strength the RMS phase error is reduced from 9.2° to 5.4° . This successful test demonstrates the ability to correct the magnetic field in a superconducting undulator with an active system.

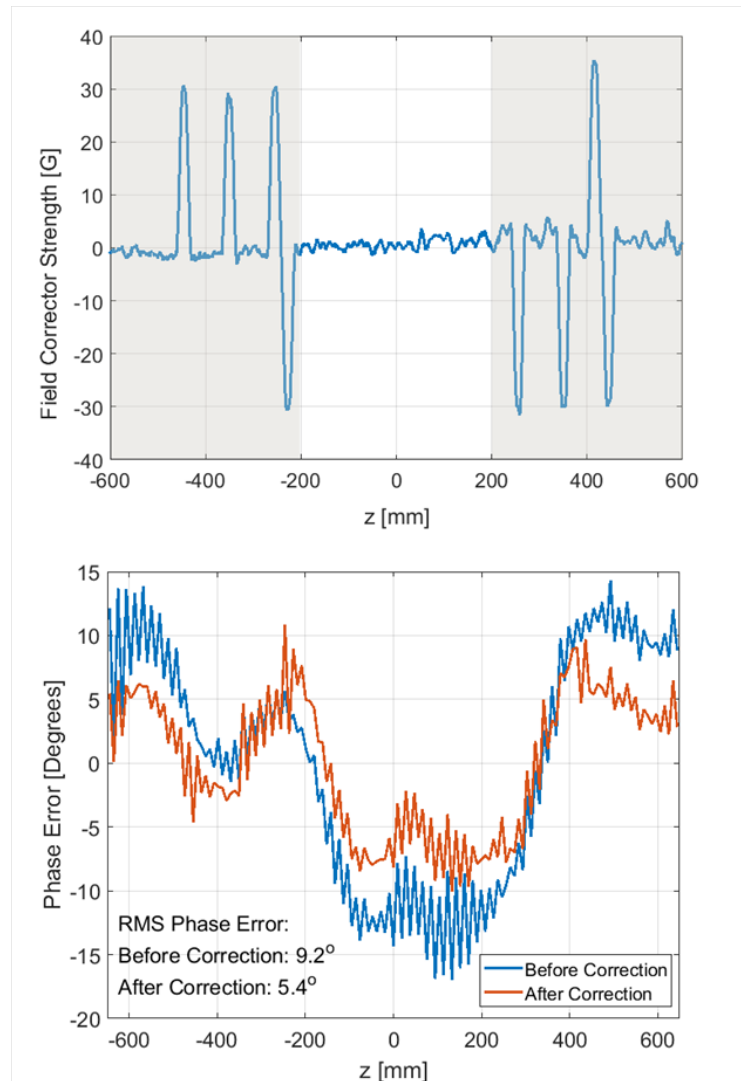


Figure 11: The local field correctors are used to improve the phase error in the device. The shaded areas in the top graphic represent the locations where corrector loops were available for the test.

2.6.7 Conclusions

In this work, the development of Nb_3Sn undulators was advanced with the fabrication of a full-length device. This demonstrated that many of the technical hurdles, due to the added complexity of the high temperature heat treatment, can be overcome. The magnetic measurements also demonstrate that stringent tolerances can be maintained through the heat treatment and that good field quality can be achieved. The phase error in the device could be further improved by better control of the undulator gap since the present errors are smooth. Alternatively, the novel correction method that was developed can be used for in-situ correction of superconducting insertion devices.

2.6.8 References

1. L.R. Elias and J.M. Madey, "Superconducting helically wound magnet for the free-electron laser," *Rev. Sci. Instrum.* **50** (1979).
2. Y. Ivanyushenkov et al., "Development and operating experience of a 1.1-m-long superconducting undulator at the Advanced Photon Source," *Phys. Rev. AB* **20** 100701 (2017).
3. "Overview of the superconducting undulator development program at ANKA," *AIP Conference Proceedings* **1741** 020002 (2016).
4. D.R. Dietderich et al., "Fabrication of a Short-Period Nb₃Sn Superconducting Undulator," *IEEE Trans. on Appl. Supercond.* **17**(2), 1243 (2007).
5. P. Emma et al., "A Plan for the Development of Superconducting Undulator Prototypes for LCLS-II and Future FELs," in *Proc. FEL2014, Switzerland, 2014*, paper THA03, pp. 649-653 (2014)
6. D. Wollmann, A. Bernhard, P. Peiffer, and T. Baumbach, "Experimental demonstration of the induction-shimming concept in superconductive undulators," *Phys. Rev. AB* **12**(4), 040702 (2009).
7. S. Chunjarean, J. C. Jan, C. H. Hwang, P. H. Lin, and H. Wiedemann, "A new field correction scheme for superconducting undulators by modification the iron pole geometry," *Superconductor Science and Technology* **24**(5) 055013 (2011).
8. S. O. Prestemon et al., "Design, fabrication, test results of undulators using Nb₃Sn superconductor," *IEEE Trans. Appl. Superconductivity* **15**(2) 1236 (2003).
9. A. Madur, F. Trillaud, D. Dietderich, S. Marks, S. Prestemon, and R. Schlueter, "Superconducting switch concept applied to superconducting undulator phase-error correction," *AIP Conf. Proc.* **1234** 552 (2010).
10. D. Arbelaez et al., "Magnetic Field Correction Concepts for Superconducting Undulators," *IEEE Trans. Appl. Supercond.* **23**(3) 4100104 (2013).

3 Workshop and Conference Reports

3.1 ICFA mini-Workshop on “Mitigation of Coherent Beam Instabilities in Particle Accelerators” (MCBI 2019)

Elias Métral (CERN), Tatiana Pieloni (EPFL) and Giovanni Rumolo (CERN),
IOC Chairs MCBI 2019

From 23-27 September 2019, more than 90 world experts gathered in the small village of Zermatt in Switzerland for the ICFA mini-Workshop on “Mitigation of Coherent Beam Instabilities in Particle Accelerators” (MCBI 2019) to discuss all the mitigation methods for all the coherent beam instabilities, to try and provide the simplest and more robust solutions for the day-to-day operation of the machines (see Fig. 1). Three quarters of the participants were coming from Europe while the last quarter was split between USA and Asia (see Fig. 2). This workshop was dedicated to our two esteemed colleagues and distinguished accelerator physicists, Yong Ho Chin and Albert Hofmann, who recently passed away and who will be greatly missed (see Fig. 3).



Figure 1: Group photo showing many of the 92 participants.

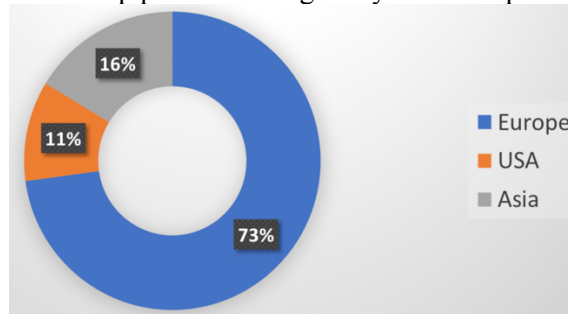


Figure 2: MCBI 2019 participation.

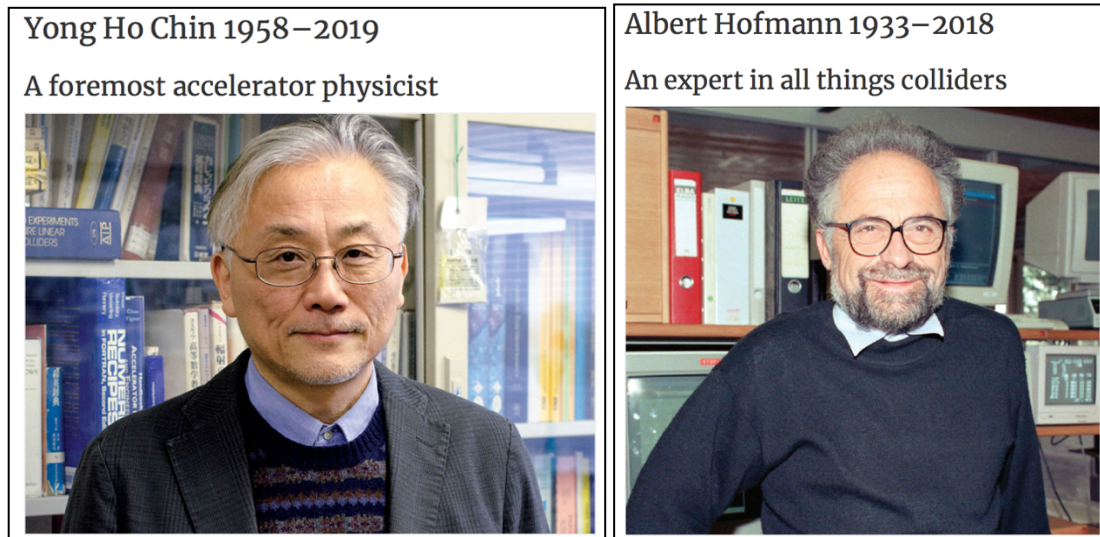


Figure 3: The MCBI 2019 workshop was dedicated to Yong Ho Chin and Albert Hofmann, two esteemed colleagues and distinguished accelerator physicists who will be greatly missed.

During the four-day workshop, 56 talks were given distributed in 8 sessions set up by the 27 members of the International Advisory Committee: (1) Review of beam instability mechanisms and mitigations, convened by G. Rumolo (CERN); (2) Landau and BNS damping, convened by E. Métral (CERN); (3) Optics and RF knobs, convened by E. Shaposhnikova (CERN); (4) Feedbacks, convened by G. Stupakov (SLAC); (5) Identification and reduction of instability sources, convened by M. Zobov (INFN LNF); (6) Diagnostics for instability observations, convened by T. Pieloni (EPFL); (7) Interplay between coherent and incoherent effects, convened by G. Franchetti (GSI); (8) Future challenges for MCBI, convened by F. Zimmermann (CERN).

In addition to the talks, 24 posters were presented. Student posters, 14 in total, have participated to the “Best Student Poster Award”, which was awarded to M. Schenk (see Fig. 4). The Poster Award Committee was composed of all the session conveners and was chaired by Q. Qin (IHEP).



Figure 4: “Best Student Poster Award” awarded to M. Schenk for his work on “Longitudinal-to-transverse Landau damping: RFQ (or Q)”. Next to him: Q. Qin (IHEP), chair of the Poster Award Committee.

The detailed program and talks are available via the workshop website: <https://indico.cern.ch/event/775147/>. We would like to thank all the sponsors (<https://indico.cern.ch/event/775147/attachments/1797894/3222764/Sponsors.pdf>), who with their contributions made it possible to organize the workshop in this beautiful location. The Swiss Institute for Accelerator Research and Technology (CHART) together with EPFL supported and sponsored the students’ participation to the workshop by offering a reduced registration fee and the best student poster prize.

3.2 The 63rd ICFA Advanced Beam Dynamics Workshop on Energy Recovery Linacs, ERL2019

Alexander Matveenko and Atoosa Meseck, Helmholtz-Zentrum Berlin, Germany
 Mail to: aleksandr.matveenko@helmholtz-berlin.de, atoosa.meseck@helmholtz-berlin.de

Energy recovery linacs generate a lot of interest in the accelerator and user communities as the recent 63rd ICFA Advanced Beam Dynamics Workshop on Energy Recovery Linacs (ERL2019, https://www.helmholtz-berlin.de/events/erl19/index_en.html) has demonstrated. The workshop was held at Helmholtz-Zentrum Berlin, Germany from September 15th to 20th, 2019 and was attended by 99 participants representing institutions from Asia, Europe and USA. ERL2019 was the 8th workshop in the series of international workshops covering accelerator physics and technology of Energy Recovery Linacs.

The scientific program of the workshop was set up by the International Program Committee, chaired by A. Matveenko (Helmholtz-Zentrum Berlin). The workshop was

hosted by Helmholtz-Zentrum Berlin, its Local Organizing Committee was chaired by A. Meseck and included J. Bierbaum, H. Ehmler, A. Matveenko, M. McAteer (editor), R. Schabardin, and J. Völker (editor).

65 talks were presented during plenary sessions. Along with “traditional” applications of ERLs such as X-ray light sources, FELs, electron-ion colliders, and electron coolers, many new proposals and ideas were presented at the workshop.

Especially pleasing was to hear about the positive developments in operation of the multiturn ERL based NovoFEL (Budker Institute of Nuclear Physics, Novosibirsk, Russia); excellent commissioning experience from CBETA (Cornell University, USA) and cERL (KEK, Japan). Detailed planning for MESA (Helmholtz Institute Mainz, Germany) was presented and MESA module integration and commissioning planning in bERLinPro (Helmholtz-Zentrum Berlin, Germany) was extensively discussed. Multi-turn upgrade of S-DALINAC was presented. The beam dynamics issues, operational experience with subsystems of the mentioned accelerators as well as ongoing developments were the topics of the corresponding working groups. ERL applications were discussed in two dedicated sessions.

The five working groups covered a wide spectrum of topics essential for ERLs.

WG1, convened by M. Abo-Bakr (HZB) and M. Arnold (TU Darmstadt), was dedicated to overview and status of the existing ERL facilities.

WG2, where conveners were G. Hoffstaetter (Cornell University) and P. Evtushenko (HZDR), addressed the optics, beam dynamics and instrumentation challenges in ERLs: lessons learnt from past and present ERL operation as well as issues arising during the design work on future ERL facilities.

WG3, convened by E. Wang (BNL) and L. Cultrera (Cornell University) was dealing with ERL electron sources and injectors exploring the results and new technologies available in injectors (lasers, cathodes, guns) since the previous ERL Workshop.

WG4 was organized by F. Gerigk (CERN) focused on Superconducting RF technology, RF control to identify the critical issues of each component in cryomodule construction, assembly works and beam operation for ERL.

Finally, D. Angal-Kalinin (STFC) and O. Brüning (CERN), conveners of WG5, arranged talks on potential applications of the ERL technology, covering a broad range of applications.

There was one poster session, where 23 posters have been presented.

A plenary session at the end of the workshop was devoted to the summary presentations from each working group.

The detailed program is available via the workshop website. The workshop proceedings will be published at JACoW.

Some statistics to the workshop venue are listed below:

By presentation type: Oral

Classification	Contributions
WG1: ERL facilities	9
WG2: ERL beam dynamics and instrumentation	16
WG3: Electron sources and injectors	14
WG4: Superconducting RF	16
WG5: ERL applications	10
Totals	65

By presentation type: Poster

Classification	Contributions
WG1: ERL facilities	1
WG2: ERL beam dynamics and instrumentation	7
WG3: Electron sources and injectors	10
WG4: Superconducting RF	2
WG5: ERL applications	3
Totals	23

Paper and contribution counts per session:

Session	Session title	paper	contribution
MOCOWBS	Workshop Opening and WG1: ERL facilities		2
MOCOXBS	WG1: ERL facilities	4	4
MOCOYBS	WG5: ERL applications	1	4
MOCOZBS	WG5: ERL applications		4
TUCOWBS	WG2: ERL beam dynamics and instrumentation		3
TUCOXBS	WG2: ERL beam dynamics and instrumentation	4	4
TUCOYBS	WG4: Superconducting RF		3
TUCOZBS	WG4: Superconducting RF	4	4
WECOWBS	WG3: Electron sources and injectors		3
WECOXBS	WG3: Electron sources and injectors	2	3
WEPNEC	Poster Session	12	23
WECOYBS	Mixed Session	1	4
THCOWBS	WG4: Superconducting RF	2	4
THCOXBS	WG4: Superconducting RF	1	4
THCOYBS	WG3: Electron sources and injectors	2	3
THCOZBS	WG3: Electron sources and injectors		4
FRCOWBS	WG2: ERL beam dynamics and instrumentation	1	3
FRCOXBS	WG2: ERL beam dynamics and instrumentation	3	4
FRCOYBS	Working group summaries	2	5
# of QA passed paper		39	
# of contributions			88

Contribution counts by country/affiliation:

#	Country	Invited Oral	Contributed Oral	Poster	Total
1	United States of America	14 32.56%	7 31.82%	5 21.74%	26 29.55%
2	Germany	7 16.28%	11 50.00%	7 30.43%	25 28.41%
3	Japan	10 23.26%	0 0.00%	1 4.35%	11 12.50%
4	Russia	4 9.30%	2 9.09%	2 8.70%	8 9.09%
5	United Kingdom	2 4.65%	1 4.55%	4 17.39%	7 7.95%
6	People's Republic of China	2 4.65%	0 0.00%	2 8.70%	4 4.55%
7	Switzerland	3 6.98%	1 4.55%	0 0.00%	4 4.55%
8	Canada	0 0.00%	0 0.00%	1 4.35%	1 1.14%
9	France	1 2.33%	0 0.00%	0 0.00%	1 1.14%
10	Italy	0 0.00%	0 0.00%	1 4.35%	1 1.14%
Total Contributions		43 48.86%	22 25.00%	23 26.14%	88

#	Affiliation	Invited Oral	Contributed Oral	Poster	Total
1	Helmholtz-Zentrum Berlin für Materialien und Energie GmbH (HZB)	2 4.65%	4 18.18%	4 17.39%	10 11.36%
2	High Energy Accelerator Research Organization (KEK)	9 20.93%	0 0.00%	1 4.35%	10 11.36%
3	Brookhaven National Laboratory (BNL)	2 4.65%	4 18.18%	3 13.04%	9 10.23%
4	Cornell University (CLASSE)	6 13.95%	1 4.55%	0 0.00%	7 7.95%
5	Thomas Jefferson National Accelerator Facility (JLab)	4 9.30%	1 4.55%	1 4.35%	6 6.82%
6	Russian Academy of Sciences (BINP SB RAS)	2 4.65%	2 9.09%	1 4.35%	5 5.68%
7	Technische Universität Darmstadt (TU Darmstadt)	3 6.98%	2 9.09%	0 0.00%	5 5.68%
8	European Organization for Nuclear Research (CERN)	3 6.98%	1 4.55%	0 0.00%	4 4.55%
9	Johannes Gutenberg University Mainz (KPH)	1 2.33%	3 13.64%	0 0.00%	4 4.55%

10	Science and Technology Facilities Council (STFC/DL/ASTeC)	2	4.65%	1	4.55%	1	4.35%	4	4.55%
11	Helmholtz-Zentrum Dresden-Rossendorf (HZDR)	1	2.33%	0	0.00%	1	4.35%	2	2.27%
12	National Research Nuclear University (MEPhI)	1	2.33%	0	0.00%	1	4.35%	2	2.27%
13	Peking University (PKU)	1	2.33%	0	0.00%	1	4.35%	2	2.27%
14	Technische Universitaet Darmstadt (TEMF, TU Darmstadt)	0	0.00%	1	4.55%	1	4.35%	2	2.27%
15	Budker Institute of Nuclear Physics (BINP)	1	2.33%	0	0.00%	0	0.00%	1	1.14%
16	Cockcroft Institute	0	0.00%	0	0.00%	1	4.35%	1	1.14%
17	Cockcroft Institute (UMAN)	0	0.00%	0	0.00%	1	4.35%	1	1.14%
18	Computer Aided Engineering and Consulting e.G. (COMPAEC e.G.)	0	0.00%	0	0.00%	1	4.35%	1	1.14%
19	Institut für Kernphysik (KPH)	0	0.00%	1	4.55%	0	0.00%	1	1.14%
20	Institute of High Energy Physics (IHEP)	1	2.33%	0	0.00%	0	0.00%	1	1.14%
21	Institute of Modern Physics, Chinese Academy of Sciences (IMP/CAS)	0	0.00%	0	0.00%	1	4.35%	1	1.14%
22	Istituto Nazionale di Fisica Nucleare (INFN-Milano)	0	0.00%	0	0.00%	1	4.35%	1	1.14%
23	Laboratoire de l'Accélérateur Linéaire (LAL)	1	2.33%	0	0.00%	0	0.00%	1	1.14%
24	Los Alamos National Laboratory (LANL)	1	2.33%	0	0.00%	0	0.00%	1	1.14%
25	Massachusetts Institute of Technology (MIT)	0	0.00%	1	4.55%	0	0.00%	1	1.14%
26	National Institutes for Quantum and Radiological Science and Technology (QST)	1	2.33%	0	0.00%	0	0.00%	1	1.14%
27	Old Dominion University (ODU)	1	2.33%	0	0.00%	0	0.00%	1	1.14%
28	SLAC National Accelerator Laboratory (SLAC)	0	0.00%	0	0.00%	1	4.35%	1	1.14%
29	The University of Liverpool	0	0.00%	0	0.00%	1	4.35%	1	1.14%
30	TRIUMF (TRIUMF)	0	0.00%	0	0.00%	1	4.35%	1	1.14%
	Total Contributions	43	48.86%	22	25.00%	23	26.14%	88	



Figure 1: Participants of the ERL2019 Workshop.



ERL2019

63rd ICFA Advanced Beam Dynamics Workshop on Energy Recovery Linacs, 15th-20th September 2019

hosted by Helmholtz-Zentrum Berlin



WORKSHOP TOPICS

- ERL facilities
- ERL beam dynamics and instrumentation
- Electron sources and injectors
- Superconducting RF
- ERL applications

CONTACT

Helmholtz-Zentrum Berlin für Materialien und Energie
Mail: erl2019@helmholtz-berlin.de | Web: hz-b.de/erl2019

VENUE

WISTA Building, Volmerstr. 2, 12489 Berlin



hz-b.de/erl2019

Online registration will be available from 15th JANUARY

LOCAL ORGANIZING COMMITTEE

- Jennifer Bierbaum
- Hartmut Ehmler
- Aleksandr Matveenko (SPC Chair)
- Meghan McAteer
- Atoosa Meseck (ERL2019 Chair & LOC Chair)
- Roswitha Schabardin
- Jens Völker

INTERNATIONAL ORGANIZING COMMITTEE

- Kurt Aulenbacher (Mainz)
- Sergey Belomestnykh (FNAL)
- Stephen Benson (JLAB)
- Ilan Ben-Zvi (BNL)
- Yong Ho Chin (KEK)
- Ryoichi Hajima (GST)
- Georg Hoffstaetter (Cornell)
- Erk Jensen (CERN)
- Kwang-Je Kim (ANL)
- Jens Knobloch (HZB)
- Kexin Liu (PKU)
- Atoosa Meseck (HZB)
- Tsukasa Miyajima (KEK)
- Oleg Shevchenko (BINP)
- Susan Smith (STFC)

SCIENTIFIC PROGRAM COMMITTEE

- Michael Abo-Bakr (HZB)
- Deepa Angal-Kalinin (ASTeC)
- André Arnold (HZDR)
- Michaela Arnold (SDALINAC)
- Kurt Aulenbacher (J Mainz)
- Ivan Bazarov (Cornell)
- Alex Bogacz (JLAB)
- Oliver Brüning (CERN)
- Andrew Burrill (SLAC)
- Yong Ho Chin (KEK)
- Pavel Evtushenko (HZDR)
- Frank Gerigk (CERN)
- Georg Hoffstaetter (Cornell)
- Walid Kaabi (LAL)
- Thorsten Kamps (HZB)
- Dmitry Kayran (BNL)
- Ivan Konoplev (ADAMS)
- Georgios Kourkafas (HZB)
- Matthias Liepa (Cornell)
- Kexin Liu (Peing U.)
- Aleksandr Matveenko (HZB)
- Peter McIntosh (STFC)
- Axel Neumann (HZB)
- Houjun Qian (PITZ)
- Bob Rimmer (JLAB)
- Hiroshi Sakai (KEK)
- Daniel Schulte (CERN)
- Oleg Shevchenko (BINP)
- Achille Stocchi (LAL)
- Christopher Tennant (JLAB)
- Nikolay Vinokurov (BINP)
- Erdong Wang (BNL)
- Juang Wang (IHEP)
- Masahiro Yamamoto (KEK)

Figure 2: ERL2019 Workshop poster.

4 Recent Doctoral Theses

4.1 Study of the Transverse Mode Coupling Instability in the CERN Large Hadron Collider

CANDIDATE: David Amorim, Université Grenoble-Alpes

SUPERVISOR: Nicolò Biancacci (CERN)

GRADUATION: October 2019

The High-Luminosity upgrade of the CERN Large Hadron Collider will increase the levelled luminosity by a factor of five compared to nominal LHC luminosity. Among others, the beam intensity will be multiplied by two. With such intensity increase, collective and in particular impedance effects are a possible performance limitation for the accelerator.

The current LHC stability limits were investigated using PyHEADTAIL, a time-domain macro-particle code, and DELPHI, a Vlasov equation solver. Simulations results were compared to dedicated measurements performed in the accelerator. From these measurements the impedance induced tune shift was found to be higher than predicted from simulations by 20% to 60% depending on the beam and plane. Despite the larger tune shifts with respect to predictions, the TMCI intensity threshold was still higher than the bunch intensities used. Beam based measurements of several LHC collimators were also performed. The measurement method and data processing used allowed to measure the impedance induced tune shifts to a level of a few 10^{-5} . For several collimators the impedance was found to be within a factor two of simulation results. These different measurements showed that the LHC model underestimates the machine impedance by a factor of 1.3 to 1.5.

An impedance reduction of the collimators is planned for HL-LHC to cope with the brightness increase. Simulations demonstrated the subsequent increase of the machine TMCI threshold. For the full collimator upgrade, this threshold would lie at $8 \cdot 10^{11}$ proton per bunch, a value three times higher than the nominal HL-LHC single bunch intensity.

The beneficial effect of the collimators impedance reduction was also demonstrated with measurements in the LHC. The machine impedance was reduced to a level similar to the one that will be reached during Run III (2021-2023) by opening a set of collimators. The tune shift versus intensity could be reduced with this configuration. Moreover the impedance of a single collimator prototype was measured with beam in the LHC. This prototype was installed in the past to confirm the choice of new low resistivity metallic materials for the collimation upgrade. The beneficial effects of these low resistivity materials compared to the current carbon based collimators could be demonstrated.

Finally, impedance and mode coupling instability simulations were performed for the High-Energy LHC, a proposed future collider. Because of the machine protection constraints, the impedance can increase by a factor up to ten over a large frequency range compared to current colliders. This results from the tight collimator gaps required to protect the machine. In consequence coherent stability margins will be much lower than in the LHC and HL-LHC and novel beam stabilization techniques should therefore be investigated.

4.2 Advanced Accelerator Interaction Region Optics for LHC Operation and Future Hadron Colliders

CANDIDATE: Leon van Riesen-Haupt

SUPERVISORS: Prof. Andrei Seryi and Dr. Emmanuel Tsesmelis

GRADUATION: 2019

This thesis covers several optics issues and solutions applicable to the Large Hadron Collider (LHC), its High Energy (HE-LHC) upgrade as well as the Future Circular Collider (FCC-hh). A key tool presented in this thesis is a final focus triplet optimisation tool to help design the interaction regions of the FCC-hh and HE-LHC. The method produces short final focus triplets with large integrated gradients whilst having an aperture sufficiently large to sustain the beams and radiation shielding. A modification of this tool is used to optimise the dynamic aperture of the Nuclotron-based Ion Collider fAcility (NICA), which is severely impacted by quadrupole fringe field effects. Finally, a ballistic alignment optics for the LHC will be presented as well as a to measure the offset of modulated quadrupoles. These efforts can be used to improve the stability and luminosity of the LHC.

4.3 Development of Feedback Algorithms for Future Linear Colliders

CANDIDATE: Rebecca Ramjiawan

SUPERVISOR: Professor Philip Burrows

GRADUATION: November 2019

This thesis is a contribution towards the design for a beam stabilisation system for a future linear collider. Low-latency, intra-train feedback systems for beam stabilisation are studied by the Feedback On Nanoseconds Timescales (FONT) group at the University of Oxford. One aspect of the thesis concerns studies of a prototype feedback system designed to provide beam stabilisation at the nominal interaction point for an electron beam at the Accelerator Test Facility (ATF) at KEK, Japan. The aim of the system is to demonstrate beam stabilisation to the 1 nm level. Studies towards improving the resolution and stabilisation performance of the feedback system are presented, with results demonstrating 20 nm resolution and 41 nm beam stabilisation.

Another focus of the thesis is the simulation of the performance of an intra-train feedback system intended for the interaction point of the International Linear Collider. The beam transport and beam-beam interactions were modelled and the performance of a bunch-by-bunch feedback system was simulated. Effects including ground motion, jitter of the damping-ring extraction kicker and both short and long-range wakefields were included. Preliminary studies suggest that a bunch-by-bunch feedback system could help achieve up to 95% of the design luminosity.

4.4 Hydrodynamic Optical-Field-Ionized Plasma Waveguides for Laser Plasma Accelerators

CANDIDATE: Rob Shalloo

SUPERVISORS: Prof Simon Hooker and Dr Laura Corner
 COMPLETION DATE: 2018

One of the key problems in the development of laser plasma accelerators is the guiding of highly-intense laser pulses over the long distances necessary for multi-GeV electron acceleration. To guide intense pulses, it is necessary to use a waveguide made of plasma. This thesis documents the experimental development of a new kind of plasma waveguide which is uniquely suited to the next generation of laser plasma accelerators operating at the multi-GeV level and at high repetition rates.

Hydrodynamic Optical-Field-Ionized (HOFI) plasma waveguides are formed by the hydrodynamic expansion of a hot column of plasma heated to high temperatures by an ultrashort, intense laser pulse. The expanding plasma drives a radial shockwave out into the cold unionized gas surrounding the plasma and in doing so creates a structure capable of guiding intense laser pulses. In this work, two proof of principle experiments show that the formation of HOFI waveguides at the low plasma densities necessary for multi-GeV electron acceleration is indeed possible and that intense laser pulses may be guided over distances long compared to the diffraction length of the pulse at these low densities.

4.5 Demonstrating High Transformer Ratio Beam-Driven Plasma Wakefield Acceleration

CANDIDATE: Gregor Loisch, Deutsches Elektronen-Synchrotron DESY, 15738 Zeuthen, Germany

SUPERVISORS: Prof. Dr. Florian Grüner (University Hamburg, CFEL), Dr. Anne Oppelt (DESY)

GRADUATION: September 2019

Particle-beam-driven plasma wakefield acceleration (PWFA) is one of the prime candidates for future compact accelerator technologies. In this scheme, a high-brightness driver particle bunch enters a plasma and initiates oscillations of plasma electrons by expelling them from their equilibrium positions. Particles trailing the driver bunch can be accelerated in the electric field between regions of negative and positive charge excess formed in this oscillation. Acceleration gradients of up to several tens of GV/m have been demonstrated in experiment, exceeding the gradients of conventional technology by orders of magnitude. PWFA could thus allow to accordingly shrink the size of an accelerator, possibly reducing size and cost of an accelerator facility significantly.

One key aspect of a PWFA is the ratio between acceleration gradient behind the driver and deceleration gradient inside the driver bunch. This so-called transformer ratio defines the maximum acceleration achievable for a given driver energy and is closely connected to the achievable efficiency. In linear wakefield theory the transformer ratio is limited to 2 for longitudinally symmetric driver bunches, which typically emerge from conventional accelerators. One proposed method to achieve high transformer ratios (HTR) exceeding this limit is to employ driver bunches with lengths of multiple plasma skin depths and sawtooth-like, “triangular” current profiles. Due to the complexity of shaping such bunches and beam-plasma instabilities that can inhibit stable acceleration, HTRs had thus far not been achieved in PWFA.

In the course of the present work, the driving of HTR PWFA has been accomplished at the Photo-Injector Test facility at DESY in Zeuthen (PITZ). Existing bunch shaping

capabilities at PITZ, based on photocathode laser pulse shaping, were extended to the production of HTR-capable driver bunches. An argon gas discharge plasma cell was built and optimised for providing the plasma acceleration medium for the PITZ electron beam parameters. A novel plasma density measurement method based on the self-modulation of long electron bunches was developed and validated, which enabled determination of plasma densities not accessible with established methods. Following these preparations, a transformer ratio of 4.6 (+2.2/-0.7) was observed experimentally and reproduced in numerical simulations.

4.6 Characterization of Ultrashort Electron Bunches at the SINBAD-ARES Linac

CANDIDATE: Daniel Marx, DESY, Hamburg, Germany

SUPERVISORS: Wolfgang Hillert (University of Hamburg), Barbara Marchetti (DESY)

DEFENSE DATE: October 2019

Daniel Marx has studied methods to measure the properties of ultrashort electron bunches. A key application of such bunches is the injection into novel accelerators with high-frequency accelerating fields, such as laser-wakefield plasma accelerators or dielectric laser accelerators.

The ARES linac at the SINBAD facility at DESY, which will begin operation in late 2019, has the goal of producing bunches at particle energies of 100 MeV to 150 MeV with rms lengths down to the subfemtosecond level and charges in the picocoulomb range. In his work, various novel techniques that will be used to characterize these bunches downstream of the photoinjector and at the end of the beamline have been investigated and developed.

In particular, he has worked on a new method to measure the transverse phase space of low-charge electron bunches based on the analysis of the shadow image of a metal grid. This technique allows the characterization of the whole 4D transverse phase-space distribution with high sensitivity in a single shot, from which the projected and intrinsic emittances are retrievable. This method has been verified with simulation studies and benchmarked against the pepper-pot technique in experiments at the PEGASUS beamline at UCLA, and it is planned to use this technique downstream of the photoinjector at the ARES linac.

Measuring the longitudinal properties of compressed, femtosecond-long bunches with sufficient resolution is another key challenge for ARES.

Two transverse deflection structures, which have the novel feature of providing a variable angle of streaking, will be installed at the end of the beamline. Detailed simulations of measurements of ARES bunches show that unprecedented resolutions may be achieved with the prospective setup, which will enable subfemtosecond bunches to be measured with high precision. A new 3D charge-density reconstruction procedure, which relies on varying the streaking angle of the deflector, has been proposed and demonstrated in simulations. Simulations of reconstructions of the energy distribution, longitudinal phase space and slice emittance are also shown in his thesis and the limitations discussed. Finally, a preliminary design of this section of the beamline is proposed based on the studies performed.

4.7 Generation of Ultra-Short Electron Bunches and FEL Pulses, and Characterization of Their Longitudinal Properties at FLASH2

CANDIDATE: Florian Christie

SUPERVISORS: Dr. Mathias Vogt, Dr. Juliane Rönsch-Schulenburg, Prof. Wolfgang Hillert, Prof. Wilfried Wurth

DISPUTATION DATE: October 2019

Florian Christie has studied the generation of ultra-short electron bunches and FEL pulses at FLASH2. A short-pulse injector laser was installed at FLASH, which generates short, low charge electron bunches directly at the cathode. These short electron bunches with a length of about 1 ps can be further compressed in the linac to produce ultra-short FEL (Free-Electron Laser) pulses down to a few femtoseconds in the FLASH2 undulators. Measurements of such pulses as well as tracking simulations of the FLASH2 beam line are presented in his thesis. Both studies demonstrate the feasibility of ultra-short FEL pulses down to single-spike lasing at FLASH2.

Up until now, no hardware to directly measure the electron bunch length has been installed in the FLASH2 beam line. As exact knowledge of the pulse duration is essential for time-resolved user experiments, the beam line downstream of the FLASH2 undulators has been redesigned for the installation of a variable polarization Transverse Deflecting Structure (TDS). In combination with a dipole magnet it is possible to map the longitudinal phase space density of the electron bunches onto a beam screen. Additionally, the photon pulse duration as well as the slice emittance in both transverse planes can be measured using such a TDS.

His thesis presents the final layout of the beam line, the accelerator optics, and also simulations for the aforementioned measurements.

5 Forthcoming Beam Dynamics Events

[64th ICFA Advanced Beam Dynamics Workshop on High Luminosity Circular e+e- Colliders \(eeFACT2020\)](#)

13-17 September 2020, Elba Island, Italy

INFN Frascati National Laboratories is organizing the ICFA Advanced Beam Dynamics Workshop on High Luminosity Circular e+e- Colliders (eeFACT2020) in Hotel Hermitage, Biodola, Elba Island (Italy).

This workshop is organized in the context and with sponsoring of the ICFA Beam Dynamics Panel and EU/ARIES funded European Network for Accelerator Performance and Concepts (APEC).

eeFACT2020 scope:

- Reviewing and documenting the state of the art in e+e- factory design
- Reviewing and drawing lessons from SuperKEKB phase 3 commissioning
- Catalyzing further contributions to the SuperKEKB, FCC, CEPC & tau-charm design efforts
- Fostering synergies and new collaborations across communities, in particular with the low-emittance light sources and between continents
- Jointly developing novel solutions to outstanding problems

[65th ICFA Advanced Beam Dynamics Workshop on High-Intensity and High-Brightness Hadron Beams](#)

5–9 October 2020, FNAL, USA

The 65th ICFA Advanced Beam Dynamics Workshop on High-Intensity and High-Brightness Hadron Beams (HB2020) will be held at Fermilab from Monday, October 4, to Friday, October 9, 2020.

The ICFA HB workshop is the premier international event focused on the latest developments and insights into the physics of high-intensity hadron beams. About 200 scientists, engineers, and industry exhibitors are expected to be in attendance. The workshop consists of plenary sessions, two parallel sessions and poster sessions covering

- Beam Dynamics in Rings,
- Beam Dynamics in Linacs,
- Accelerator Systems,
- Commissioning and Operations, and
- Beam Instruments and Interactions.

The ICFA HB workshop series originated in 2002 at Fermilab. Previous recent HB workshops were held in Lansing, Michigan (USA, 2014), Lund (Sweden, 2016) and Daejeon (Korea, 2018).

5.1 ICFA Beam Dynamics Panel Members

Name	eMail	Institution
Rick Baartman	baartman@lin12.triumf.ca	TRIUMF, 4004 Wesbrook Mall, Vancouver, BC, V6T 2A3, Canada
Marica Biagini	marica.biagini@lnf.infn.it	INFN-LNF, Via E. Fermi 40, C.P. 13, Frascati, Italy
John Byrd	jbyrd@anl.gov	Accelerator Systems Division, Argonne National Laboratory, 9700 S. Cass Ave, Building 401-C4263, Argonne, IL 60439, U.S.A.
Yunhai Cai	yunhai@slac.stanford.edu	SLAC, 2575 Sand Hill Road, MS 26, Menlo Park, CA 94025, U.S.A.
Jie Gao	gaoj@ihep.ac.cn	Institute for High Energy Physics, P.O. Box 918, Beijing 100039, China
Ajay Ghodke	ghodke@rrcat.gov.in	RRCAT, ADL Bldg., Indore, Madhya Pradesh, 452 013, India
Eliana Gianfelice-Wendt	eliana@fnal.gov	Fermilab, Mail Station 312, PO Box 500, Batavia IL 60510-5011, U.S.A.
Ingo Hofmann, Chair	i.hofmann@gsi.de	High Current Beam Physics, GSI Darmstadt, Planckstr. 1, 64291 Darmstadt, Germany
Sergey Ivanov	sergey.ivanov@ihep.ru	Institute for High Energy Physics, Protvino, Moscow Region, 142281 Russia
In Soo Ko	isok@postech.ac.kr	Pohang Accelerator Lab, San 31, Hyoja-Dong, Pohang 790-784, South Korea
Elias Metral	elias.metral@cern.ch	CERN, CH-1211, Geneva 23, Switzerland
Peter Ostroumov	Ostroumov@frib.msu.edu	FRIB, National Superconducting Cyclotron Laboratory, Michigan State University, 640 S. Shaw Lane, East Lansing, Michigan 48824, U.S.A.
Mark Palmer	mpalmer@bnl.gov	Brookhaven National Lab, Upton, NY 11973, U.S.A.
Chris Prior	chris.prior@stfc.ac.uk	STFC/RAL, Harwell Campus, Didcot, Oxon OX11 0QX, U.K.
Ji Qiang	jqiang@lbl.gov	Lawrence Berkeley National Laboratory, MS 71J-100a, One Cyclotron Road, Berkeley, CA 94720-8211 U.S.A.
Yuri Shatunov	Yu.M.Shatunov@inp.nsk.su	Akad. Lavrent'eva, Prospekt 11, 630090 Novosibirsk, Russia
Yoshihiro Shobuda	yoshihiro.shobuda@j-parc.jp	J-PARC, Shirakata 2-4, J-Tokai-Mura, Naka-Gun, Ibaraki-Ken 319-1195, Japan
Jiu-Qing Wang	wangjq@ihep.ac.cn	Institute for High Energy Physics, P.O. Box 918, 9-1, Beijing 100039, China
Rainer Wanzenberg	rainer.wanzenberg@desy.de	DESY, Notkestrasse 85, 22603 Hamburg, Germany
Zhentang Zhao	zhaozhentang@sinap.ac.cn	SINAP, Jiading Campus: 2019 Jia Luo Road, Jiading District, Shanghai 201800, P.R. China; and Zhangjiang Campus: 239 Zhang Heng Road, Pudong New District, Shanghai 201203, P.R. China

*The views expressed in this newsletter do not necessarily coincide with those of the editors.
The individual authors are responsible for their text.*